

Copyright  
by  
Lorena Gina Moscardelli  
2007

**The Dissertation Committee for Lorena Gina Moscardelli Certifies that this is the approved version of the following dissertation:**

**Mass Transport Processes and Deposits in Offshore Trinidad and Venezuela, and their role in Continental Margin Development**

**Committee:**

---

Lesli Wood, Supervisor

---

William Fisher

---

Ron Steel

---

David Mohrig

---

Charles Kerans

---

Ursula Hammes

**Mass Transport Processes and Deposits in Offshore Trinidad and  
Venezuela, and their role in Continental Margin Development**

**by**

**Lorena Gina Moscardelli, B.Sc.**

**Dissertation**

Presented to the Faculty of the Graduate School of

The University of Texas at Austin

in Partial Fulfillment

of the Requirements

for the Degree of

**Doctor of Philosophy**

**The University of Texas at Austin**

**May, 2007**

## **Acknowledgements**

First of all, I would like to thank all of those that supported me through the process of obtaining my PhD. I am very grateful to my supervisor Dr. Lesli Wood for her guidance, patience, and her willingness to open doors of opportunities for all her students. Special thanks to Dr. William Fisher who played an important role supporting my research. I also want to thank the rest of my committee members for all their technical support, and good advices: Dr. David Mohrig, Dr. Ron Steel, Dr. Charles Kerans, and Dr. Ursula Hammes.

I acknowledge The Jackson School of Geosciences, and specially the Bureau of Economic Geology for the financial support that I received during all these years. Special thanks to the company members of the Quantitative Clastic Laboratory consortium: bhpbilliton, Anadarko, bg, ConocoPhillips, Shell, Chevron, Talisman Energy, Hydro, Total, Amerada Hess, Agip, ExxonMobil, IMP, KerrMcGee and Noble Energy, for their generous contributions. I also appreciate all the support provided through contributions of data by the Ministry of Energy and Energy Industries of Trinidad and Tobago.

I thank Dallas Dunlap, John Andrews, Sean Sullivan, Moraima Aponte, Nysha Chaderton, Julie Maher, and Carla Sanchez for their friendship and for all their support during this process. Finally, I thank my grandfather, Giovanni Moscardelli, for inspiring me to become a scientist, and the rest of my family for providing me with the unconditional support necessary to finish this dissertation.

# **Mass Transport Processes and Deposits in Offshore Trinidad and Venezuela, and their role in Continental Margin Development**

Publication No. \_\_\_\_\_

Lorena Gina Moscardelli, PhD

The University of Texas at Austin, 2007

Supervisor: Lesli Wood

Mass transport complexes (MTC) form a significant component of the stratigraphic record in ancient and modern deep water basins. One such basin, the deep marine margin of eastern offshore Trinidad, situated along the obliquely converging boundary of the Caribbean and South American plates and proximal to the mouth of the Orinoco River, is characterized by catastrophic shelf margin processes, intrusive and extrusive mobile shales, active tectonics and possible migration and sequestration of hydrocarbons. Major structural elements found in the deep water slope regions include: large transpressional fault zones along which mobile shales extrude to form seafloor ridges; fault-cored anticlinal structures overlain by extrusive seafloor mud volcanos; shallow-rooted sediment bypass grabens near the shelf break; and normal and counter-regional faults. A data volume consisting of 10,708 km<sup>2</sup> of several merged 3D seismic data volumes enable subseafloor interpretation of several mass transport event deposits and the erosional surfaces that form their boundaries. The data shows numerous mass

transport complexes which are characterized by chaotic, mounded seismic facies and fan-like geometries. Their extent (up to 2017 sq. km) and thickness (up to 250 m) is strongly influenced by seafloor topography. Depositional and erosional architectures identified with these units includes: large magnitude lateral erosional edges, thrust faulting, linear basal scours, side-wall failures, flow geometries, possible displaced blocks and chaotic matrix material. Active tectonism in the region, high sedimentation rates associated with the Orinoco Delta System, and abundant unstable gas hydrates suggest the presence of higher frequency mechanisms at work for MTCs generation than sea-level fluctuations alone.

Three types of mass transport complexes are identified in offshore Trinidad; shelf-attached systems that were fed by shelf edge deltas whose sediment input is controlled by sea level fluctuations, slope- attached systems which occur when upper slope sediments catastrophically fail due to gas hydrate disruptions, earthquakes and/or storm activity, and locally detached systems formed when local instabilities in the sea floor trigger small collapses. Such classification of the relationship between slope mass failures and the sourcing regions enables an understanding of the nature of initiation, length of development history, petrography and petrophysics of MTC's.

In addition, a collection of morphometric parameters of MTCs from different continental margins are analyzed in order to better understand their causal mechanisms, and to establish whether systematic morphometric parameters characterize these deposits across different tectonic settings. Observations suggest that there is a clear relationship between morphometric parameters of MTC and their causal mechanisms.

## Table of Contents

List of Tables .....	x
List of Figures .....	xi
Chapter 1: Introduction, Objectives and Dissertation Overview .....	1
1.1. Introduction.....	1
1.2. Previous Work in Mass-Transport Complexes.....	2
1.3. Geological Elements of the Study Area.....	7
Sedimentary Sources and Distribution.....	7
Structural Setting and Features that Influence Deep-Marine Sedimentation .....	9
1.4. Methodology and Data Set.....	12
1.5. Anthropogenic Impact of Mass Transport Complexes .....	14
Tsunamigenic Hazards.....	14
Geotechnical Hazards .....	15
1.6. Objectives .....	17
1.7. Organization of Chapters .....	17
1.8. References.....	19
Chapter 2: Architectural Description and Geomorphology of Mass Transport Complexes in Offshore Trinidad .....	26
2.1. Introduction.....	26
2.2. General Description of the MTC_1 .....	29
Seismic Facies.....	37
Erosional Morphologies.....	38
Erosional Escarpment .....	42
Basal Mega-Scours .....	42
Cat-Claw Scours .....	44
Secondary Scours and Scratches.....	44
Syndepositional Thrusts.....	45
Erosional Shadow Features.....	47
Pressure Ridges.....	50
2.3. Character Variability of Axial and Peripheral Parts of the Complex ....	50

Basal Flow Processes .....	51
2.4. Interpreted Causes and Controls for MTC Generation .....	55
Sea Level Fluctuations, High Sedimentation Rates and MTC's.....	59
Tectonism, Gas Hydrates, Free Gas and MTC's .....	61
2.5. Mass-Transport Complex Reservoir Elements .....	62
2.6. Conclusions.....	64
2.7. References.....	66
 Chapter 3: A Genetic Classification of Mass Transport Complexes – Offshore Trinidad.....	 69
3.1. Introduction.....	69
Terminology, Dimensions and Relevance of Mass Transport Complexes .....	 70
Seismic Character of Mass Transport Complexes .....	72
Physical and Lithological Characteristics of Mass Transport Complexes in Cores and Outcrops.....	 74
Sequence Stratigraphy, Eustatic Control and Mass Transport Complexes .....	 79
3.2. Methodology and Data Sets .....	82
3.3. Structural Setting and Paleobathymetry in Offshore Trinidad and its Influence in Deep Water Sedimentation .....	 87
3.4. Synthesis of the Evolution of the Deep Marine Margin of Offshore Trinidad .....	 90
P60-P20 Time Interval .....	90
P20-P15 Time Interval.....	91
P15-P10 Time Interval.....	91
P10-P4 Time Interval.....	95
P4-P0 Time Interval.....	96
3.5. Mass Transport Complexes in Offshore Trinidad .....	99
Attached Mass Transport Complexes .....	100
Detached Mass Transport Complexes (MTC_2.2, MTC_2.3 and MTC_2.4).....	 111
3.6. Morphometry of mass transport complexes.....	116
3.7. Classification of Mass Transport Complexes and Causal Mechanisms	117
3.8. Conclusions.....	120



3.9. References.....	123
Chapter 4: A New Insight into the Morphometry of Mass Transport Complexes and its Significance.....	128
4.1. Introduction.....	128
Quantitative data from Worldwide Mass Transport Deposits .....	128
Can we predict sediment nature from deposit geometry?.....	129
4.2. Morphometry of Mass Transport Complexes .....	130
4.3. The scale and geometry of mass transport complexes.....	139
4.4. The Missing Link between the Morphometry of Mass Transport Complexes and Their Causal Mechanisms .....	141
4.5. The Thickness of Mass Transport Complexes.....	148
4.6. Conclusions.....	151
4.7. References.....	153
Appendices.....	156
Appendix 1. Data base of basic morphometric parameters of mass transport complexes around the world .....	156
Appendix 2. Classification of mass transport complexes .....	158
References.....	160
Vita.....	172

## **List of Tables**

Table 3.1: Worldwide Occurrence and Distribution of Offshore Mass Transport Complexes.....	78
Table 3.2: Classification, Causal Mechanisms and Source Areas of Mass Transport Complexes.....	100
Table 3.3: Classification and Morphometry of Mass Transport Complexes in Offshore Trinidad.....	113

## List of Figures

Figure 1.1: Classification of gravity induced deposits.....	3
Figure 1.2: Annual sediment discharge in the Columbus Basin. ....	8
Figure 1.3: Area of study and 3D mega merge. ....	9
Figure 1.4: Seismic line parallel to the axis of the paleocanyon (MTC_1). ....	11
Figure 1.5: Seismic line showing dip view across northern part of block 25. ....	13
Figure 2.1: Seismic surveys in study area and index map. ....	26
Figure 2.2: Three main surfaces that define the shallowest depositional sequence in the deep-marine area of offshore Trinidad. ....	28
Figure 2.3: Erosional surface that defines the base of MTC_1.....	30
Figure 2.4: Geomorphological interpretation of the basal erosional surface of the MTC_1.....	31
Figure 2.5. Isochron map that composites the youngest MTC and the overlying LCC. .....	32
Figure 2.6: Isochron map of LCC overlying MTC_1.....	33
Figure 2.7: Visualization subvolume Area 2 / Mega Scours.....	34
Figure 2.8: Visualization subvolume Area 3 / Syndepositional Thrusts. ....	38
Figure 2.9: Seismic line showing western boundary of MTC_1. ....	40
Figure 2.10: Seismic facies MTC_1. ....	41
Figure 2.11: Visualization subvolumes areas 4 and 5 / Cat Claw Scours and Eastern Mega Scour. ....	43
Figure 2.12: Close-up seismic line showing rafted blocks above the basal incision.	45
Figure 2.13: Shortening Syndepositional Thrusts.....	46
Figure 2.14: Geomorphology of an Erosional Shadow Remnant (ESR's).....	48

Figure 2.15: Flow patterns according to geometry of erosional shadow remnants.	49
Figure 2.16: Geomorphology proximal part MTC_1 and MTC_2.	58
Figure 3.1: Worldwide distribution of mass transport complexes	77
Figure 3.2: Map showing the area of study and outline of MTC_2.	84
Figure 3.3: Map showing the main structures that are present in the study area.	85
Figure 3.4. Conceptual method that was used to generate RSA extraction maps.	86
Figure 3.5: Visualization paleocanyon MTC_1.	88
Figure 3.6: Visualization NE termination of the Darien Ridge.	89
Figure 3.7: Isochron maps between key stratigraphic surfaces.	93
Figure 3.8: RMS amplitude extraction map showing : MTC_2, MTC_2.1, MTC_2.2, MTC_2.3 and MTC_2.4.	97
Figure 3.9: Stratigraphic surface P15, this erosional surface defines the base of the stratigraphic interval (P15-P10).	98
Figure 3.10: RMS amplitude extraction map from basal portion of MTC_2	103
Figure 3.11: RMS amplitude extraction map from the basal portion of the P15-P10 stratigraphic interval.	107
Figure 3.12. Seismic lines across MTC_2.1 and MTC_2.2	108
Figure 3.13: RMS amplitude extraction map near the top of the MTC_2.1	112
Figure 3.14: A) RMS amplitude extraction map near the top of mass transport complexes MTC_2.3 and MTC_2.4.	115
Figure 3.15: Run-out distance versus length concept in MTCs.	118
Figure 3.16: Schematic depiction of the different kinds of mass transport complexes and the processes associated with their genesis.	122
Figure 4.1: Log-log plot showing the relationship between area (A) and length (L) of mass transport complexes around the world.	131

Figure 4.2: Relationship between area and length of MTCs .....	132
Figure 4.3: Run-out distance versus length concept in MTCs II .....	135
Figure 4.4: Relationship between area (A) and volume (V) of MTCs. ....	136
Figure 4.5: Relationship between area and volume of MTC's and power function.	137
Figure 4.6: Estimation of the area and volume of MTC's.....	138
Figure 4.7: Geometric relationships of MTC's - Lower and Upper fields.....	143
Figure 4.8: Area versus length log-log plot and the distribution of attached versus detached MTC's .....	144
Figure 4.9: Area versus volume log-log plot and the distribution of attached versus detached MTC's. ....	145
Figure 4.10: Relationship between causal mechanisms and morphometry of MTC's. ....	146
Figure 4.11: (A) Area versus thickness plot of MTC's around the world. (B) Area versus thickness of attached versus detached MTC's. ....	150

# **Chapter 1: Introduction, Objectives and Dissertation Overview**

## **1.1. INTRODUCTION**

Mass transport complexes (slides, slumps and debris flows) deposits pose a problem for hydrocarbon exploration and development in deep-water facies. These units typically have low porosities and permeabilities (Shipp et al., 2004), and their episodic and recurrent nature in many basins of the world means that they have the potential to constitute significant stratigraphic components of deep-water traps. Erosiveness of mass-movement processes, controlled by sea floor irregularities, can result in deep and widely dispersed truncation and removal of underlying levee-channel deposits. Mass transport complexes (MTCs) can then act as both lateral and top seal for these depositional remnants forming effective stratigraphic traps (see Moscardelli et al., 2006).

MTCs form a large stratigraphic component of many ancient and modern deep-water margins around the world. In some settings, up to 70% of the entire slope and deep-water stratigraphic column is composed of MTCs and associated deposits (Maslin et al., 2004; Newton et al., 2004). The prevalence of mass failures represents a significant hazard to engineering infrastructure located on the continental slope and in deep-marine areas of the world's oceans (Hoffman et al., 2004; Pirmez et al., 2004; Shipp et al., 2004). Such hazards can have a significant impact on the financial aspects of hydrocarbon exploration and thus a significant impact on development of deep-water locations. Recent interest in global warming has prompted a large number of climate researchers to consider the influence of catastrophic landslides in episodic release of methane into the atmosphere (Haq, 1993 and 1995; Kvenvolden, 1993; Maslin et al., 1998 and 2004). Paleomarine landslides and mass failures, known to occur throughout the world's marine margins, disrupt the pressure/temperature conditions that maintain stable frozen methane

in large portions of the world's continental margins, resulting in release of these gases (Maslin et al., 2004). Likewise, destabilization of pressure/temperature regimes by changing water temperatures, shifting ocean currents, or lowering sea level can cause melting of frozen clathrates and initiate failures along marine margins. These episodes of catastrophic mobilization of huge amounts of slope sediments not only present a risk for submarine installations but also have the potential to generate tsunamis, a phenomenon that represents a significant hazard for coastal communities and near-shore navigation (Nisbet and Piper, 1998; Hearne et al., 2003; O'Loughlin and Lander, 2003).

Three key questions must be addressed if we are to gain an understanding of the risks that MTC's present, the role that they play in forming continental margins around the world, and the effect that they have on fluid flow and reservoir development within deep-water basins: (1) how do we recognize and map MTC's in the world's submarine margins and what role do they play in the filling of deep-water basins; (2) how do these MTC's influence underlying and overlying strata and what factors are involved in MTC initiation, duration, and termination; and (3) what role do these processes, elements, and facies play in the creation and destruction of hydrocarbon traps? It is the main goal of this research to answer the three questions posed.

## **1.2. PREVIOUS WORK IN MASS-TRANSPORT COMPLEXES**

Terminology in MTC's study remains a confusing mix of terms compiled by scientists working in subaerial and submarine environments, settings that have different fluid-flow parameters, and in modern (Masson et al., 1997; Masson et al., 1998; Norem et al., 1990; Gee et al., 1999 and 2001) versus ancient rocks (Martinez et al., 2005; Sohn, 2000; Wach et al., 2003), where our ability to view the deposits and their details varies. The term mass-transport complex includes all kinds of gravity- induced or downslope deposits, with the exception of turbidites (Figure 1.1). For purposes of this discussion,

turbidite deposits are grouped into a different subcategory. Remotely sensed information contained in seismic, sonar, and well and core data is often inadequate to identify those sedimentary structures and textures within a deposit that constrain the relevant flow parameters and conditions. Therefore, the term gravity-induced or downslope processes will be used when it is impossible to make a distinction between turbidites, debris flows, slides, and slumps. In this work, debris flows, slides, and slumps are considered to be constituents of MTC's, and these elements can co-occur in the same event or depositional unit (Figure 1.1).





CLASSIFICATION FOR GRAVITY INDUCED DEPOSITS					
		Definition	Common Characteristics (all scales)	Seismically Recognizable Features (dependant on data quality and the scales of the features)	
GRAVITY INDUCED OR DOWNSLOPE DEPOSITS MASS TRANSPORT COMPLEXES	<b>Slides</b>		Mass or block that moves downslope on a shear surface and shows no internal deformation.	The block preserves its original internal feature and fabrics - No internal deformation.	Mega rafted and/or detached blocks, compressional ridges, imbricate slides, irregular upper bedding contacts, lateral pinch-out geometries, duplex structures, contorted layers, braided patterns, oriented ridges and scours.
	<b>Slumps</b>		Blocks that move downslope and undergoes rotation that causes internal deformation.	Internal folds, contorted bedding, layers with various orientations, changes in fabric, breccias, clastic injections.	
	<b>Debris Flows</b>		Debris flows are generated by flows with plastic rheology (a yield limit of cohesive sediment is exceeded) and laminar state.	Sharp upper and lower contacts, floating or rafted clasts, planar clast fabric, inverse grading, basal shear zone.	Discontinuous units. Chaotic reflectors.
TURBIDITE	<b>Turbidity Current</b>		Deposits generated by a turbidity current with Newtonian rheology and turbuletn state.	Normal size grading, sharp basal contacts, gradational upper contacts.	Lobate features. Lateral continuous.

Figure 1.1: Terminology in MTC study remains a confusing mix of terms compiled by scientists working in subaerial and submarine environments. Slides, slumps and debris flows are considered to be constituents of MTC's.

MTC's can occur at any time during a margin's history (Masson et al., 1997) but often have been hypothesized to develop early in cycles of shoreline fall toward lowstand, when sedimentation to the shelf edge is at its peak and water overburden weight is being reduced over shelf regions (Posamentier and Kolla, 2003). Resulting deposits occupy areas on the slope and on the basin floor, usually accumulating near the toe of slope. The volume of MTC's can vary enormously, ranging from a few meters in



thickness and a few hundred square meters in area, to more than 200 m in thickness and tens of thousand of square kilometers in area. They often develop initial bathymetry that later influences sedimentation in deep-water settings (Shanmugam, 2000; Marr et al., 2001; Posamentier and Kolla, 2003; Moscardelli et al., 2004). MTC's occur in a variety of both carbonate and siliciclastic settings; however, this research will deal with only siliciclastic MTC deposits and processes.

With recent advances in seafloor imaging and visualization, relatively young, modern MTC's are being studied extensively as process and reservoir analogs for older deposits. For example, the genesis and stratigraphic features of Pleistocene-age MTC's in the north part of the Gulf of Mexico have been studied as analogs to older, Tertiary-age mass-transport deposits. A series of papers by several researchers (Beaubouef and Friedmann, 2000; Winker and Booth, 2000; Anderson et al., 2003; Armentrout, 2003; Beaubouef et al., 2003a and 2003b; Piper and Behrens, 2003) document the latest Pleistocene in the Texas offshore area in the Brazos-Trinity slope system and in the Louisiana offshore area in the Mississippi system, where high-quality seismic data show episodic MTC development. Each MTC unit is characterized by the presence of low-amplitude, semitransparent, chaotic seismic reflections (Beaubouef and Friedmann, 2000). Several wells and continuous core taken in upper- to mid-slope-situated, mud-rich complexes in the Gulf of Mexico suggest that these elements (Winker, 1996) are composed of slumps, slides, and debris-flow events. These MTC's are usually embedded in a repetitive stratigraphic succession that is composed of sandy, levee-channel complexes and hemipelagic drapes (Beaubouef and Friedmann, 2000). Bami et al. (2000) documenting deep water strata in offshore Trinidad found that most of the fill within their study area was composed of repetitious cycles of MTC's and levee-channel complexes. The authors attributed this repetition to Pleistocene sea-level change inducing

sediment-supply fluxes to the shelf edge. Similar observations and interpretations of causal mechanisms have been made in the intraslope basin system in the Gulf of Mexico (Beaubouef and Friedmann, 2000) and in the Amazon Fan (Manley and Flood, 1988), where the vertical cyclic distribution of different depositional systems has been related to sea-level fluctuations. However, other authors have suggested that tectonic events may be a major cause of slope destabilization (Moscardelli et al., 2004 and Martinez et al., 2005) and gas hydrate dissolution events may also be responsible for many shelf edge and slope failures (Knapp, 2000).

Pirmez et al. (1997) describing several sand-rich intervals in the Amazon Fan of offshore Brazil infer these deposits to be a series of sediment gravity flows intercalated with channel-levee complexes. These deposits are interpreted by the authors to have been emplaced as slides of large coherent blocks (meters to decimeters) and relatively small amounts of deformed matrix and deformed weaker blocks (slumps). Matrix-rich deposits with small clasts at the top of some of these slides are considered true debris flows (Piper and Deptuck, 1997; Piper et al., 1997). Several authors (Damuth et al., 1988; Manley and Flood, 1988 and Piper and Deptuck, 1997), have reported that MTC deposits in the Amazon Fan can reach maximum thicknesses of 200 m and to cover areas of more than 15,000 km<sup>2</sup>. Maslin et al. (1998), attributed the genesis of these deposits to catastrophic failures in the continental margin and slope, generated by rapid drops in sea level during the Pleistocene, and episodic flushing of Amazon River sediments onto the upper slope.

Actual physical characteristics of mass-transport deposits have been documented by few authors. Shipp et al. (2004), using analyses from cores, logs, and geotechnical parameters in the Amazon Fan in Brazil (Piper et al., 1997b), the Na Kika Basin debris flows in the Gulf of Mexico and in shallow mass-transport deposits in offshore Trinidad (East Prospect - block 25A), concluded that several physical characteristics seem to be

common in these kinds of MTC's. The lithology is generally made up of muddy sediments, although in some cases sands can be also present; log responses tend to show an increase in resistivity, compressional velocity, density, and porosity; and geotechnical measurements indicate an increase in shear strength, with a corresponding decrease in void ratio and water content (Pirmez et al., 2004; Shipp et al., 2004). All these characteristics suggest that MTC's may be considerably more consolidated shortly after deposition than other deep-water deposits, such as levee-channel complexes or hemipelagic drapes. As a consequence of this physical nature, certain factors have to be considered to prevent complications during the drilling phase (low penetration rates and problems in installation of jetted conductors) of exploration in regions of MTC development (Shipp et al., 2004). However, the same authors pointed out that the lithology of MTC's always depends on the kind of materials composing the slope failure.

Additional consideration must be given to the distance over which these deposits might travel and impact engineering facilities. Several studies in debris flows of the Gulf of Mexico have also suggested that yield strength is inversely proportional to run-out distances, whereas run-out is proportional to failure volume (Gee et al., 1999; Pirmez et al., 2004). On the basis of quantitative study of several geomorphic parameters in submarine landslides located in different tectonic settings in the U.S. continental slope (Oregon, California, Gulf of Mexico, and New Jersey), McAdoo et al. (2000) established that (1) steepness of the slope adjacent to the failure tends to be inversely proportional to the run-out length, and (2) landslides that encompass large areas occur in regions where weaker, perhaps younger, material is present and past rapid accumulations of sediment and subsequent salt or mud tectonics may combine to create high fluid overpressures and steep slopes. These observations lead to the conclusion that sedimentation, erosion, and

local geology are more important factors in determining landslide location and morphology than slope or proximity to seismic centers (McAdoo et al., 2000).

### **1.3. GEOLOGICAL ELEMENTS OF THE STUDY AREA**

#### **Sedimentary Sources and Distribution**

The principle sediment source to the present day Columbus Basin shelf and deep water margin is the Orinoco River and Delta (Herrera et al., 1981; Meade et al., 1990; Warne et al., 2002; Aslan et al., 2003). The offshore area of Trinidad and Venezuela has been influenced by the Orinoco Deltaic depositional systems since the late Miocene (Diaz de Gamero, 1996). Several efforts have been made to examine the marine processes on the offshore area of Trinidad and Venezuela and the influence that the Orinoco exerts on recent basin fill (Nota, 1958; Van Andel, 1967; Carr-Brown, 1972; Bami et al., 2000; Ercilla et al., 2000); however, intrarelationships between structure, tectonics, and marine processes in this offshore area are still unclear. The Amazon River is also believed to be a major contributor to the finer-grained material component filling the basin (Figure 2.1). At present sea-level highstand-marine currents transport huge amounts of suspended sediment from the Amazon and Orinoco Delta northwest along the northern South American coast (Warne et al., 2002). Most of the fine-grained Amazonian sediments are deposited as extensive mud capes along the Guyana and Suriname margins. However, some of the sediments and nutrients from these major river systems are carried far into the northern reaches of the Caribbean Sea before dissipating into the water column. Within the Trinidad offshore, currents strongly rework sands and silt along the eastern continental shelf during modern highstand (Wood, 2000; Sydow et al., 2003).

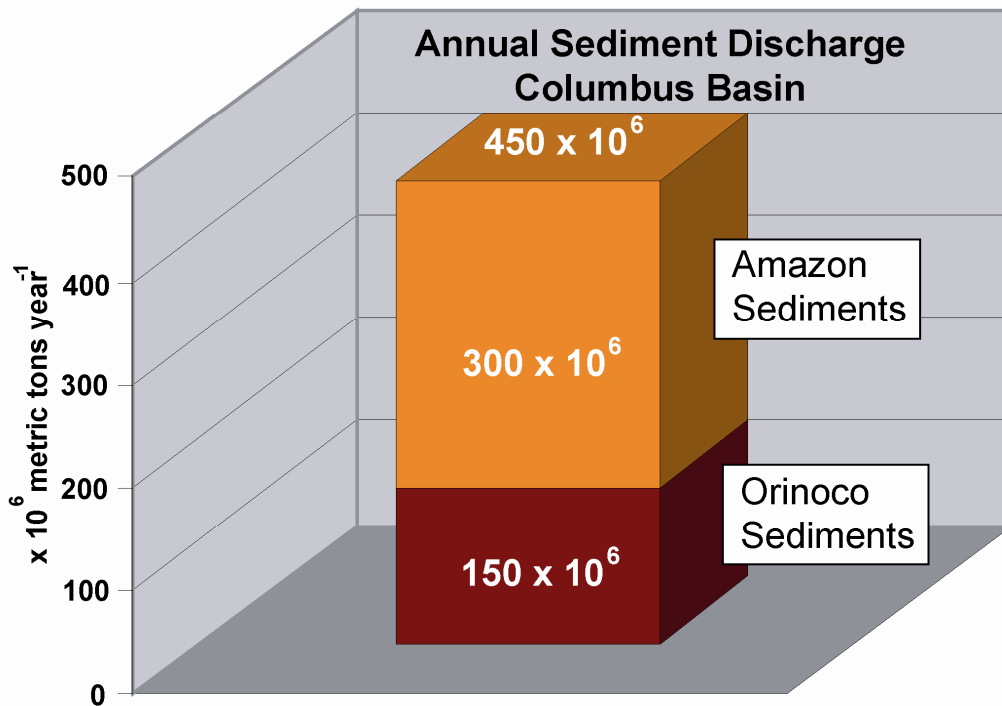


Figure 1.2: Annual Sediment Discharge in the Columbus Basin (Sources: Kuehl et al., 1986; Meade et al., 1990 and Eisma et al., 1978).

The Orinoco and Amazon have persisted in the geologic past as major supplier of sediment to the basin. A strong body of evidence exists that, during the most recent lowstand ~ 18,000 years BP, sea level fell almost 125 m in the study area, exposing a large part of the Trinidad and Tobago shelf (Carr-Brown, 1972). Deltas prograded to the present shelf edge (Sydow et al., 2003), building lowstand wave-dominated shelf-margin deltas that, at least in northern areas of the Columbus Basin, fed sediment almost directly into canyons that impinged upon the lowstand shelf break. Channels documented by recent seismic (Brami et al., 2000; Sullivan et al., 2004) and sonar imagery (Belderson et al., 1984; Ercilla et al., 2000; Deville et al., 2003a; Deville et al., 2003b) currently transport deep-marine sediments to the northeast to sites of deposition in accretionary

prism piggyback basins or, ultimately, to the modern Orinoco Fan (Belderson et al., 1984; Deville et al., 2003a and Deville et al., 2003b).

### Structural Setting and Features that Influence Deep-Marine Sedimentation

Extensive seismic interpretation in the offshore area of Trinidad reveals a variety of structural features that influence sediment transport and distribution in the deep-marine margin. These include mud volcanoes, seafloor ridges, and normal and counternormal faults (Figure 1.3).

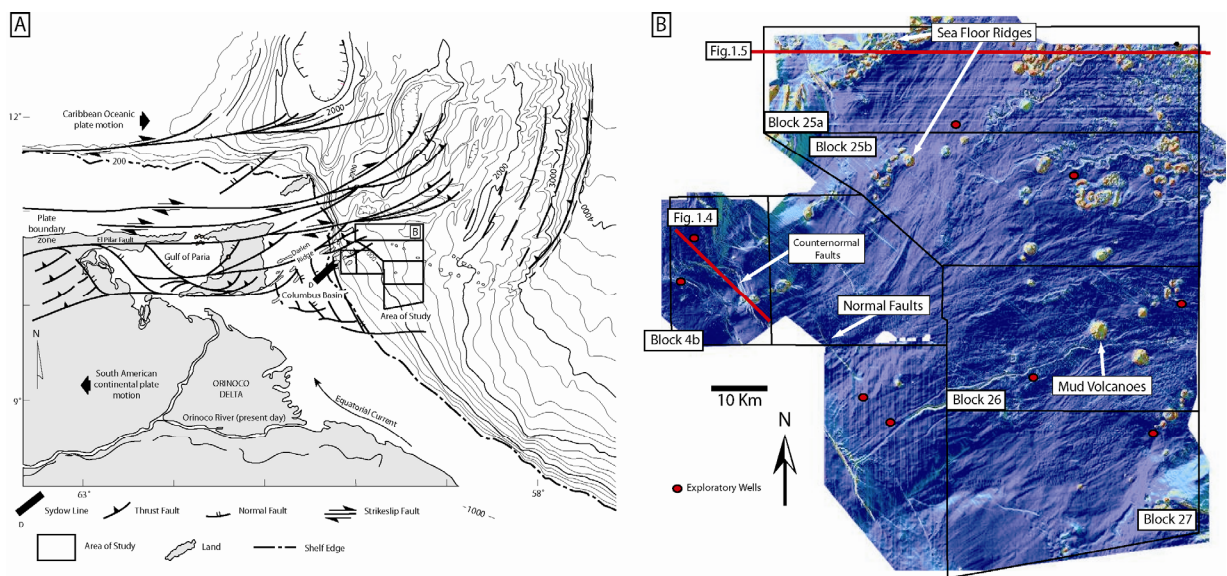


Figure 1.3: A) Map showing the area of study located in the area of the northeastern South America along the Caribbean Plate Boundary Zone where the Caribbean Plate (to the north) and the South American Plate (to the south) meet. The area of 3D seismic is outlined in black lines. The shelf break is shown as a heavy black dashed and dotted line along the 200-300 meter contour. The Orinoco Delta system in Venezuela is the primary supplier of sediments to the eastern shelf and continental slope. B) Seismic surveys in study area correspond to Block names and sea floor (Sullivan et al., 2004). The locations of subsequent figures is shown.

Mud volcanoes in the study area occur in a variety of sizes, shapes, and arrangements. These features have been extensively studied by Sullivan et al. (2004) and

grouped into five different provinces/categories: mud volcanoes located in the fault-focused province, mud ridge province, basin fill province, collapse mud volcanoes and buried mud volcanoes. Some occur as isolated individual features; others occur as clusters or trains that align northeast-southwest. It is important to note that some of these systems are still active. The majority of these mud-volcano features are documented to rise above the present seafloor several hundred meters and have a significant impact on the distribution of gravity-driven margin sediments in deep-marine environments. Sullivan et al. (2004) identified 161 mud volcanoes in the study area, from this amount only 13 have been classified as collapse features or buried mud volcanoes. Often radial normal faults associated with mud-mass deflation and mud-volcano collapse have a propensity to redirect channel systems to moat-shaped areas of accommodation developed around the mud-volcano flanks (Mize et al., 2004). In addition, the majority of the mud volcanoes form bathymetric highs on the seafloor, which the channels and debris flows are forced to navigate around.

A major transpressive fault system occurs in the study area and is associated with the oblique collision occurring between the Caribbean Plate to the north with the South American plate, the host plate for the Columbus Basin (Figure 1.3A). This fault system is most prevalent in the northwest parts of the study area, where large faults break the seafloor surface, forming a seafloor structure called the Darien Ridge. This ridge is a narrow zone of uplift (20 km wide) comprising multiple complexly folded and thrust structures. Extensional forces associated with this boundary form pull-apart grabens along the shelf edge, in the north parts of the study area. In addition to graben structures (Figure 1.3A), several large, down-to-the-northeast normal faults affect the slope areas (Figures 1.3A and 1.4). These faults appear to be the eastward most occurrence of a family of northwest-southeast-oriented extensional structures that dominate the

Columbus Basin shelf located to the west of the study area (Heppard et al., 1998; Wood, 2000). On the shelf, similar normal faults are Pliocene and Pleistocene in age and have throws of up to 1,300 m. In the study area, shelf-edge normal faults appear to be relatively recent structures, expressing several meters of seafloor relief. These normal faults are often coupled with counter-normal faults, striking in the same orientation but downthrown to the west (Figure 1.4). These faults appear to form localized areas of accommodation for sediments in the upper slope, temporarily ponding sediments that later spill downslope in gully channels.

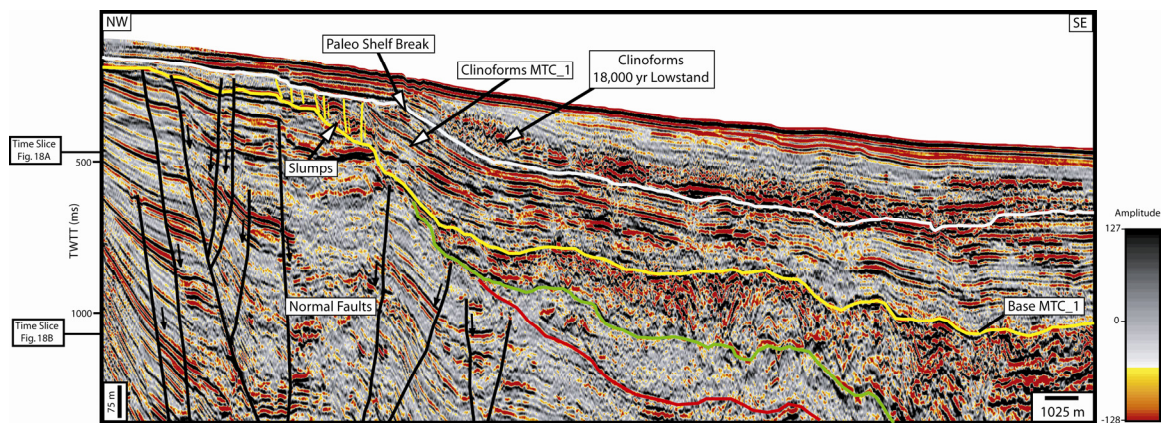


Figure 1.4: Northwest to southeast seismic line in block 4ab (see figure 1B for relative location) showing normal faults, which dip towards the southeast, and counter-normal faults near the shelf break area. The interpreted horizons represent the stratigraphic boundaries of stacked cycles of mass-transport complexes and levee channel complexes in the areas proximal to the shelf-break. Several aggradational clinoform packages overlie the Base MTC\_1 horizon in more updip locations confirming the connection between the shelf-edge prograding deltaic systems and the upper slope. A much younger clinoform package, dated by Sydow et al. (2003) at 18, 000 kyr overlies the MTC\_1 deposits.

Deeper seismic data reveal several buried anticlinal ridges aligned northeast-southwest across the length of the study area that appear to exert a long-lived influence on sediment pathways. They show little expression on the seafloor, except for a line of



seafloor mud volcanoes paralleling the subterranean anticlinal crest. Sediments thicken off axis in basins to the north and south of these anticlines. These anticlines continue on trend southwest through the substrata of the Columbus Basin shelf where they are buried beneath the extensive upper Tertiary overburden of the Trinidad marine shelf. The anticlinal axis of these structures appears to align with several prolific shelfal hydrocarbon fields (Wood et al., 2004). Deep regional seismic studies suggest that these anticlines are cored by transpressive faulting that is associated with regional compression along the Caribbean-South American plate boundary (Boettcher et al., 2003), the same forces responsible for the uplifting of the Darien Ridge.

#### **1.4. METHODOLOGY AND DATA SET**

The primary tool for study of the deep-water architecture and nature of the offshore Trinidad continental margin is three-dimensional seismic data. Using 3D data offers a range of visualization and attribute-analysis techniques not afforded researchers working with 2D seismic or seafloor imaging sonar. Unfortunately, few seismic surveys are large enough to encompass an entire mass-transport deposit's stage area and depocenters. To mitigate this problem in the Trinidad study area, five separate 3D seismic data volumes were merged into a single contiguous volume spanning approximately 10,708 km<sup>2</sup>. Depths of data provided from individual surveys vary from a low of 1,500 milliseconds (block 4B) in the westernmost part of the area to a high of 5,000 milliseconds (block 25B) of coverage over central and eastern areas (Figure 1.3B). These data are all late-1990's vintage, and although they were acquired by various companies working in the area, their acquisition parameters and quality are remarkably similar. Time-migrated volumes have an approximate bin spacing volume of 25 m by 12.5 m and 4 ms vertical sampling rate. All the seismic volumes were processed to zero-phase and the average frequency content of the full stack seismic data was 30-35 Hz. For

approximate time-depth conversions at shallow depths, 1 millisecond is equivalent to 0.75 m. Seismic interpretation and attribute analyses were done on seismic workstations using Landmark Seisworks, OpenVision, and GeoProbe software.

The quality of the 3D data makes it possible to correlate units across the slope into the deep-marine basin with a high degree of confidence. Seven regional seismic horizons have been mapped. Figure 1.5 (see location in Figure 1.3B) is a seismic line that shows a dip view across the north part of the study area on which some regional horizons are correlated from an area proximal to the slope on the west, across a mud-diapir province, to the deep-marine environments on the east. These surfaces were mapped to define the gross architecture of the continental margin fill.

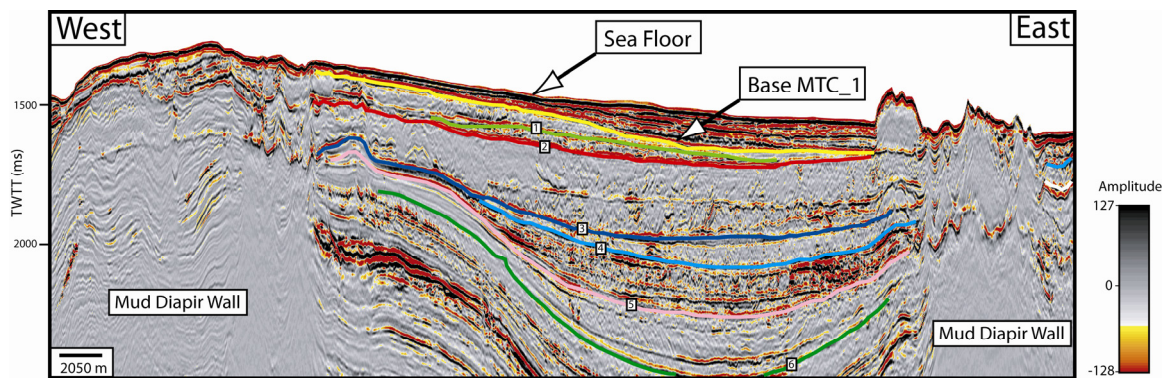


Figure 1.5: Seismic line showing dip view across north part of study area (block 25). Six regional horizons that represent major erosional surfaces have been correlated from an area proximal to the slope on the west, across a mud diapir province, to the deep-marine environments on the east. These surfaces were mapped in order to define gross architecture of continental margin fill. Stratigraphic units between surfaces represent stacked cycles of mass-transport complex and levee channel system development.

In each case, all surfaces were seeded with the picking tool and then interpolated along key amplitude horizons. These surfaces were then adjusted by hand where the picking tool strayed from the horizon.

Although more than 200 drop-cores exist across the study area (Sullivan et al., 2004), none penetrates the section of interest. Several exploration wells have been drilled in the area, but no direct access to this data was available to the authors. However, Shipp et al. (2004) described the lithologic and physical characteristics of these deposits using data from two exploratory wells in block 25A. Their observations and descriptions are used in this work.

## **1.5. ANTHROPOGENIC IMPACT OF MASS TRANSPORT COMPLEXES**

### **Tsunamigenic Hazards**

It is well known that a sudden displacement of the seafloor through faulting can potentially disrupt the overlying water column and generate tsunamigenic waves (Dawson et al., 2004). A similar phenomenon can be generated by catastrophic slumps and downslope slides initiated by a variety of processes. One of the most economically devastating modern tsunamigenic events recorded was associated with a landslide related to the Unimak (eastern Aleutians, south coast of Alaska) earthquake that occurred in April 1946. Although the earthquake was relatively small, it caused a landslide on the slope that initiated a huge remobilization of the substratum, resulting in a sudden displacement of water above the seafloor. The result was an enormous tsunami with wave heights between 8 and 20 m that killed 167 people and affected coastal regions from as far away as the Aleutian chain to Hawaii (Fryer et al., 2004). Of even more historic note was the submarine landslide in the offshore area of Newfoundland, Canada that occurred on November 18, 1929. The landslide, initiated by an earthquake around the Grand Bank area, severed a series of submarine cables. The timing of each cut was recorded, and for the first time, scientists were able to document both the speed and direction of a submarine mass failure. More than 200 km<sup>3</sup> of debris was mobilized into the deep water

in this erosive and turbulent sediment flow that reached a calculated velocity of 65 km per hour. The flow and the water displaced by it generated waves more than 30 m high that killed 27 people along the Newfoundland coast (Nisbet et al., 1998; Dawson et al., 2004). Even small slides have the capacity to do large damage. In 1979 a small landslide that occurred off the French coast mobilized 0.15 km<sup>3</sup> of debris near the Nice airport, causing a tsunami that killed 11 people (Rothwell et al., 1998).

The southern Caribbean region (the focus of this study) is a province of active tectonic activity that has experienced its share of landslide-generated tsunamigenic events. The tsunamis in this region are often associated with earthquake events, but not always (O'Loughlin and Lander, 2003). In 1726, a 10-m tsunami hit Peninsula de Araya (Venezuela), and the waves destroyed La Salina (the salt works) and partly ruined the Spanish Fort located on the coast of Araya. It is thought that this event was related to offshore landslides, but the trigger mechanism for such a slide has not been documented. More recently, on September 13, 1928, a tsunami was reported in Carupano (Peninsula de Paria, Venezuela), which could not be linked to the occurrence of any earthquake in the area. However, it is thought that a large hurricane over 1,000 km away might have destabilized the continental margins of the hurricane-affected region, initiating underwater landslides that generated the Carupano tsunamigenic waves.

### **Geotechnical Hazards**

MTC's and gravity-induced mass movements in general represent a dangerous geotechnical hazard for submarine installations, such as pipelines and communication lines. Often exploration and development planning costs are increased to allow for planning in the face of MTC hazards. Hoffman et al. (2004) documented a case study in Falcon field (EB 579/623), located in the northwestern Gulf of Mexico, where planning for the placement of seafloor infrastructure was significantly influenced by the presence

of the East Breaks Slide MTC. The slide, generated nearly 15 kyr ago by sediments shed from the lowstand shelf-break regions of the relict Colorado and Brazos Deltas, extends between 73 and 100 miles downslope and covers some 2,760 km<sup>2</sup>. Thickness of the deposit is about 77 m (250 ft). 3D seismic data show chaotic reflectors and tilted, rafted blocks of undeformed sedimentary strata. Identification of paleoslide regions necessitated design of a longer, more costly, but much more stable and safer pipeline route from Falcon field to its host platform in Mustang Island Block A-13.

Shipp et al. (2004) also documented the importance of describing the physical characteristics of MTC's in order to improve drilling strategies in the so called foundation zone (upper 100 m below seafloor). Three different case studies—Amazon Fan, Brazil; Na Kika Basin, Gulf of Mexico; and offshore Trinidad—document MTC deposits to be more consolidated than neighboring conformable sediments, showing an increase in resistivity, compression velocity, and density with an associated decrease in porosity. Conductor penetration rates on MTC deposits are much slower than in conformable deposits, causing delays in installation of conductor casings. An extreme case study was documented in the east part of block 25(a) offshore Trinidad, where difficulty in conductor penetration caused the casing to tilt, resulting in subsequent abnormal flow outside of the housing. This flow disturbed the stability of surrounding soil, eventually compromising the security of the well and causing its abandonment and considerable economic loss (Shipp et al., 2004).

## **1.6. OBJECTIVES**

This dissertation aims to set a series of parameters and guidelines to better recognize and map mass transport complexes in the world's submarine margins. It also intends to clarify the role that mass transport complexes play in the fill of deep-water basins, and how these deposits influence underlying and overlying strata, as well as to

understand the controlling factors that are involved in the initiation, development, and termination of mass transport complexes. This information will be useful to determine the role that the processes, elements, and facies of mass transport complexes play in the creation and destruction of hydrocarbon traps, and their role as potential anthropogenic risks. Finally we compare and contrast the morphology, causal mechanisms and nature of mass transport deposits around the world to examine the similarities, trends and uniqueness of these types of deposits and develop some common equations for predicting their occurrence and nature in both the ancient and modern record.

## **1.7. ORGANIZATION OF CHAPTERS**

This dissertation is organized into four main chapters:

1. Chapter 1 presents an overview of MTC's (terminology and previous works), and introduces a brief description of the main geological elements that are present in the study area. It also describes the data set (3D mega merge) and explains the main objectives of this research.
2. Chapter 2 describes in detail the main geomorphological elements that constitute the architecture of MTCs. This chapter also analyses the causal mechanisms associated with MTCs, and explains how to identify specific triggering mechanisms based on the geomorphology observed in the source areas associated with these deep-water deposits. In addition, Erosional Shadow Remnants (ESR's) are defined for the first time in this work as potential stratigraphic traps, these traps are formed as the result of the interaction between mass-wasting processes, pre-existing bathymetric barriers (mud volcanoes), and previous sedimentation (levee-channel complexes). This chapter has been published as Moscardelli and Wood (2006).

3. Chapter 3 introduces a new genetic classification for MTCs. This new classification scheme was elaborated taking into account the causal mechanisms associated with MTCs, and incorporating the quantitative relationships that exist between their morphometric parameters (area, length, width, thickness, and volume). The classification intends to provide with elements that can be used to elucidate triggering mechanisms based on the morphometry of the deposits. This chapter also addresses the discussion associated with the role that mass transport complexes play in the traditional sequence stratigraphic model. In addition, a deep insight into the structural setting and paleobathymetric evolution of the deep marine margin of offshore Trinidad is provided, this discussion intends to better illustrate the influence of paleobathymetric barriers in the development of deep water sedimentation pathways. This chapter is currently under review for publication.
4. Chapter 4 presents a collection of morphometric parameters (area, length, and volume) of MTC's from different continental margins, and tectonic settings around the world, this data was analyzed in order to better understand the causal mechanisms of MTC's, and to establish whether systematic morphometric parameters characterize these deposits along different continental margins around the world. The results presented in this chapter validate, through quantitative data from all over the world, the classification scheme that was proposed in chapter 3, and it also provides with a series of simple equations that can be used to predict unknown morphometric parameters of MTC's based on existing data. This chapter will be submitted for publication this year.

## 1.8. REFERENCES

- Anderson, J. B., J. Wellner, K. Abdulah, S. R. Sarzalejo, H. H., N. C. Rosen, R. H. Fillon, and J. B. Anderson, 2003, Late Quaternary shelf-margin delta and slope-fan complexes of the East Texas-western Louisiana margin: variable response to eustasy and sediment supply: Shelf Margin Deltas and Linked Down Slope Petroleum Systems: Global Significance and Future Exploration Potential, p. 67-78.
- Armentrout, J. M. R., H. H., N. C. Rosen, R. H. Fillon, and J. B. Anderson, 2003, Timing of Late Pleistocene shelf-margin deltaic depositional and mass-transport events, East Breaks 160-161 shelf-edge minibasin, Gulf of Mexico: Shelf Margin Deltas and Linked Down Slope Petroleum Systems: Global Significance and Future Exploration Potential, p. 91-114.
- Aslan, A., W. A. White, A. G. Warne, and E. H. Guevara, 2003, Holocene evolution of the western Orinoco Delta, Venezuela: GSA Bulletin, v. 115, p. 479-498.
- Beaubouef, R. T., V. Abreu, J. C. R. Van Wagoner, H. H., N. C. Rosen, R. H. Fillon, and J. B. Anderson, 2003, Basin 4 of the Brazos-Trinity slope system, western Gulf of Mexico: the terminal portion of a late Pleistocene lowstand systems tract: Shelf Margin Deltas and Linked Down Slope Petroleum Systems: Global Significance and Future Exploration Potential, p. 45-47.
- Beaubouef, R. T., S. J. W. Friedmann, P., R. M. Slatt, J. Coleman, N. C. Rosen, H. Nelson, A. H. Bouma, M. J. Styzen, and D. T. Lawrence, 2000, High resolution seismic/sequence stratigraphic framework for the evolution of Pleistocene intra slope basins, western Gulf of Mexico: depositional models and reservoir analogs: Deep-Water Reservoirs of the World.
- Beaubouef, R. T. V. W., J. C., and N. L. Adair, 2003, Ultra-high resolution 3-D characterization of deep-water deposits; Part II; Insights into the evolution of a submarine fan and comparisons with river deltas, Annual Meeting Expanded Abstracts - American Association of Petroleum Geologists, United States, American Association of Petroleum Geologists and Society of Economic Paleontologists and Mineralogists (AAPG) : Tulsa, OK, United States, p. 10.
- Belderson, R. H. K., N. H., A. H. Stride, and C. D. Pelton, 1984, A 'braided' distributary system on the Orinoco deep-sea fan, Marine Geology, Netherlands, Elsevier : Amsterdam, Netherlands, p. 195.
- Boettcher, S. S. J., J. L., M. J. Quinn, and J. E. Neal, 2003, Lithospheric structure and supracrustal hydrocarbon systems, offshore eastern Trinidad, AAPG Memoir, United States, American Association of Petroleum Geologists : Tulsa, OK, United States, p. 529.



- Brami, T. R., C. Pirmez, C. Archie, K. W. Holman, P., R. M. Slatt, J. Coleman, N. C. Rosen, H. Nelson, A. H. Bouma, M. J. Styzen, and D. T. Lawrence, 2000, Late Pleistocene deep-water stratigraphy and depositional processes, offshore Trinidad and Tobago: *Deep-Water Reservoirs of the World*, p. 104-115.
- Carr-Brown, B., 1972, The Holocene/Pleistocene contact in the offshore area east of Galeota Point, Trinidad, West Indies, *Transactions of the Caribbean Geological Conference = Memorias - Conferencia Geologica del Caribe*, United States, Queens College Press : Flushing, NY, United States, p. 381.
- Damuth, J. E., R. D. Flood, R. O. Kowsmann, R. H. Belderson, and M. A. Gorini, 1988, Anatomy and growth pattern of Amazon deep-sea fan as revealed by long-range side-scan sonar (GLORIA) and high-resolution seismic studies: *AAPG Bulletin*, v. 72, p. 885-911.
- Dawson, A. G., P. Lockett, and S. Shi, 2004, Tsunami hazards in Europe: *Environment International*, v. 30, p. 577-585.
- Deville, E., A. Battani, R. Griboulard, S. Guerlais, J. P. Herbin, J. P. Houzay, C. Muller, and A. Prinzhofer, 2003a, The origin and processes of mud volcanism; new insights from Trinidad: *Geological Society Special Publications*, v. 216, p. 475-490.
- Deville, E., A. Mascle, S. H. Guerlais, C. Decalf, and B. Colletta, 2003b, Lateral changes of frontal accretion and mud volcanism processes in the Barbados accretionary prism and some implications: *AAPG Memoir*, v. 79, p. 656-674.
- Diaz de Gamero, M. L., 1996, The changing course of the Orinoco River during the Neogene: a review: *Palaeogeography, Palaeoclimatology, Palaeoecology*, v. 123, p. 385-402.
- Ercilla, G., B. Alonso, J. W. Baraza, P., R. M. Slatt, J. Coleman, N. C. Rosen, H. Nelson, A. H. Bouma, M. J. Styzen, and D. T. Lawrence, 2000, High resolution morpho-sedimentary characteristics of the distal Orinoco turbidite system: *Deep-Water Reservoirs of the World*, p. 374-388.
- Fryer, G. J., P. Watts, and L. F. Pratson, 2004, Source of the great tsunami of 1 April 1946; a landslide in the upper Aleutian forearc: *Marine Geology*, v. 203, p. 201-218.
- Gee, M. J. R., D. G. Masson, A. B. Watts, and N. C. Mitchell, 2001, Passage of debris flows and turbidity currents through a topographic constriction; seafloor erosion and deflection of flow pathways: *Sedimentology*, v. 48, p. 1389-1409.
- Gee, M. J. R. M., D. G., A. B. Watts, and P. A. Allen, 1999, The Saharan debris flow; an insight into the mechanics of long runout submarine debris flows, *Sedimentology, International*, Blackwell : Oxford-Boston, International, p. 317.

- Haq, B. U., 1993, Deep sea response to eustatic changes and significance of gas hydrates for continental margin stratigraphy: International Association of Sedimentologists Special Publication, v. 18, p. 93-106.
- Haq, B. U., 1995, Growth and decay of gas hydrates: a forcing mechanism for abrupt climate change and sediment wasting on ocean margins?: Akademie Wetenschap, v. 44, p. 191-203.
- Hearne, M. E., N. R. Grindlay, and P. Mann, 2003, Landslide deposits, cookie bites, and crescentic fracturing along the northern Puerto Rico-Virgin Islands margin: implications for potential tsunamigenesis: Eos Transactions American Geophysical Union, v. 84, p. 46.
- Heppard, P. D., H. S. Cander, and E. B. Eggertson, 1998, Abnormal pressure and the occurrence of hydrocarbons in offshore eastern Trinidad, West Indies: AAPG Memoir, v. 70, p. 215-246.
- Herrera, L., G. Febres, and R. Avila, 1981, Las mareas en aguas Venezolanas y su amplificacion en la region del delta del Orinoco: Acta Cientifica Venezolana, v. 32, p. 299-306.
- Hoffman, J. S., M. J. Kaluza, R. Griffiths, G. McCullough, J. Hall, and T. Nguyen, 2004, Addressing the challenges in the placement of seafloor infrastructure on the East Breaks slide—a case study: the Falcon Field (EB 579/623): Northwestern Gulf of Mexico: Offshore Technology Conference, p. 17.
- Knapp, J. H., C. C. Diaconescu, and Anonymous, 2000, Evidence for buried gas hydrates and their role in seafloor instability in the South Caspian Sea, Azerbaijan: Abstracts with Programs - Geological Society of America, v. 32, p. 102.
- Kvenvolden, K. A., 1993, Gas hydrates, geological perspective and global change: Reviews of Geophysics, v. 31, p. 173-187.
- Manley, P. L., and R. D. Flood, 1988, Cyclic sediment deposition within Amazon deep-sea fan: AAPG Bulletin, v. 72, p. 912-925.
- Marr, J. G., P. A. Harff, G. Shanmugam, and G. Parker, 2001, Experiments on subaqueous sandy gravity flows: The role of clay and water content in flow dynamics and depositional structures: GSA Bulletin, v. 113, p. 1377-1386.
- Martinez, J. F., J. A. Cartwright, P. M. Burgess, and J. V. Bravo, 2004, 3D seismic interpretation of the Messinian unconformity in the Valencia Basin, Spain: Memoirs of the Geological Society of London, v. 29, p. 91-100.

- Martinez, J. F., J. A. Cartwright, P. M. Burgess, and J. V. Bravo, 2005, 3D seismic interpretation of the Messinian unconformity in the Valencia Basin, Spain: *Memoirs of the Geological Society of London*, v. 29, p. 91-100.
- Maslin, M., N. Mikkelsen, C. Vilela, and B. Haq, 1998, Sea-level- and gas-hydrate-controlled catastrophic sediment failures of the Amazon Fan: *Geology*, v. 26, p. 1107-1110.
- Maslin, M., M. Owen, S. Day, and D. Long, 2004, Linking continental-slope failures and climate change: Testing the clathrate gun hypothesis: *Geology*, v. 32, p. 53-56.
- Masson, D. G., M. Canals, B. Alonso, R. Urgeles, and V. Huhnerbach, 1998, The Canary debris flow; source area morphology and failure mechanisms: *Sedimentology*, v. 45, p. 411-432.
- Masson, D. G., B. van Niel, and P. P. E. Weaver, 1997, Flow processes and sediment deformation in the Canary debris flow on the NW African continental rise: *Sedimentary Geology*, v. 110, p. 163-179.
- McAdoo, B. G., L. F. Pratson, and D. L. Orange, 2000, Submarine landslide geomorphology, US continental slope: *Marine Geology*, v. 169, p. 103-136.
- Meade, R. H., F. H. Weibezahn, W. M. Lewis, D. Perez Hernandez, F. H. Weibezahn, H. Alvarez, and W. M. Lewis, 1990, Suspended-sediment budget for the Orinoco River: *El Rio Orinoco como ecosistema--The Orinoco River as an ecosystem*, Impresos Rubel, 55-79 p.
- Mize, K. L., L. J. Wood, and P. Mann, 2004, Controls on the morphology and development of deep-marine channels, eastern offshore Trinidad and Venezuela AAPG Annual Meeting Program, v. 13.
- Moscardelli, L., L. J. Wood, and P. Mann, 2004, Debris flow distribution and controls on slope to basin deposition, offshore Trinidad AAPG Annual Meeting Program, v. 13.
- Newton, C., G. Wach, U. Dalhousie, C. Shipp, and D. Mosher, 2004, Importance of mass transport complexes in the Quaternary development of the Nyle Fan, Egypt: *Offshore Technology Conference*, p. 10.
- Nisbet, E., and D. J. W. Piper, 1998, Giant submarine landslides: *Nature (London)*, v. 392, p. 329-330.
- Norem, H., J. Locat, and B. Schieldrop, 1990, An approach to the physics and the modeling of submarine flowslides: *Marine Geotechnology*, v. 9, p. 93-111.
- Nota, D. J. G., 1958, *Sediments of the western Guiana shelf*, diss., Utrecht, Univ.

- O'Loughlin, K. F., and J. F. Lander, 2003, Caribbean tsunamis – a 500 year history from 1498 – 1998: advances in natural and technological hazards research: Boston, Kluwer Academic Publishers, 263 p.
- Piper, D. J. W., E. W. R. Behrens, H. H., N. C. Rosen, R. Fillon, and J. Anderson, 2003, Downslope sediment transport processes and sediment distributions at the East Breaks, Northwest Gulf of Mexico: Shelf Margin Deltas and Linked Down Slope Petroleum Systems: Global Significance and Future Exploration Potential, p. 359-385.
- Piper, D. J. W., M. Deptuck, R. D. Flood, D. J. W. Piper, A. Klaus, S. J. Burns, W. H. Busch, S. M. Cisowski, A. Cramp, J. E. Damuth, M. A. Goni, S. G. Haberle, F. R. Hall, K.-U. Hinrichs, R. N. Hiscott, R. O. Kowsmann, J. D. Kronen, D. Long, M. Lopez, D. K. McDaniel, P. L. Manley, M. A. Maslin, N. Mikkelsen, F. Nanayama, W. R. Normark, C. Pirmez, J. R. dos Santos, R. R. Schneider, W. J. Showers, W. Soh, and J. Thibal, 1997a, Fine-grained turbidites of the Amazon Fan; facies characterization and interpretation: Proceedings of the Ocean Drilling Program, Scientific Results, v. 155, p. 79-108.
- Piper, D. J. W., C. Pirmez, P. L. Manley, D. Long, R. D. Flood, W. R. Normark, W. J. Showers, R. D. Flood, D. J. W. Piper, A. Klaus, S. J. Burns, W. H. Busch, S. M. Cisowski, A. Cramp, J. E. Damuth, M. A. Goni, S. G. Haberle, F. R. Hall, K.-U. Hinrichs, R. N. Hiscott, R. O. Kowsmann, J. D. Kronen, D. Long, M. Lopez, D. K. McDaniel, P. L. Manley, M. A. Maslin, N. Mikkelsen, F. Nanayama, W. R. Normark, C. Pirmez, J. R. dos Santos, R. R. Schneider, W. J. Showers, W. Soh, and J. Thibal, 1997b, Mass-transport deposits of the Amazon Fan: Proceedings of the Ocean Drilling Program, Scientific Results, v. 155, p. 109-146.
- Pirmez, C., J. G. Marr, C. Shipp, and F. Kopp, 2004, Observations and numerical modeling of debris flows in the Na Kika Basin, Gulf of Mexico: Offshore Technology Conference, p. 13.
- Pirmez, C. H., Richard N., and J. D. Kronen, Jr., 1997, Sandy turbidite successions at the base of channel-levee systems of the Amazon Fan revealed by FMS logs and cores; unraveling the facies architecture of large submarine fans, Proceedings of the Ocean Drilling Program, Scientific Results, United States, Texas A & M University, Ocean Drilling Program : College Station, TX, United States, p. 7.
- Posamentier, H. W., and V. Kolla, 2003, Seismic Geomorphology and Stratigraphy of Depositional Elements in Deep-Water Settings: Journal of Sedimentary Research, v. 73, p. 367-388.
- Rothwell, R. G., J. Thomas, and G. Kaehler, 1998, Low-sea-level emplacement of very large late Pleistocene "megaturbidite" in the Western Mediterranean Sea: Nature (London), v. 392, p. 377-380.

- Shanmugam, G., 2000, 50 years of the turbidite paradigm (1950s-1990s); deep-water processes and facies models; a critical perspective: *Marine and Petroleum Geology*, v. 17, p. 285-342.
- Shipp, C., J. A. Nott, and J. A. Newlin, 2004, Physical characteristics and impact of mass transport complexes on deepwater jetted conductors and suction anchor piles: *Offshore Technology Conference*, p. 11.
- Sohn, Y. K., 2000, Depositional Processes of Submarine Debris Flows in the Miocene Fan Deltas, Pohang Basin, SE Korea with Special Reference to Flow Transformation: *Journal of Sedimentary Research*, v. 70, p. 491-503.
- Sullivan, S., L. J. Wood, and P. Mann, 2004, Distribution, nature and origin of Mobile mud features offshore Trinidad: *Salt-Sediment Interactions and Hydrocarbon Prospectivity: Concepts, Applications, and Case Studies for the 21st Century*, p. 840-867.
- Sydow, J. C., J. Finneran, A. P. R. Bowman, H. H., N. C. Rosen, R. H. Fillon, and J. B. Anderson, 2003, Stacked shelf-edge reservoirs of the Columbus Basin, Trinidad, West Indies: Shelf Margin Deltas and Linked Down Slope Petroleum Systems: *Global Significance and Future Exploration Potential*, p. 411-465.
- Van Andel, T. H., 1967, The Orinoco Delta: *Journal of Sedimentary Research*, v. 37, p. 297-310.
- Wach, G., A. H. Bouma, T. Lukas, H. D. Wickens, R. K. R. Goldhammer, H. H., N. C. Rosen, R. H. Fillon, and J. B. Anderson, 2003, Transition from shelf margin delta to slope fan—outcrop examples from the Tanqua Karoo, South Africa: *Shelf Margin Deltas and Linked Down Slope Petroleum Systems: Global Significance and Future Exploration Potential*, p. 849-861.
- Warne, A. G., R. H. Meade, W. A. White, E. H. Guevara, J. Gibeaut, R. C. Smyth, A. Aslan, and T. Tremblay, 2002, Regional controls on geomorphology, hydrology, and ecosystem integrity in the Orinoco Delta, Venezuela: *Geomorphology*, v. 44, p. 273-307.
- Winker, C. D., 1996, High-resolution seismic stratigraphy of a late Pleistocene submarine fan ponded by salt-withdrawal minibasins on the Gulf of Mexico continental slope, p. 619-628.
- Winker, C. D., J. R. W. Booth, P., R. M. Slatt, J. Coleman, N. C. Rosen, H. Nelson, A. H. Bouma, M. J. Styzen, and D. T. Lawrence, 2000, Sedimentary dynamics of the salt-dominated continental slope, Gulf of Mexico: Integration of observations from the seafloor, near-surface, and deep subsurface: *Deep-Water Reservoirs of the World*, p. 1059-1086.

Wood, L. J., 2000, Chronostratigraphy and Tectonostratigraphy of the Columbus Basin, Eastern Offshore Trinidad: AAPG Bulletin, v. 84, p. 1905-1928.

Wood, L. J., S. Sullivan, and P. Mann, 2004, Influence of mobile shales in the creation of successful hydrocarbon basins: Salt-Sediment Interactions and Hydrocarbon Prospectivity: Concepts, Applications, and Case Studies for the 21st Century, p. 892-930.

## Chapter 2: Architectural Description and Geomorphology of Mass Transport Complexes in Offshore Trinidad

### 2.1. INTRODUCTION

The main objectives of this chapter are to document in detail the architecture and character of a major MTC in eastern offshore Trinidad (Figure 2.1) and to apply these observations toward an understanding and discussion of the processes active in deposits and the nature of mass-transport deposits.

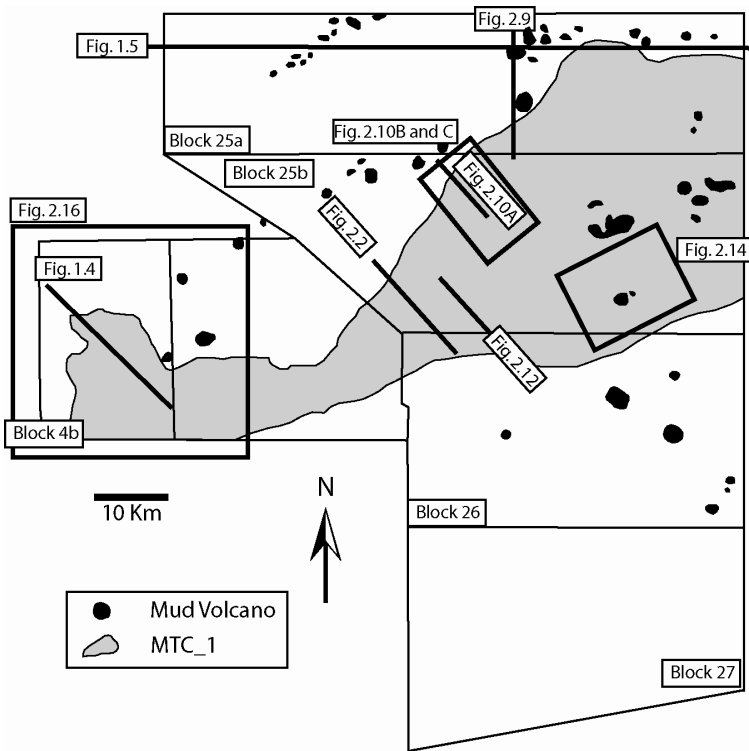


Figure 2.1: Seismic surveys in study area correspond to Block names and the locations of subsequent figures is shown. Black dashed lines define lateral boundaries of the large mass transport unit discussed in this chapter.

Brami et al. (2000) published the most comprehensive work on the deep water stratigraphy to date in the offshore area of Trinidad using 3,000 Km<sup>2</sup> of 3D seismic data (Figure 2.1 - blocks 25B and 26). The authors characterized seven depositional facies as the main architectural elements encountered in the area. These include; mass-transport

complexes (MTC), confined channel complexes (CCC), levee channel complexes (LCC), distributary channel complexes or sheet complexes (DCC), slope with minor channels, undifferentiated slope, and mud diatremes. In this chapter, we will present data from five separate 3D seismic data volumes (Figure 2.1 - blocks 25A, 25B, 26, 27 and 4B), including the survey used by Bрами et al. (2000). These data were merged into a single contiguous volume spanning approximately 10,708 Km<sup>2</sup>. This process added 7,708 Km<sup>2</sup> of high quality 3D seismic coverage to the original data set that was used by Bрами et al. (2000). These data provide an exceptional opportunity to document and study an entire mass-transport deposit from its staging area in the shelf break to its more distal ends.

Although, Bрами et al. (2000) identified mass transport complexes as important component elements of the stratigraphic sequences in the study area, provided descriptions and formulated observations on various aspects of these strata, a lack of updip data hampered some consideration of the controls and causes associated with these gravity induced deposits. Likewise, Bрами et al. (2000) being the first publication regarding the deep water processes and deposits of this area, was not specifically focused on the architecture, processes and morphology associated with MTCs. The more extensive nature of the 3D seismic data sets used in this research, allowed to better document and understand the processes that are operating in this deep water region, making special emphasis on mass-movement processes and deposits. The youngest mass transport complex identified in the area (MTC\_1) is the principal subject of study of this chapter. The exceptional quality of the data allowed to produce a detailed map of the MTC\_1 event, showing its main geomorphological elements (Figure 2.1) from the paleo-shelf break (block 4B) to the middle-slope area (block 25A). This approach provided with a comprehensive and detailed image of an entire MTC and its component elements.



MTC\_1 is equivalent to the mass-transport deposit described by Brami et al. (2000) in the stratigraphic interval P10-P20. According to these authors, the interval also contains other types of depositional complexes such as single levee channel complexes, weakly confined channel complexes, and distributary channel complexes. However, the focus of this chapter will be concentrated in the description of depositional facies and processes associated with MTC\_1 (Figure 2.1). Three key surfaces were mapped in the 3D mega merge to define the gross architecture of the continental margin fill and, to study and describe the geomorphology of MTC\_1, these three primary surfaces are: the modern seafloor, the basal surface of the uppermost MTC event, and the basal surface of the uppermost slope levee-channel complex documenting the most recent MTC–levee-channel sequence, the focus of this chapter (Figure 2.2; see location in Figure 2.1).

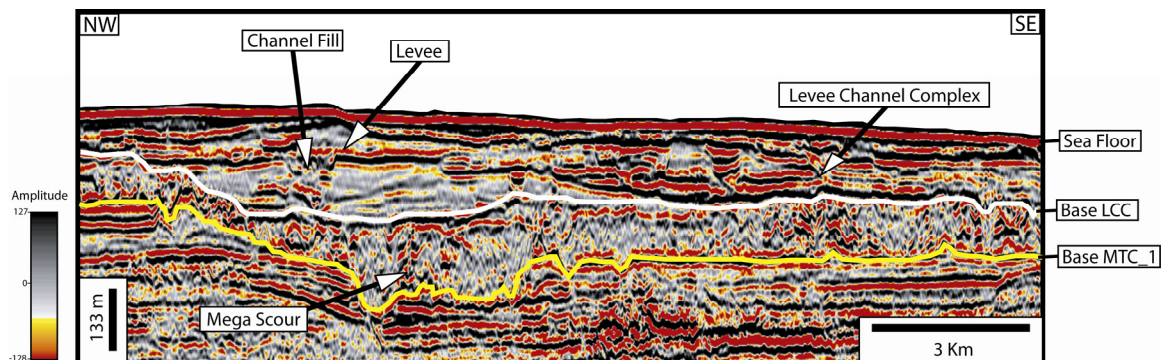


Figure 2.2: Northwest to southeast seismic line (see figure 1B for relative location) showing three main surfaces that define the shallowest depositional sequence in deep-marine area of offshore Trinidad. Base mass-transport complex (MTC\_1), base levee-channel complex (LCC) and seafloor. Note the differences in seismic character between MTC material (located between surfaces MTC\_1 and LCC) which are composed of chaotic, discontinuous, low-amplitude reflections and the overlying leveed channel complex (located between surfaces Sea Floor and Base LCC), where high-amplitude and continuous reflectors are dominant.

## 2.2. GENERAL DESCRIPTION OF THE MTC\_1

The MTC\_1 in the deep Columbus Basin covers a region of approximately 2017 Km<sup>2</sup>. However, the axial part of the complex, where deposits exceed 250 m in thickness, is restricted to an elongate central body that covers approximately 800 km<sup>2</sup> (Figures 2.3 and 2.4). The estimate volume of MTC\_1 is 242 Km<sup>3</sup>; the thickness of this unit is variable, reaching a maximum of 250 m in the core area, progressively decreasing in thickness to the east (Figure 2.5). The MTC\_1 is overlain unconformably by a thick levee-channel complex, which is in turn overlain by the modern seafloor (Figures 2.2, 2.6 and 2.7A). The thickness of the overlying levee-channel complex is greatest along the axial trace of the underlying mass-transport system, and it appears to have occupied space left underfilled by the mass-transport deposits (Figure 2.6). The levee-channel complex reaches thicknesses of approximately 150 m. For more detailed discussion of levee-channel systems in this area see Mize et al. (2004).

A buried paleocanyon trending southeast-northwest and located near the seaward projection of the Darien Ridge in the slope area (Figure 2.3) appears to be the main feeder of the MTC\_1 (Figure 2.4). The paleocanyon, located on the upper slope, is bounded along both margins by normal faults forming a structural depression that is nearly 200 m deep. The northern border of the canyon coincides with a fault escarpment that marks the boundary between the canyon on the south and a structurally higher block on the north (horst block) (Figure 2.3). The paleocanyon, less than 2 km wide on its upper section (updip), widens downslope, reaching more than 10 km on its lower end (toe of slope). Figure 1.4 shows aggradational clinoforms that represent a paleo Orinoco shelf-edge delta. The paleocanyon captures gravity induced sediment derived from this unstable delta front and funnels them as a point-source into deep-water settings.

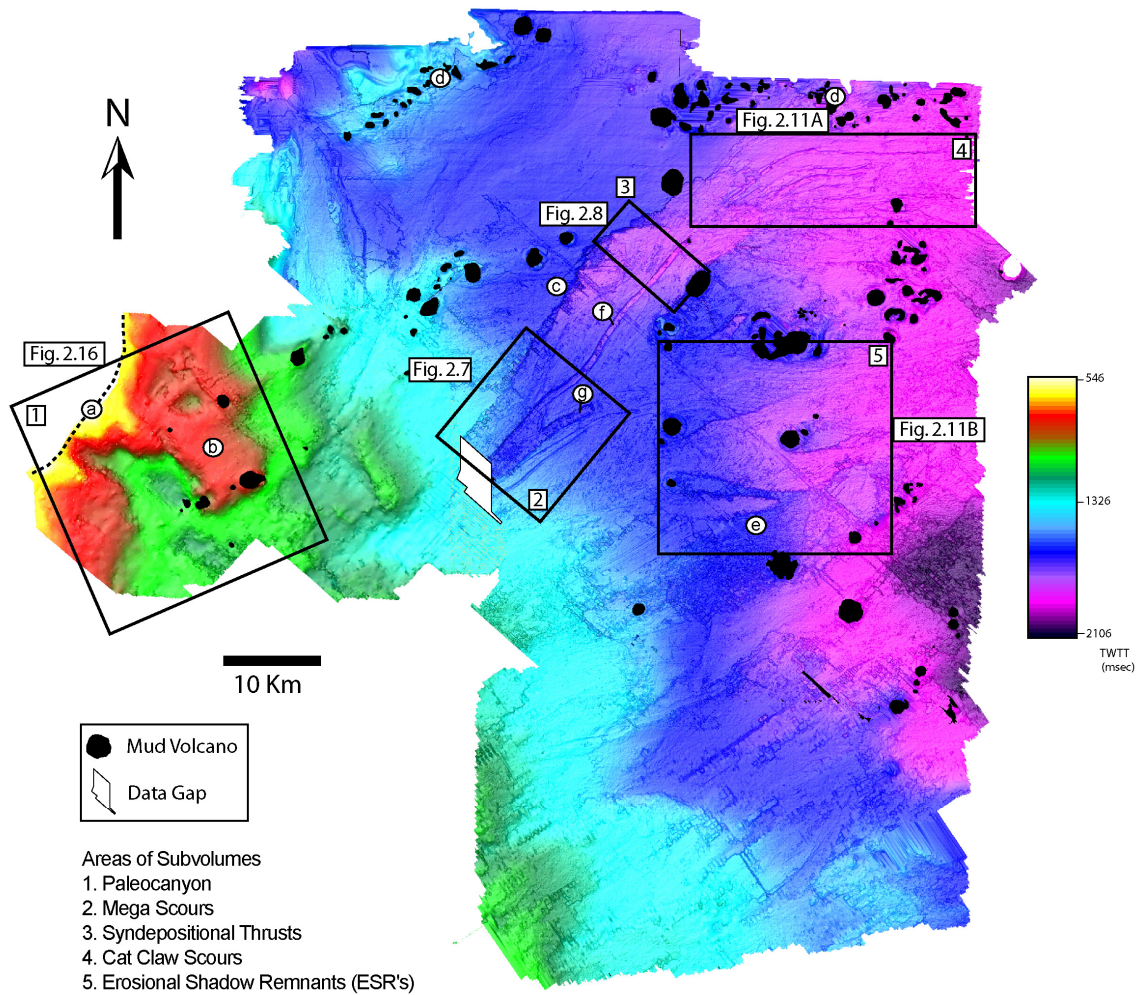


Figure 2.3: Erosional surface that shows the main geomorphological elements that characterize the base of the shallowest mass-transport complex in offshore Trinidad (MTC\_1). These elements include, incised paleocanyon (1), scours (2, 3, 4), and several erosional shadow remnants (ESR's)(5). The black squares outline individual subvolumes that have had more detailed evaluation. Additional geomorphological elements include: (a) paleo-shelf break, (b) horst block, (c) erosional edge, (d) mud volcano walls and (e) eastern boundary of MTC\_1. Colors represent depth in milliseconds with shallower depths in brighter colors and deeper depths in darker colors.

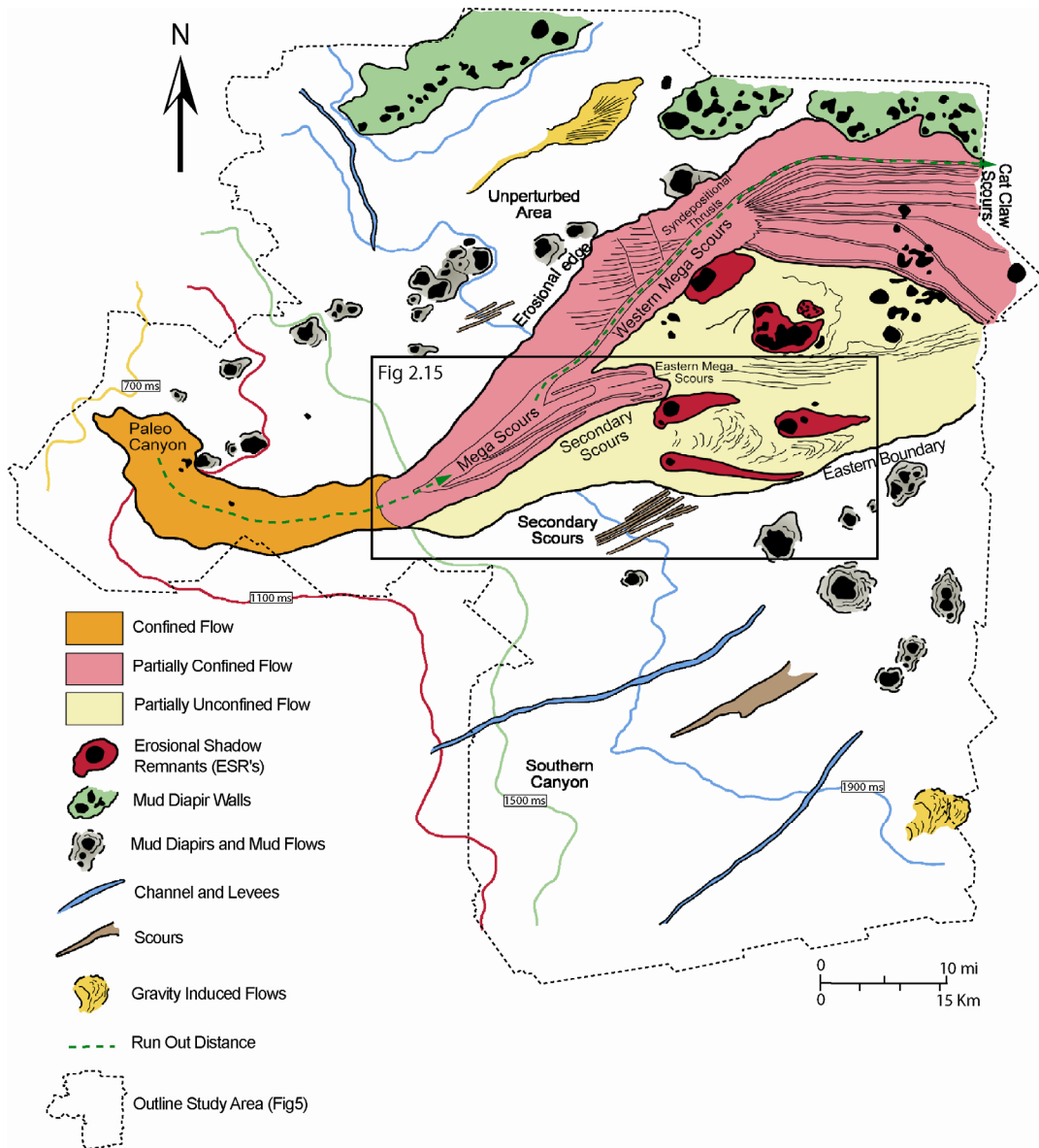


Figure 2.4: Geomorphological interpretation of the basal erosional surface of the MTC\_1. Several stratigraphic features that show significant basal incision are located in core area (scours in pink) and indicate significant scour occurring at the base of the flow. Bathymetric features confined the flow increasing the potential energy. The peripheral part of the mass-transport complex shown in yellow where the absence of deep basal incision suggests that the flow was in large part unconfined. However, the presence of significant erosional shadow remnants (ESR's) is evidence of the flows' large-scale lateral erosive energy.

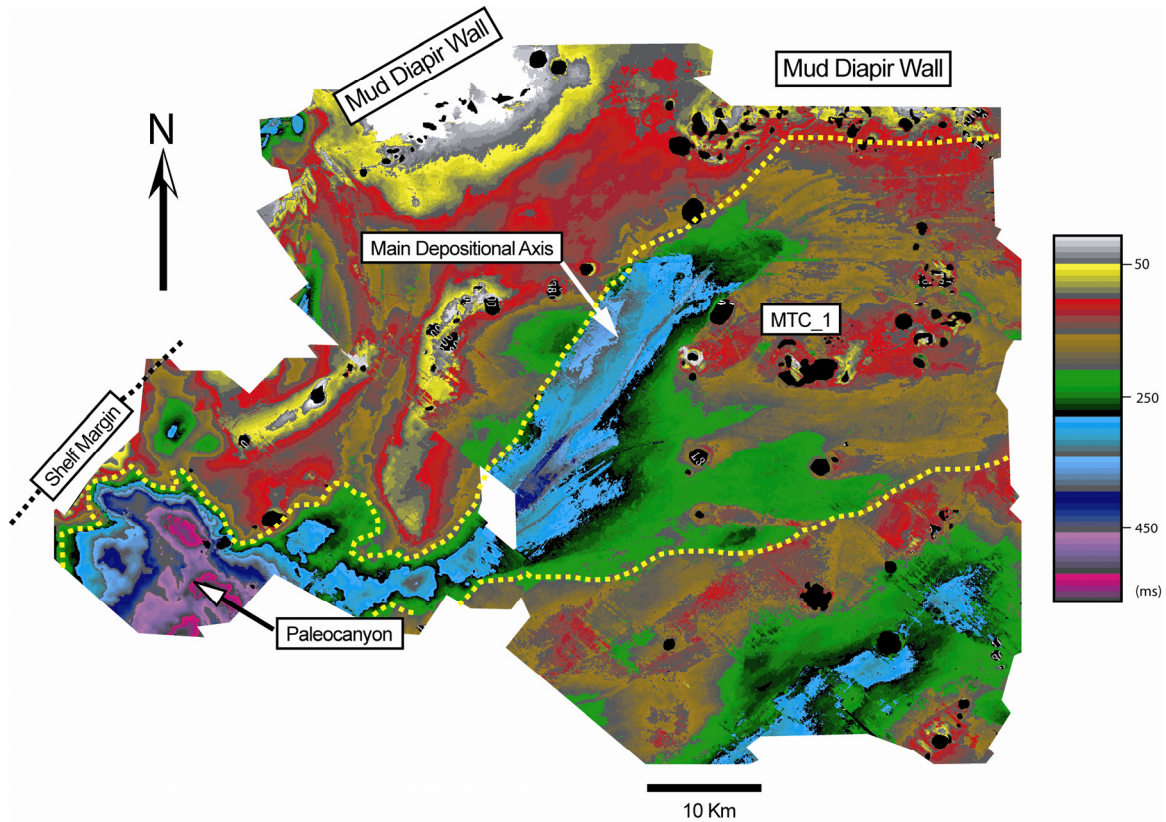


Figure 2.5. An isochron map that composites the youngest mass-transport complex (MTC\_1) and the overlying levee channel complex cycle, shows a main depositional axis defined by dark purple and blue colors, where thickness of both units reach maximum values. Along this trend, the erosive phase of mass-transport complex development created areas of maximum accommodation. The MTC material failed to completely fill the underlying scour and the subsequent levee channel complex occupied the same axial trend.. The yellow dotted line represents the lateral boundaries of the mass-transport complex. Colors represent thickness in milliseconds.

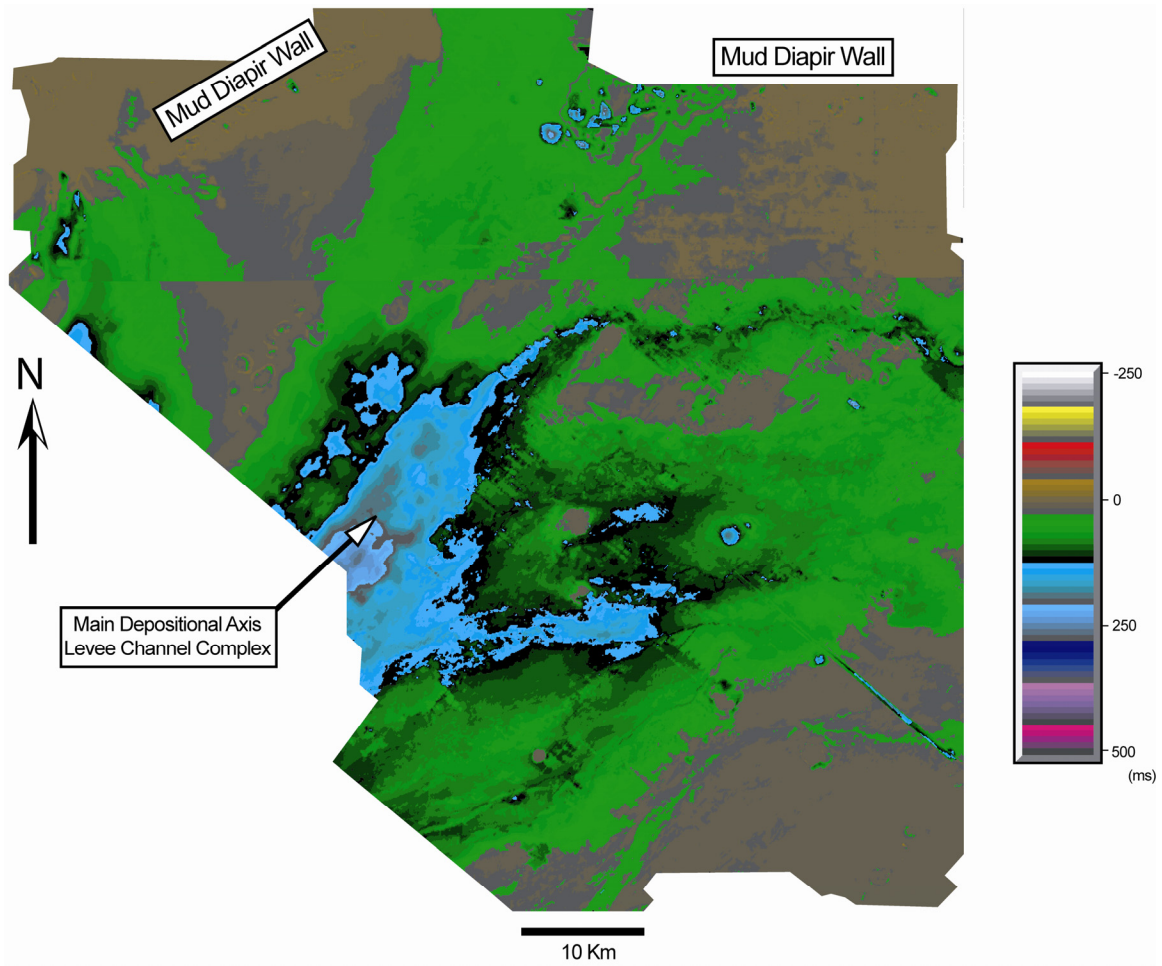
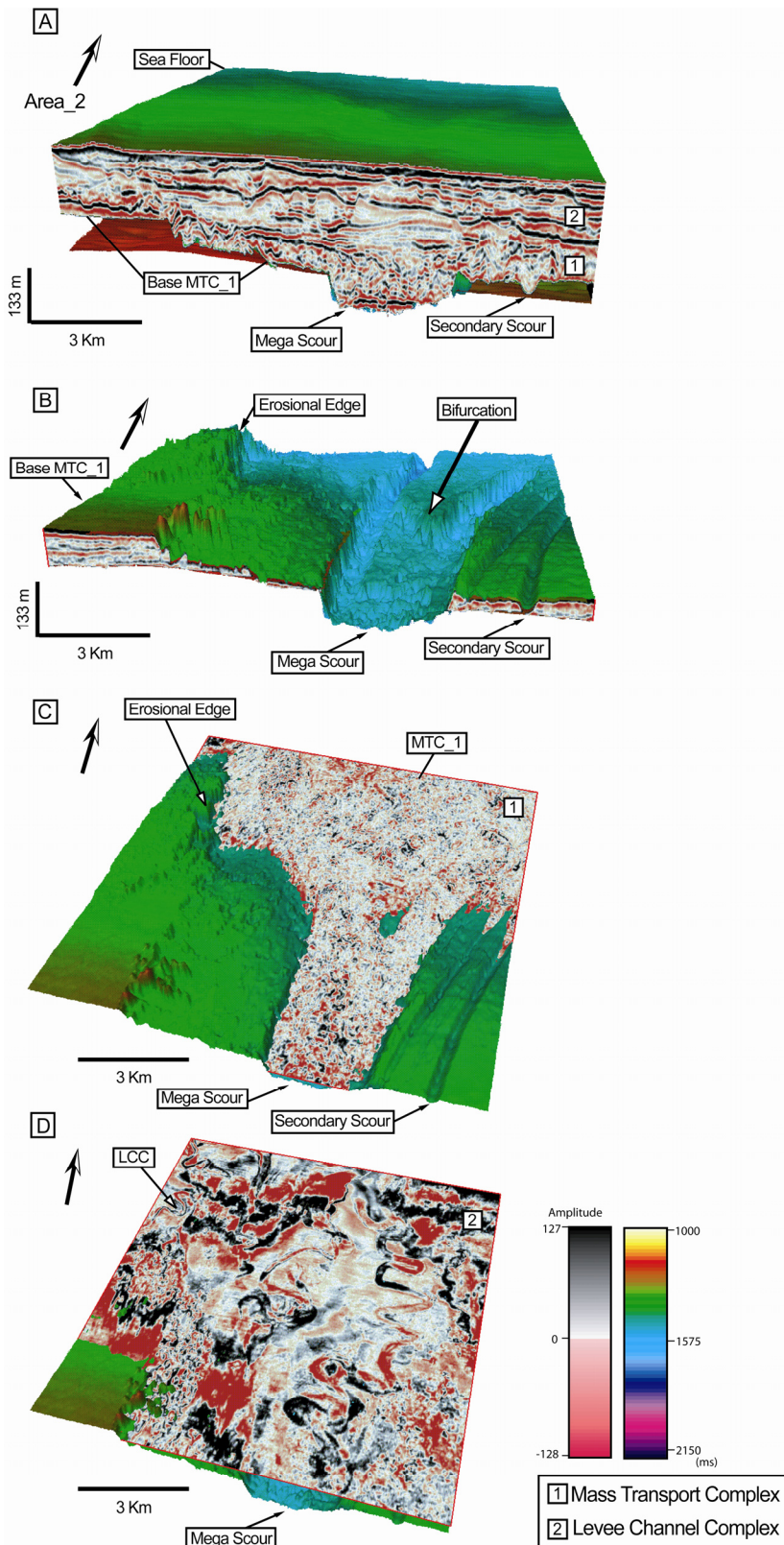


Figure 2.6: An isochron map of levee-channel complex overlying the MTC\_1 deposit shows the thickest intervals (blue colors) paralleling the main axis of the underlying mass transport complex (see Figure 2.5) in more proximal portions of the study area. Colors represent thickness in milliseconds.

Figure 2.7: A) Images of the seismic subvolume in Area 2 show an oblique view looking from the south of three stratigraphic surfaces (from base to top) including (a) erosional surface affected by overlying MTC\_1, (b) erosional surface defining base of MTC\_1 and (c) actual seafloor bathymetry. A sculpted subvolume between surfaces b and c was generated, showing two well-defined units, numbered 1 and 2 on the Figure 9A. Unit 1, interpreted as a mass-transport complex fill is composed of reflectors that are chaotic and discontinuous. Unit 2, interpreted as a levee-channel complex, is composed of reflectors that are more continuous, with channels and levees that are easily recognizable. B) Backstripped image showing several geomorphological elements in base of MTC\_1, including the erosional edge on the west, mega scours in center of image, and secondary scours on the east side. C) A time slice taken 1500 milliseconds down from the seafloor illustrates chaotic character of reflectors that represent filling of the MTC\_1. D) Time slice taken 1300 milliseconds down from the seafloor shows the abundant channels associated with the overlying levee-channel complex.





The MTC\_1 is bounded at its base by an extensive and irregular erosional surface (Figure 2.3). Internally, the MTC\_1 presents multiple geometries; in the MTC core area, basal features that resemble linear grooves or scours can be observed (Figures 2.4 and 2.7B). However, toward the east (peripheral area), the unit has a more sheetlike geometry, and grooves or incisions are absent (Figures 2.3 and 2.4). In general, the unit tends to be relatively straight and narrow, thinning gradually toward the margins. Total length distance of the deposit from the platform margin down to the east boundary of the seismic coverage (deep basin) is approximately 140 km. The total length was calculated taking into account the length of the axis of the canyon and the lengths of the western mega scour and the northernmost cat claw scour (see Figure 2.4). Near the slope, the unit is less than 20 km wide, widening progressively toward the northeast until it reaches 50 km in its distal part. The basal surface is irregular, presenting steep erosional edges that can reach 250 m in relief (Figure 2.8B) and elongated linear scours that are more than 30 m deep (Figures 2.7B). The slope of this surface changes along its extent, becoming steeper on the west where the walls of the feeder paleocanyon cut into the slope. Toward the northeast, slopes on the basal surface become subtler; however, seafloor topography and mud volcanoes frequently confine the flow, reducing its cross-sectional area and increasing its erosive power. Therefore, in some places, there is a steeper gradient on the basal surface. The upper boundary of the unit is represented by a prominent surface that defines the base of the overlying levee-channel system.

The western lateral boundary of the MTC is a significant erosional escarpment cut by the same processes that transported debris downslope. On the northwest side of this escarpment, strata are undisturbed and appear as conformable, continuous, high-amplitude reflectors (Figure 2.9). These strata were not affected by the younger MTC\_1, and appear to represent an older stratigraphic unit that was partly eroded by gravity-

induced processes that affected the central part of the study area. The east boundary of the MTC\_1 is less clear (Figures 2.3 and 2.4). It is seismically interpreted on the basis of three main observations: (1) lateral change in seismic facies character—from low-amplitude, semitransparent, chaotic reflections in the MTC unit to relatively continuous, high-amplitude reflectors in the area outside the complex; (2) an east edge defined by the change from west-east orientation to a more southwest-northeast orientation of associated flow scours and erosional shadow remnants (ESRs); and (3) geomorphologic and stratigraphic elements present in the southeast corner of the data set that are of a character and form completely different from those that are within the area of the MTC\_1 (Figure 2.4). These criteria provide compelling evidence with which to define the southern boundary of MTC\_1 and will be discussed in further detail.

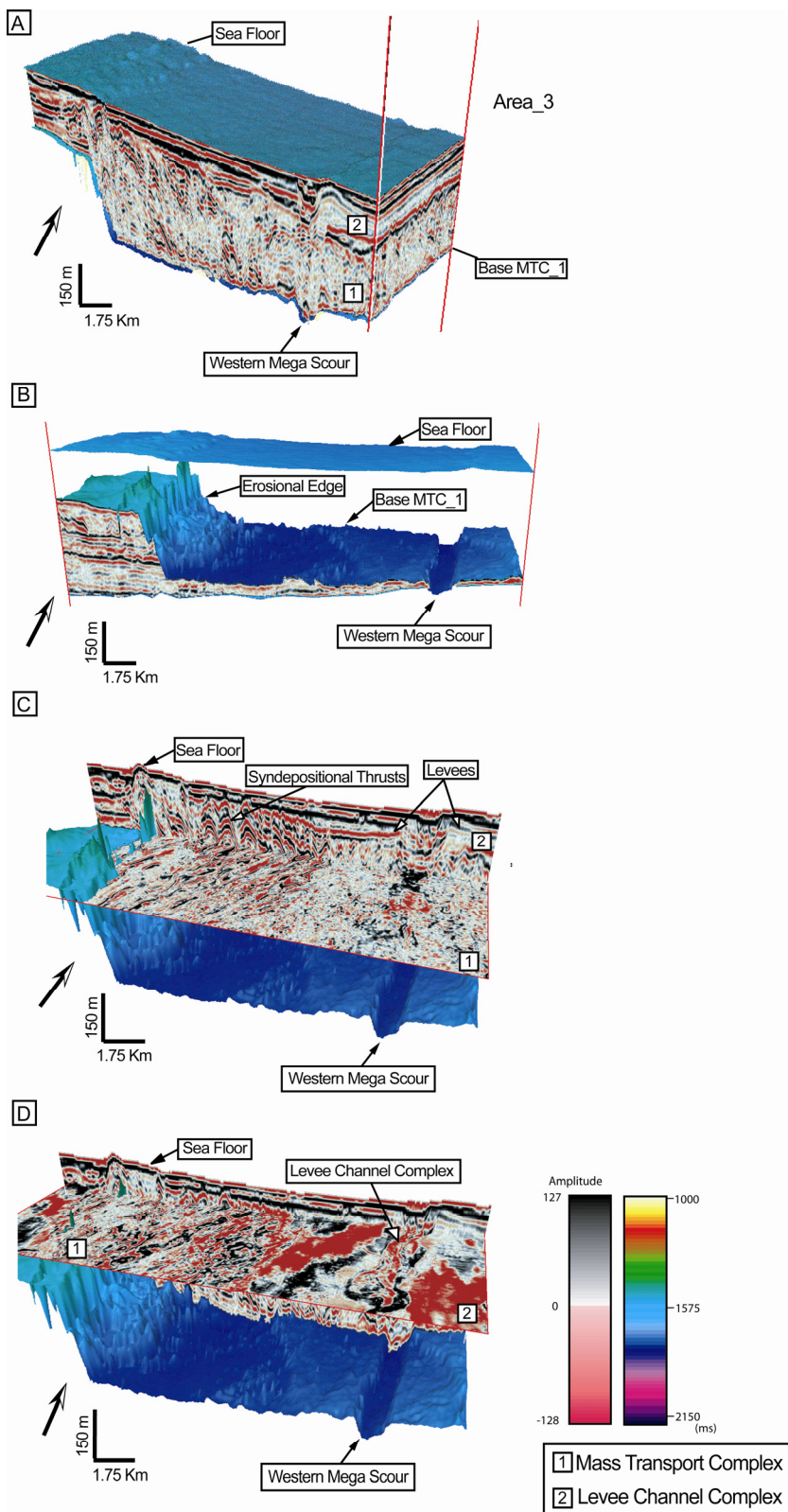
### **Seismic Facies**

Three seismic facies are distinct within the study interval of interest. Seismic facies SF1 is composed of low-amplitude, semitransparent, chaotic reflections that have been associated around the world with distinctive patterns for these MTC units (see Posamentier and Kolla, 2003) (Figure 2.10). Seismic facies SF2 is a mixture of low- and high-amplitude reflections, geometrically arranged as though deformed through compressive stresses. Seismic facies of this type are frequently folded and show multiple inverse fault planes and evidence of syndepositional deformation of the units (Figures 2.10A and 2.10B). Seismic facies SF3 is continuous, with high-amplitude reflection packages that seem to typify the overlying levee-channel system. They are also found in the undeformed unit located lateral to the MTC deposits (Figure 2.10C). These facies types were used to assist in interpreting the extent of the MTC\_1 and its lateral, upper, and lower boundaries.

## Erosional Morphologies

Several erosional morphologies exist in association with the MTC\_1 deposit and can be used to better understand the flow behaviors that characterize the deposit. These features include an erosional escarpment, deep basal scours, multiple cat-claw basal scours, erosional shadow remnants (ESR's), smaller scale scratch marks, wavy ridges, and imbricated thrust complexes (Figure 2.3 and 2.4). These features offer insight into the processes active in and behavior of these deposits during their transport and deposition.

Figure 2.8: A) Images of the seismic subvolume in Area 3 show an oblique view looking from the south. The volume is sculpted between the Base of MTC\_1 and Seafloor surfaces. The mass-transport complex and levee-channel complex units can be easily differentiated on the basis of seismic character. Erosional Edge reaches its maximum depth incision in the core area, and Syndepositional Thrusts were developed against walls of Erosional Edge. B) Backstripped image shows the area of maximum incision of the Erosional Edge and the northern continuation of Western Mega Scour. C) A time slice taken 1600 milliseconds down in the data is composited with a seismic line across the zone of Syndepositional Thrusts, showing the compressional folds generated by syndepositional deformation are aligned with northeast striking micro-thrusts shown on the time slice (strike in plan view). D) A time slice taken 1500 milliseconds down in the data, is laid over the basal MTC\_1 scour surface and composited with a seismic line showing the well defined, overlying leveed channel complex. This channel system within the levee-channel complex parallels underlying western mega scour of the MTC\_1.



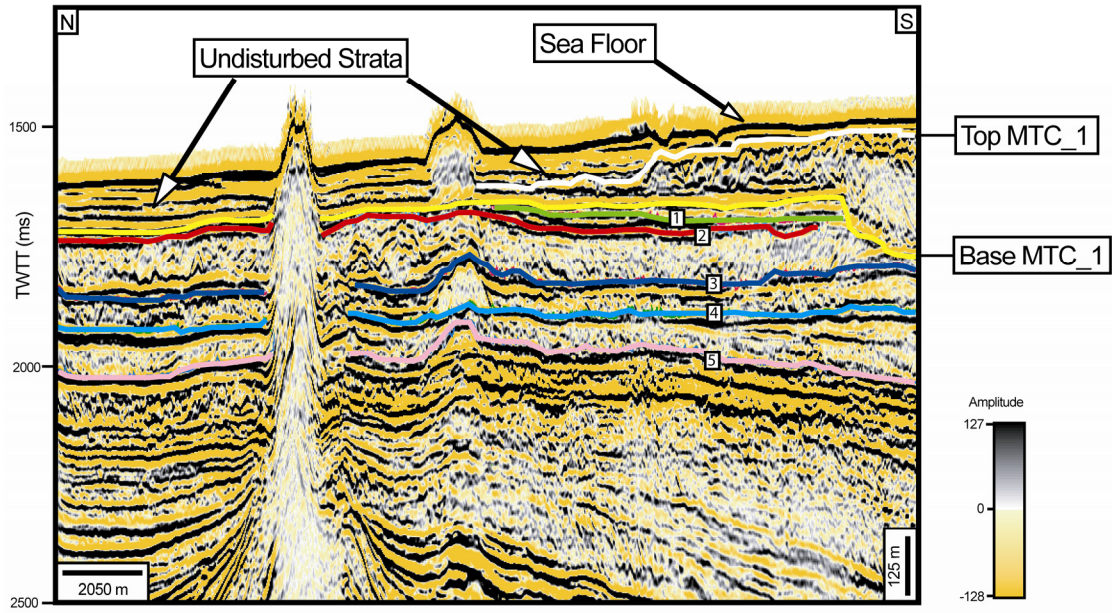


Figure 2.9: Seismic line oriented north to south across the northwest side of erosional escarpment, shows the defining west boundary of mass-transport complex (MTC). Here, the strata appear undisturbed and are characterized by conformable, continuous, high-amplitude reflectors. These strata were unaffected by the younger MTC\_1 and appear to represent an older stratigraphic unit.

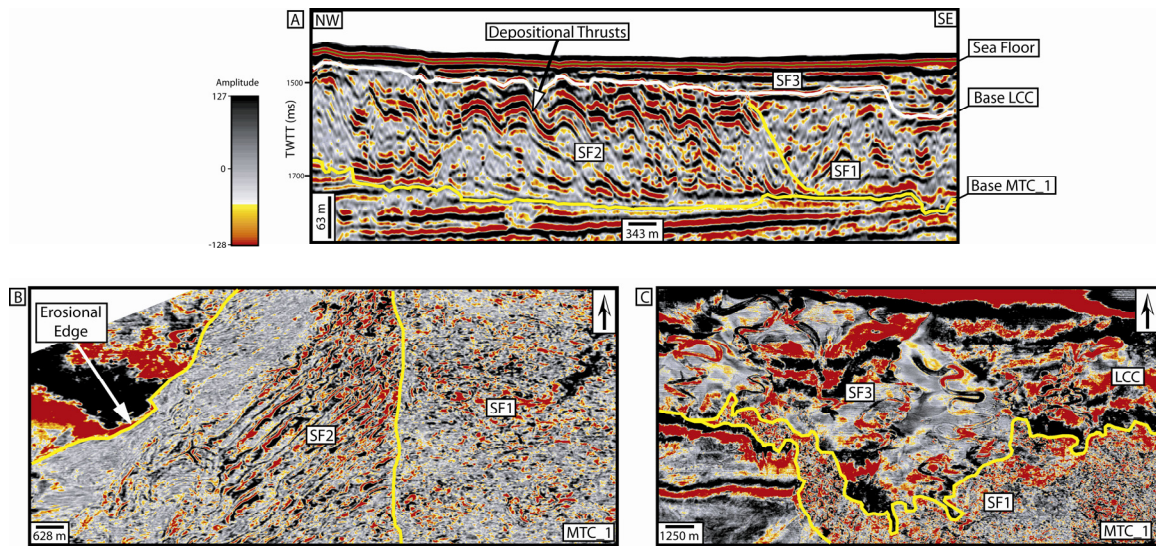


Figure 2.10: A) A seismic line shows seismic facies that have been identified within MTC\_1 and levee-channel complex, including SF1 – low-amplitude, semitransparent, chaotic reflections, SF2 – mixture of low- and high-amplitude reflections, geometrically arranged as though deformed through compressive stresses, and SF3 – high-amplitude and semicontinuous reflection packages. B) A time slice showing the morphologic character of SF1 and SF2 in plan view. On the east SF1 shows only a chaotic, non-oriented arrangement. In contrast, to the west SF2 shows northeast-southwest oriented lineaments associated with similarly striking syndepositional thrusts C) A time slice showing the character of SF3 in plan view. Channel patterns and their trajectories are an easily recognizable component of SF3. Seismic facies SF1 and SF2 are within the MTC\_1 unit.

## **Erosional Escarpment**

The western boundary of the northern feeder paleocanyon turns toward the northeast after 20 Km in the down-dip direction and transitions into an erosional escarpment that defines the western boundary of the MTC\_1 (Figure 2.3 and 2.4). This erosional escarpment, oriented northeast-southwest, is approximately 70 km long. Relief along this escarpment between the base of the MTC\_1 and the seafloor is variable but ranges between 65 m along the southernmost edge (Figure 2.7B) to 300 m along the north edge (Figure 2.8B). The depth of erosional relief within the axis of the MTC\_1 is 250 m. The erosional escarpment presents an irregular geometry in plan view (Figure 2.3 and 2.4) and can easily be mistaken for a fault until examined in vertical seismic profiles. The escarpment is especially prominent where the overlying MTC\_1 flow comes in contact with bathymetric barriers to its downslope path, such as areas of mud-volcanic uplift (Area 3 in Figure 2.3). Further downslope, the steep erosional escarpment turns eastward and gradually decreases in height more distally (Figure 2.11A). The sharp profile of the escarpment is interpreted to be a function of the shearing and plowing of the MTC sediments as they moved downslope.

## **Basal Mega-Scours**

The base of the MTC\_1 is characterized by a deep, wide, erosional scour located in the midslope region that then bifurcates downslope near the toe-of-slope region into two separate mega-scours (Figure 2.7B). The midslope scour is less than 2 km wide at its upper section (updip), but it becomes wider downdip, reaching more than 7 km at its lower end. It appears to initiate in the region around the upper-slope graben paleocanyon. Once the scour bifurcates, the two mega-scour features, here termed the western and eastern mega-scours, tend to parallel the erosional escarpment previously described

(Figures 2.7C, 2.8B and 2.11A). The western mega-scour is less than 2 km wide, but 60 km long. After about 50 km of run-out distance, it changes orientation to run nearly east-west (Figures 2.3 and 2.11A). This abrupt change in orientation is due to the presence of a mud-diapir wall that deflected the sediments eastward. The depth of the incision in the western mega-scour varies from 33 m in the south to less than 13 m in the northern region. The eastern mega-scour is also 2 km wide but only 20 km long. Its average depth of incision is 26 m. The eastern mega-scour bifurcates toward the east and ends abruptly after 20 km of run-out distance (Figures 2.3, 2.4, 2.7B and 2.11B). The bifurcation is more likely due to the splitting of a single flow than by the action of two different flows.

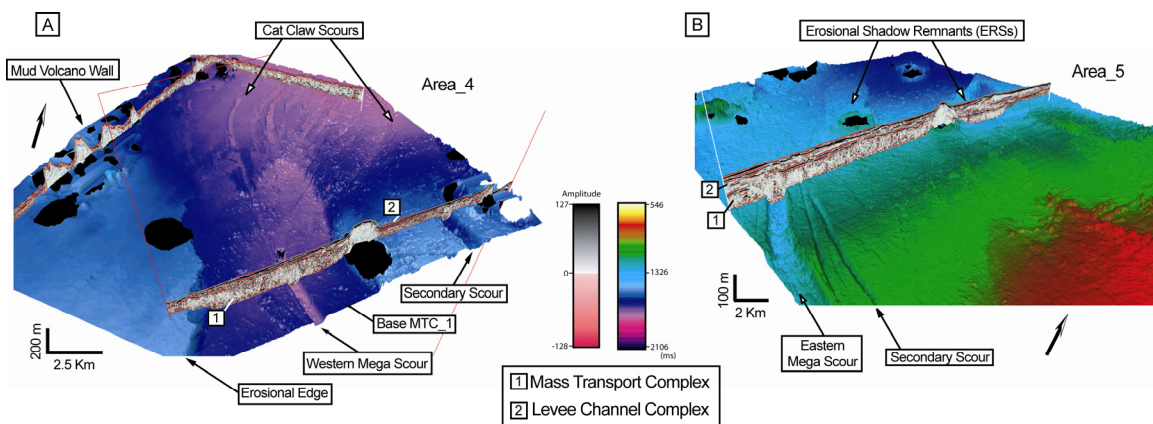


Figure 2.11: A) Images of the seismic subvolume in Area 4 show the cat-claw scours, erosional edge and western mega scour. The western mega scour bifurcates into several small and shallow erosional branches in a dispersive radiating pattern as the surfaces progresses to the northeast. To the north, a highly populated area of mud volcanoes defines a mud diapir wall that inhibited flows from breaching further to the north. B) Images of the seismic subvolume in Area 5 show the eastern mega scour and secondary scours along the basal surface. Seismic line shows the chaotic fill of the MTC\_1 deposits overlain by the more continuous reflectors of the levee-channel complex. Several mud diapiric uplifts within the area favor development of erosional shadow remnants (ESR).



### **Cat-Claw Scours**

The north end of the western mega-scour defines the apex of a series of radiating small scour features that have been termed “cat-claw scours” (Figures 2.3, 2.4 and 2.11A). Each of these features is a single, shallow, erosional scour (10 m deep or less). They are fairly consistent in appearance and, as a group, radiate from the north end of the western mega-scour (Figure 2.11A). As they impinge upon an east-west-oriented mud volcano wall, these cats-claw scours turn eastward and diverge in a radiating pattern to the east.

### **Secondary Scours and Scratches**

Several secondary scours occur across the entire area of the MTC\_1 basal surface. The most prominent of these are located next to the eastern mega-scour (Figure 2.11B). These smaller scale scours are less than 1 km wide, and their extent is variable, ranging in length from 10 to 20 km. The average depth incision on these features is less than 20 m. They parallel the eastern mega-scour, but their tracks diverge from one another as they progress eastward (Figures 2.3 and 2.4). Several additional fields of elongated “scratches” that follow the orientation of these secondary scours can be seen in the regions between the mud diapirs in the northeast part of the study area (Figures 2.3 and 2.4).

Another system of similar-sized scours is located 15 km southeast of the previous group (Figures 2.4). This group of small-scale scours is shorter and less incised than the ones that are located next to the eastern mega-scour, but they also have a distinguishable pathway that indicates transport toward the northeast (Figure 2.4). It is possible that these features are formed by an earlier and older flow traveling more northeastwardly.

The secondary scours documented here are similar in form and appearance to those defined by Nissen et al. (1999) in the Nigerian continental slope of West Africa as

glide tracks. The authors could identify out-runner blocks that most likely tooled the scours. Here we have identified localized high-amplitude reflections located immediately above the small scours that contrast with the surrounding low amplitude and chaotic character of the reflections of the remaining MTC. The high amplitude of these subunits suggests that they may be composed of more consolidated material that was rafted as blocks to their present location (Figure 2.12).

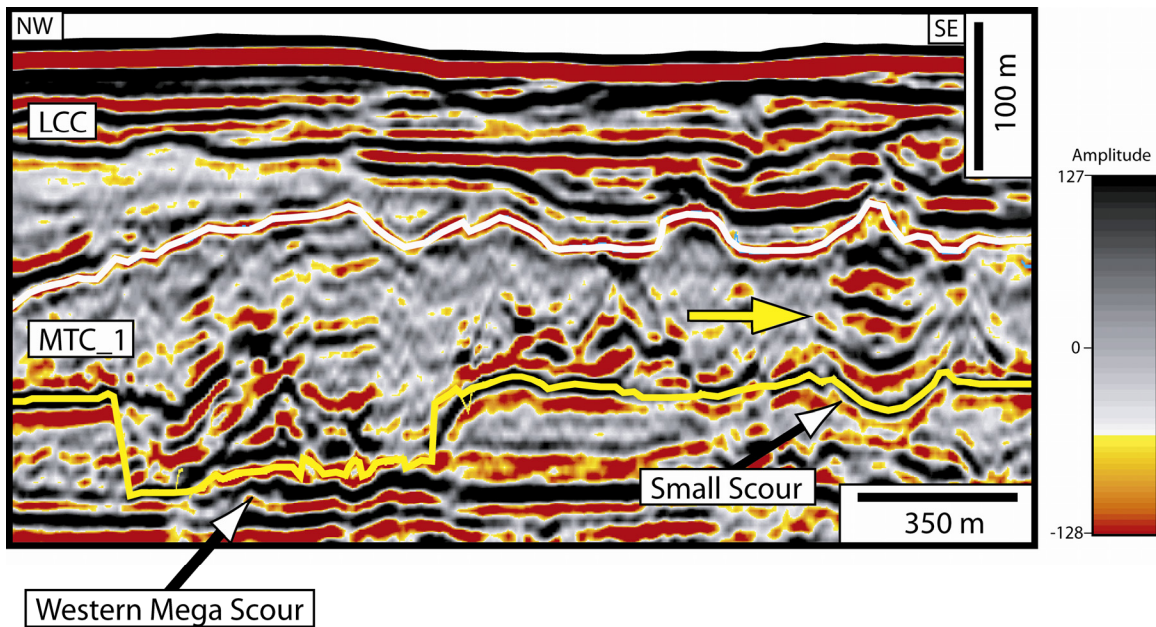


Figure 2.12: Close-up seismic line showing the bright amplitude, discontinuous, stacked reflectors within the base of the MTC\_1 deposit that are interpreted to represent more consolidated, rafted blocks above the basal incision.

### Syn depositional Thrusts

Spectacular syn depositional-thrust imbricate fields are identified in the mass-transport core area (Figures 2.8, 2.10 and 2.13). These regions of thrusting are localized and appear to be associated with areas of topographic confinement of the flow. As sediments moved downslope, topographic features acted as a barrier to the catastrophic downslope movement of the flow, compressing and compacting it in

successive events and causing the flow to ramp up over confining walls of the erosional escarpment (Figures 2.8A and 2.8C). As the flow was compressed, lack of space favored generation of a series of syndepositional imbricated thrusts (Figure 2.13).

The degree of shortening in this deposit was examined in two cross sections of the area of thrusting. Analyses show that amount of shortening varies across the imbricated area. Areas of the flow proximal to mud diapirs show shortening of around 1,530 m (Figure 2.13A). Several kilometers farther downslope, where flow appears unconfined by mud diapirs, shortening within the deposits is less, only 412 m (Figure 2.13B). When bathymetric features confine flow, thrust imbricates reflect an attempt by the flow to accommodate the decreased cross-sectional area and dissipate flow energy.

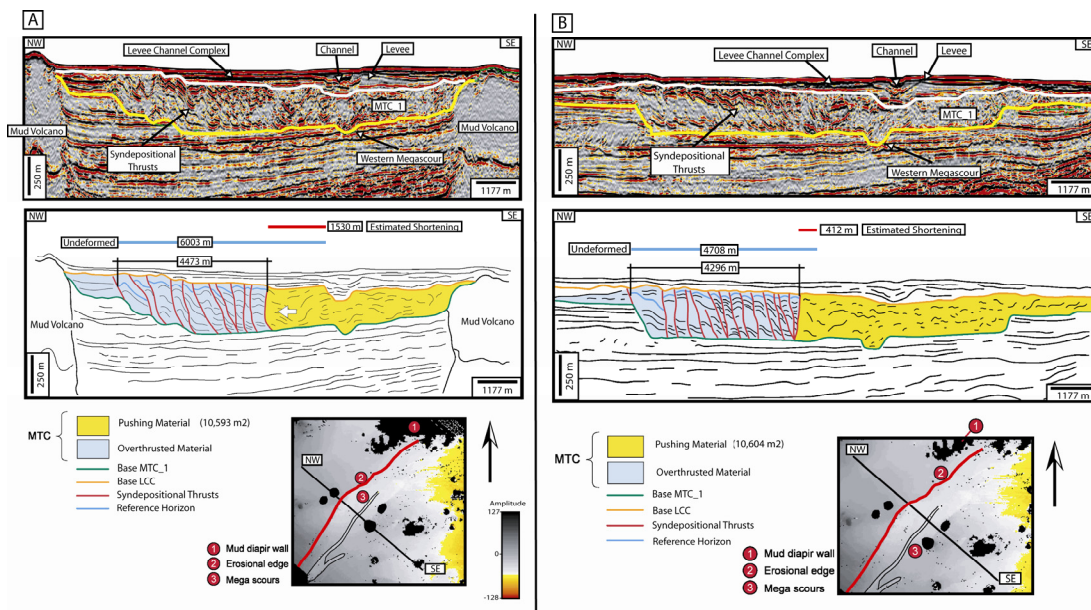


Figure 2.13: A) Seismic line cross-section, accompanying line drawing and map view of the confined regions of the mass transport deposit. In these regions where MTC flow cross-sectional area was confined by diapiric uplift shortening of the flow by thrust faulting can reach 1,530 meters. B) Seismic line cross-section, accompanying line drawing and map view of the more non-confined regions of the mass transport deposit. In these regions where MTC flow cross-sectional area was less confined by diapiric uplift shortening of the flow by thrust faulting decreases to less than 412 meters.

## **Erosional Shadow Features**

Several depositional remnants, here termed erosional shadow remnants or ESR's for their apparent association with the shadowing effect of mud volcanoes, are found preserved on the downslope side of individual mud volcanoes (Figures 2.11B and 2.14). These diapiric features acted as physiographic barriers that prevented parts of the older seafloor from being eroded by passing mass-transport flows. These preserved remnants of older seafloor have average areas of 20 km<sup>2</sup> and a maximum height of 152 m (Figures 2.14). The remnants are most likely composed of older slope or other deep-marine deposits. These remnants provide the opportunity to preserve potentially older, sandy levee-channel or sheet sand sediments trapped in accommodation moats around the mud volcanoes (see previous discussion) that would have otherwise been eroded by the voracity of passing gravity-induced flows (Figure 2.14). These remnants are then draped by low-porosity and low-permeability mass-transport deposits, creating an effective baffle or seal. The mud volcanoes, often fault-cored active fluid-migration pathways in the basin, can hydrocarbon-charge these erosional remnants, which may have reservoir volumes of greater than  $3 \times 10^6$  m<sup>3</sup>. This study is the first to document the presence of such a stratigraphic trapping mechanism in deep-water settings.

The main axes of these erosional shadow features (Figure 2.15) align in a radial pattern that converges to a specific area upslope. This point of convergence marks the location where the mass-transport sediments started to become unconfined and can be extrapolated updip.

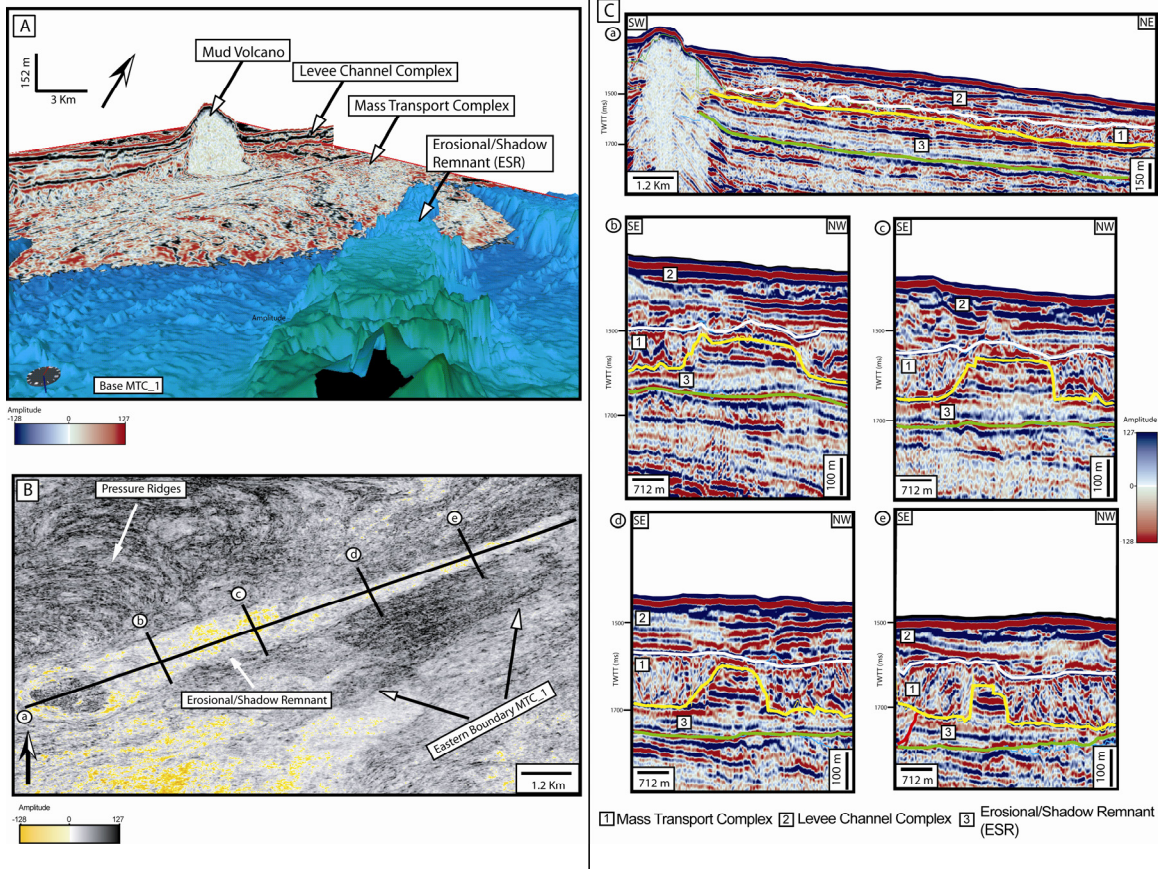


Figure 2.14: A) An image of the basal erosional surface of MTC\_1 draped with a time slice showing the chaotic nature of the mass transport fill surrounding a triangular shaped erosional shadow remnant (ESR) that tapers away from the viewer. The seismic line in the background shows the flat, continuous reflectors of the overlying leveed channel deposits and the non-reflective core of an adjacent mud diapir. B) Coherency image showing triangular-shaped plan view geometry and high amplitude character of a single ESR. The deposit tapers in the direction of flow, in this case to the east-northeast. C) Several dip and strike seismic lines across the ESR whose location is indicated in Figure 16c, show the sharp truncation along the edges. The short-length, high amplitude reflectors within the core of the ESR are interpreted to represent leveed channel deposits of an older system.

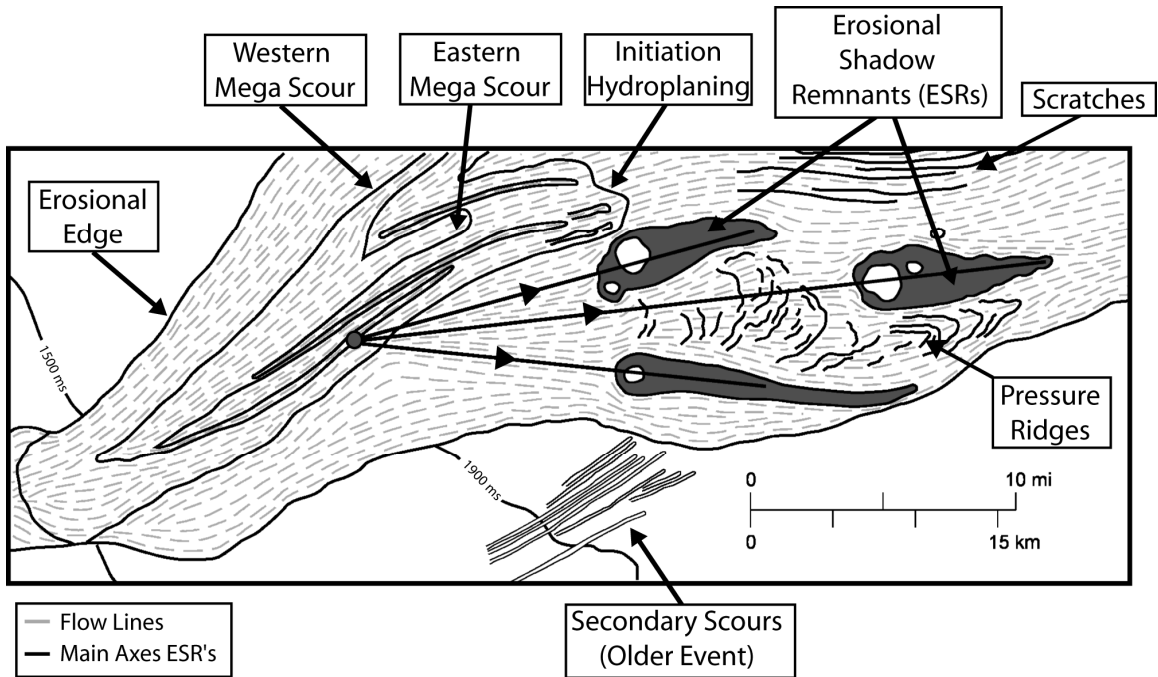


Figure 2.15: Erosional shadow remnants (ESR's) are found preserved on downslope side of individual mud volcanoes. These preserved remnants of older deposits have average areas of 20 km<sup>2</sup> and maximum heights of 152 m. Dashed lines represent interpreted flow patterns for the original trajectory of scouring MTC\_1 flow. Main axes of the erosional shadows converge to a specific area upslope (see dark heavy straight lines). This convergence point (black dot) represents the location where sediments began to become unconfined.

## **Pressure Ridges**

A field of pressure seafloor ridges occurs in the area between prominent erosional shadow features. These features were previously described by Brami et al. (2000) (Figures 2.3, 2.4 and 2.15). Pressure ridges are a relatively shallow seafloor phenomenon, and their specific occurrence is most likely associated with debris-flow confinement between seafloor mud volcanoes. The features are similar to those identified in experimental debris-flow studies of Marr et al. (2001). Similar features have also been documented by Posamentier and Kolla (2003) in the Green Canyon area of the Gulf of Mexico.

### **2.3. CHARACTER VARIABILITY OF AXIAL AND PERIPHERAL PARTS OF THE COMPLEX**

The axial part of the complex is less than 250 m thick, and it has an area of 800 km<sup>2</sup> (Figure 2.4). It covers an elongate central area, where several mega-stratigraphic architectures show significant amounts of basal incision (erosional escarpment, mega-scours, and cat-claw scours). Syndepositional structures that show considerable amounts of compressional strength are also present in the core area (Figures 2.8, 2.10 and 2.13). We assume that a certain degree of confinement on the flow that affected this area was necessary in order for the incision created by the erosional morphologies (erosional escarpment, mega-scours, and cat-claws scours) to be generated, and the compression appreciated in some internal depositional morphologies (syndepositional thrusts).

In contrast, the peripheral part of the complex is less than 100 m thick and 864 km<sup>2</sup> in extent (Figure 2.4). The unit in this area has a more sheet like geometry, and deep basal grooves or incisions are absent. The flow that affected this area was under partly unconfined conditions because it is characterized by signs of lateral or frontal erosion. The presence of erosional shadow remnants (ESR's) (Figure 2.14) is evidence of the

flow's large-scale erosive energy; however, there are neither deep basal scours nor bounding erosional escarpments in this area.

## **Basal Flow Processes**

### ***Origin of Mega-Scour Features***

McGilvery and Cook (2003) identified elongate grooves offshore Brunei that are similar to the mega-scours that we have identified in the offshore area of Trinidad. According to these authors, the features suggest some component of gouging during the transport of sediments. Posamentier and Kolla (2003) also pointed out that these types of large scour features are distinctive attributes of debris-flow deposits and commonly characterize the basal surface upon which the debris flows are deposited; they documented some features offshore eastern Borneo (Indonesia) that are similar to the mega-scours that we have described in offshore Trinidad (Figure 2.7). These authors reported divergence seaward similar to the divergence that we see when the eastern and western scours bifurcate near the lower end of the western feeder canyon (Figure 2.7B). According to their findings, the common divergence of grooves down system suggests divergent flow vectors in an unconfined setting. We agree with the idea of divergence of flow, but we think that the mega-scours were generated during a transitional state in which the flow was under partly confined conditions (Figure 2.4). Clearly, in the offshore eastern Trinidad setting of uplifted seafloor ridges and mud-volcano highs, confined flow is a typical state of many of these deposits. In our interpretation, at least some sort of confinement was probably necessary to sustain the energy needed to generate the extreme basal incision. At the same time, note that the western mega-scour is at least 60 km long. Some sort of confinement was likely necessary to preserve the effectiveness of the flow over long distances (Figures 2.3 and 2.4).



The eastern mega-scour is shorter than the western mega-scour, and it bifurcates toward the east, abruptly ending after 20 km of run-out distance (Figures 2.7B and 2.11B). This abrupt end is related either to a lack of flow competence, preventing further erosion from occurring on the basal surface, or to the initiation of flow and drag-block hydroplaning as it moved downslope (Figure 2.15). The presence of several secondary scours immediately north of the eastern mega-scour and in apparent geometrical continuation suggests that the theory of hydroplaning is the more appropriate one to explain the abrupt termination of the eastern mega-scour (Figures 2.4 and 2.15). Moreover, several additional fields of elongated “scratches” that seem to represent the northeastern continuation of the secondary scours can be seen between the mud diapirs in the northeastern part of the study area (Figures 2.4 and 2.15). We think that the north end of the eastern mega-scour defines the boundary or the transitional area where the flow started to pass from partly confined to partly unconfined conditions.

It is important to define when the flow is frictionally attached to the substrate and when it has the capacity to hydroplane because these attributes are closely related to the physical properties of debris-flow mixtures and can be used indirectly to infer their gross lithologic composition. Sohn (2000) pointed out that the style of flow transformation may change depending on clast size, viscosity of interstitial fluid, and permeability. According to the same author and the study of Miocene fan deltas in South Korea, a debris flow rich in coarse gravel clasts may become longitudinally segregated, developing a frontal concentration on a large scale. Such a debris flow is not likely to hydroplane. On the other hand, a debris flow composed of small gravel clasts and a muddy matrix may hydroplane, involving various flow-transformation processes. The predominance of fine-grained sediments in the offshore area of Trinidad and Venezuela and evidence associated with the abrupt termination of the eastern mega-scour suggest

that a significant part of the studied MTC in this area behaves like a hydroplaning debris flow composed mainly of small gravel clasts and a muddy matrix.

### ***Origin of Cat-Claw Scouring***

The north end of the western mega-scour defines the apex of a series of small radiating scour features that have been termed “cat-claw scours” (Figure 2.11A). Similar features, referred to by McGilvery and Cook (2003) as “monkey fingers” have been described in the deep-marine environments in offshore Brunei. McGilvery and Cook (2003) pointed out that these features diverge down flow and exhibit squared-off ends at their terminal extent, suggesting an origin related to basal gouging, followed by lift-off from the seafloor bottom of the gouging “tool.” These authors also suggested that the geometry and orientation of this divergence provide information regarding relative distance and direction of transport. Additionally, using side-scan sonar, Klauke et al. (2004) identified similar “finger-shaped features” in the Monterey channel-mouth lobe in the offshore area of California that they interpreted as small erosional depressions whose formation is associated with massive sand deposits.

In offshore Trinidad, the cat-claw scouring is interpreted to represent a response to an abrupt change in deposit flow conditions (Figure 2.4). At some point during formation of the gravity-induced deposit, a mixed mass of sediments and water coming from the southwest (following the partly confined pathway) encountered a mud-volcano wall located on the northeast corner of the region (Figures 2.3, 2.4 and 2.11A). This wall acted as a physiographic barrier that prevented the flow from continuing on its natural trajectory northward, effectively redirecting it to the east (Figures 2.3 and 2.4). As a consequence, the flow was locally spread out from the apex (north end of the western mega-scour) (Figure 2.11A). However, the associated flow energy remained high enough and the flow competent enough to incise and erode the substratum. This high-energy,

competent expansion of the flow's cross-sectional area resulted in the formation of radially distributed cat-claw scours and a broadening of the overlying debris-flow deposit.

### ***Origin of Syndepositional Thrusting***

Syn depositional thrusts have been described as one of the internal depositional morphologies located in the core area of the axial part of the unit (Figure 2.4). The maximum incision here is 250 m (Figure 2.8B); the area is constrained by irregularities of the erosional escarpment and several mud diapirs. Marr et al. (2001) were able to document the presence of imbricate slices in laboratory gravity transport experiments. In these experiments, geometry associated with previously detached bodies of static sediment allowed the flow to ramp up over these bodies, creating different slides that are in contact with sharp surfaces. Shanmugam et al. (1988) also documented similar, but much smaller scale duplexlike features in an outcrop of the Jackfork Formation (Lower Pennsylvanian) of the Ouachita Mountains in Arkansas. They described soft deformation features associated with the Ouachita flysch succession exposed at the DeGray Dam Spillway in the Upper Jackfork Formation. This unit was deposited in a deep-water, submarine-fan complex and is composed of pebbly and massive sandstones, with beds showing upward-thinning trends (Morris, 1971; Muiola and Shanmugam, 1984). Deformation of unlithified turbidites into duplex like structures in the succession has been attributed to the action of high-energy sediment gravity flows. Similar duplex features were described in the Jurassic-lower Tertiary pelagic carbonates in the Umbria-Marches Apennines of northern Italy, where synsedimentary submarine slide deposits are common (Alvarez et al., 1984). McGilvery and Cook (2003) also described contractional imbricate toe thrusts in the distal part of a cohesive slump complex in a stepped slope profile offshore Brunei. Posamentier and Kolla (2003) mentioned the presence of

pressure ridges indicative of thrust faults commonly present near the boundaries of debris flows; they documented these features in the Green Canyon area of the Gulf of Mexico. Nissen et al. (1999) also studied pressure ridges in the continental Nigerian slope in Africa, defining them as regularly spaced undulations caused by compression within the main body of the debris flow. For the syndepositional thrusts that we documented, the process was not related directly to slumps or to the terminal part of the debris flow; imbrications were generated when the material contained within the partly confined flow area encountered lateral barriers (irregularities in the geometry of the erosional escarpment and individual mud diapirs) (Figure 2.4) that caused them to overthrust owing to a lack of space for accommodation. These syndepositional thrusts are very similar to the compressional features described as ridge-like structures in slump complexes from the continental margin of Israel (Martinez et al., 2005). This process was generated while sediments were still unconsolidated and sedimentation was still actively moving downslope.

#### **2.4. INTERPRETED CAUSES AND CONTROLS FOR MTC GENERATION**

Mass transport complexes can be generated as the result of a series of processes, most of them associated with slope failures. Gravitational instabilities in the upper slope can be triggered by a variety of factors, including high sedimentation rates, gas hydrate dissolution, sea-level fluctuations, storms and/or tectonic activity. Brami et al. (2000) have compared the apparently cyclic repetition of seismic facies (Figure 1.5) in the studied area as similar to those observed in the passive margins of the Gulf of Mexico and offshore Brazil (Amazon Fan). They interpreted this “apparent cyclicity” as primarily driven by Pleistocene high frequency sea level changes. However, the complexity of the geology in the area (close proximity to an active tectonic margin and the high

sedimentation rates associated with the Orinoco Delta System) suggests, in our opinion, a higher frequency mechanism at work than sea-level fluctuations alone.

It is difficult to pinpoint individual causes for each MTC event in the complex geologic environment of the study area, since several mechanisms could be acting at the same time and overlapping their signatures. However, data covering the paleoshelf break and slope areas (Figure 2.1 - block 4B) reveal interesting clues regarding the origin of these MTC deposits. Figure 2.16A shows a time slice at 492 msec in the shelf edge and upper slope regions where the southeast-northwest trending paleocanyon that is the main feeder of MTC\_1 can be found. Figure 2.16B shows a deeper flattened horizontal coherence-slice at 1126 msec taken over the same area but stratigraphically located below the erosional surface that defines the base of MTC\_1 (see Figure 1.4 for reference). This deeper coherency image shows the updip portions of an older MTC (MTC\_2) failure event. In this deeper interval (Figure 2.16B), several geomorphological features are revealing the presence of gravitational collapses that are located in the upper slope area near the paleo-shelf edge (Figure 2.16B). At least three major collapses can be seen updip. Two of these collapses are located on the north-western corner of the area presenting a distinctive semi-circular shape (“cookie bite shape”) with average diameters of 4.5 Km. The average length of the perimeter around individual heads of the collapses is 6 Km and both “cookie bite” features cover an approximate area of 28 Km<sup>2</sup> in the upper slope (Figure 2.16B). These collapses have a concave upward appearance and they are cutting the upslope strata. This area represents the depletion zone of the older MTC\_2. In addition, abundant gullies that are perpendicular to the collapse can be observed through the margin and multiple minor headscarps are interpreted (Figure 2.16B). It is quite apparent from the geomorphological evidence that the formation mechanisms of these two MTC events were different. As previously noted, the sourcing

mechanism for MTC\_1 does not appear to be failure of the upper slope, but rather a direct point source from shelf-edge deltas. The distinct differences in the origin of two similarly massive shelf and slope failures, so close in geologic time suggest a variety of mechanism destabilizing the continental margin in this region. In the following sections, further discussion is provided regarding the issue of possible causes generating these mass failure phenomena in this region of the world.

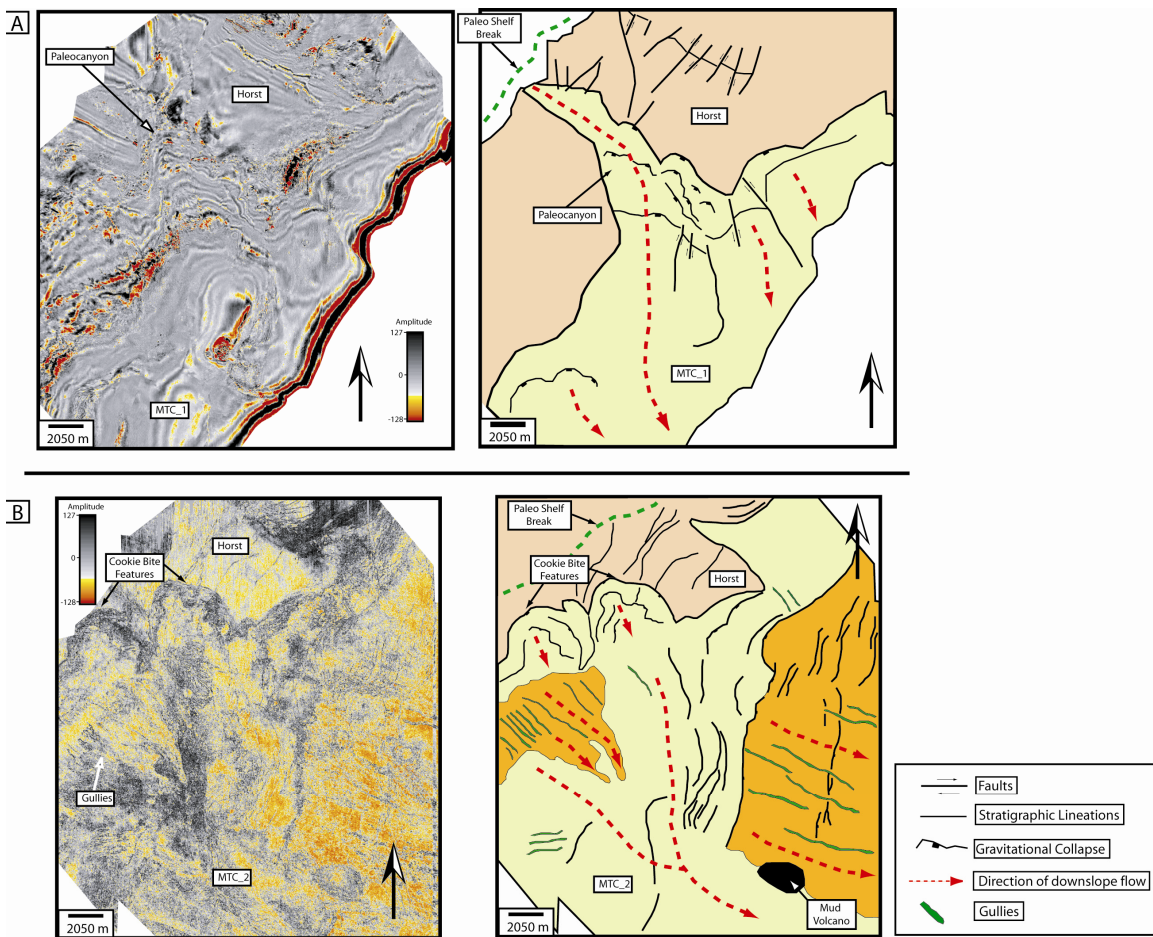


Figure 2.16: A) Seismic amplitude time slice taken 492 milliseconds down in the data and an accompanying seismic geomorphologic interpretation show the continental shelf edge and upper slope regions (block 4B) where the southeast-northwest trending paleocanyon that is the main feeder of MTC\_1 is located. B) Seismic coherence time slice and taken over the same exact area as Figure 18A 1126 milliseconds down in a volume flattened from the modern seafloor. This images the older shelf edge and shows significantly large “cookie bite” failures associated with older mass slumping events along the margin.

## **Sea Level Fluctuations, High Sedimentation Rates and MTC's**

Establishing recognition criteria to differentiate causal mechanisms of MTCs is a crucial step to better understand these deposits. In this work two causal mechanisms have been identified: (1) gravity-induced deposits that are generated by variations in relative sea level fluctuations and high sedimentation rates (MTC\_1) and (2) catastrophic failures of upper slope sediments due to gas hydrate disruption and/or earthquakes (MTC\_2). These differentiations have a huge impact in reservoir characterization issues and risk assessment for coastal communities.

Sydow et al. (2003) suggested the most recent shelf-edge event to have occurred at the last glacial lowstand, approximately 18,000 yr BP. At that time, sea level was thought to be nearly 100 m lower than at present. Such a drop would have exposed the present-day Columbus Basin shelf and brought the shoreline to approximately the location of the present-day shelf slope break (Carr-Brown, 1972 and Sydow, et al., 2003). Butenko and Barbot (1980), conducting a geotechnical study in the shelf break and upper slope of the Orinoco Delta system, identified a major buried erosional surface with paleochannel development, which they interpreted to have formed during a sea-level drop at the end of the Pleistocene. The same authors identified a large area of irregular seafloor topography in the continental margin, an active area of rotational slumping where northwest-southeast-trending seafloor scarps with a maximum throw of 45 m were reported. Sydow et al. (2003) presented four northeast-southwest seismic lines located in the outer shelf and upper slope areas of the Columbus Basin. One of these lines (seismic line D – see relative location on Figure 2.1A) is adjacent to the southwestern corner of block 4B, where the paleocanyon of MTC\_1 is identified. The northeastern portion of seismic line D clearly shows sigmoid clinofolds that are interpreted by the authors to be



composed of unstable delta front facies. Based on available well data, the authors identified this unit as the 18,000 yr shelf-edge delta; debris flows and slump deposits have been identified as the dominant constituents of these facies (Sydow et al., 2003).

MTC\_1 appears to have been point-source fed by a single paleocanyon (Figures 1.4, 2.3 and 2.4) that have captured sediments directly from aggradational clinofoms. Figure 1.4, a northwest-to-southeast, depositional dip-oriented seismic line across the main axis of the paleocanyon located proximal to MTC\_1 shows a series of aggradational clinofoms that are prograding to the southeast. These prograding clinofoms are located in the updip portions of the paleocanyon confirming the connection between the shelf-edge systems and the upper slope area. The paleocanyon geometry and orientation is structurally controlled by faults associated with transtensional plate margin structural forces. The underlying structural graben generates sea floor irregularities, indicating ongoing transtensional deformation that defines a preferential northwest-southeast sedimentary pathway. The aggradational clinofoms located in the upper portions of the paleocanyon are interpreted as a paleo Orinoco shelf-edge delta whose delta front facies were increasingly unstable, affected by gravitational tectonics and slumping. The aggradational character of the clinofoms (Figure 1.4) is interpreted to reflect the response of the shelf-edge delta to a rising shoreline following lowstand conditions. This increasing accommodation prompted the accumulation of sediments in the unstable shelf-break, oversteepening of the clinofoms and eventually gravitational collapses that fed the downslope systems.

Stratigraphic relationships inferred from the seismic lines published by Sydow et al. (2003) indicated that the clinofom unit associated with the 18,000 yr shelf-edge delta (Low Stand System Tract) may be slightly younger than the aggradational clinofom unit described in this work. Notice that clinofoms reported by Sydow et al. (2003) are

prograding towards the northeast and the aggradational clinoforms reported in this work, and associated with the MTC\_1 event are prograding towards the southeast, indicating a different origin. Moreover, the aggradational character of the clinoforms associated with MTC\_1 and their relative stratigraphic position and orientation suggests that this unit was generated during times of prevalent still-stand conditions or during the early stages of relative sea level rise. This interpretation of deposition of MTC\_1 during late lowstand and early transgression is a different interpretation from that presented by Brami et al. (2000). Although the previous authors believed the MTC\_1 deposits to have been deposited during maximum shoreline lowstand, we are placing the timing of the genesis of the unit in the rising limb of a cycle. The high sedimentation rates associated with the paleo Orinoco Delta System are believed to be a key factor for the formation of the shelf-edge delta that fed MTC\_1. Although frozen gas hydrates have been reported as a causal mechanism for other slope failures around the world, it is believed that the staging area for the MTC\_1 was in too shallow a water to generate or destabilize hydrates.

### **Tectonism, Gas Hydrates, Free Gas and MTC's**

Figure 2.16B presents a complete different scenario for deep marine debris flow development than that documented for the younger MTC\_1 deposits (Figure 2.16A). The kilometer-diameter scale “cookie-bite collapses” can be found in several locations along the margin. This geomorphology provides a more line-source, upper slope source of material for MTC\_2 deposit. Although not described in this chapter in detail (see chapter 3 for detail descriptions of MTC\_2), the MTC\_2 deposits appear to be generated by failures in numerous locations. Such broadly distributed, isolated pods of source material imply a broadly active process for slope failure. Although a relative drop in sea level might destabilize hydrates, it is still unlikely that significant amounts of hydrate occur in

the upper slope where the “cookie-bite” scars are found. A second destabilizing process may have been large storms or tropical depressions and hurricanes.

A more likely scenario is that a tectonic event, such a major earthquake, caused the destabilization of a broad area of the upper slope and subsequent failure. In contrast to the point-source, clinoform fed deposits of MTC\_1, the materials that failed and comprise the MTC\_2 deposits would be mainly composed by shaly slope sediments. Martinez et al. (2005), documented similar tectonically driven collapse features in the continental margin of Israel, the authors pointed out that the high occurrence of slumping processes in this area was possible because a combination of seismic activity, presence of free gas within the sediments and slope oversteepening. All these influences are present in the Trinidad offshore. In the study area, significant and frequent earthquakes occur due to the interaction between the Caribbean and South America plates, abundant free gas associated with the inner and outer shelf regions, slope oversteepening associated with shelf-edge deltas and the presence of abundant gas hydrates.

Submarine landslides triggered by earthquakes have also been documented in the upper slope area of the eastern Aleutian Islands (south coast of Alaska) caused by a significant earthquake in 1946, (Fryer et al., 2004), and by a 1929 earthquake which triggered a landslide and subsequent 30 m high tsunami in the Grand Bank area in the offshore area of Newfoundland (Canada) (Nisbet et al., 1998 and Dawson et al., 2004). We believe that the mechanisms that triggered MTC\_2 in the offshore area of Trinidad are similar to those that generated these submarine landslides in Alaska (1946) and in offshore Newfoundland (1929).

## **2.5. MASS-TRANSPORT COMPLEX RESERVOIR ELEMENTS**

Few authors have reported quantitative information on the lithology, petrophysics, and general character of mass-transport deposits in the subsurface. The ability for mass-

transport deposits to act as subsurface fluid reservoirs or barriers is at present a poorly understood phenomenon. Shanmugam et al. (1995) noted that plastic flows, believed to characterize some debris flows, generate laterally discontinuous and disconnected sand bodies that are harder to predict in terms of their spatial distribution and geometries. In contrast, turbidity currents produce some high-reservoir-quality deposits that are laterally continuous making them more attractive exploration and development targets. This difference in the nature of sediments deposited from plastic flows (debris flows) versus turbidity currents (turbidites) makes it all the more important to distinguish between these two processes active in continental margins. Such ability will enable accurate prediction of reservoir geometries and aid in defining reservoir uncertainty and quality.

Mass-transport deposits may constitute a critical factor in modeling fluid flow because they have been reported to have poor porosity and permeability values with respect to turbidite sands (Pirmez et al., 2004; Shipp et al., 2004). In contrast, some research (Shanmugam et al., 1995; Shanmugam 2000) has shown that slumps and debris flows can contain thick, amalgamated sands bodies with high porosity (27 to 32%) and permeability (900 to 4,000 md) values. The Frigg Formation in the North Sea has been pointed out as one of such units. Similarly, Jennette et al. (1999) interpreted four different sequences in the evolution of the Tay and Forties/Sele basin floor fans in the central part of the North Sea, with the sandstone bodies of the upper sequences being interpreted as sandy debris flows. Based on well data, Jennette et al. (1999) recognized that these phases of debris flows fan building leads to high quality reservoir sandstones that have strongly mounded cross-sectional geometries. However, limited lateral continuity of these deposits and the ability to predict their occurrence may still be major issues to overcome before the deposits are viable reservoir targets (Shanmugam et al., 1995; Shanmugam, 2000; Jennette et al., 1999).

Finally, although the deposits themselves may not prove viable reservoirs, many of the erosive processes and subsequent stratigraphic relationships surrounding debris flow development provide the opportunity to create stratigraphic trapping opportunities. It is shown in this research and reviewed in other studies (Shipp et al., 2004), that MTC\_1 is a Pleistocene fine-grained, low porosity and low permeability gravity induced deposit that does not appear to have any reservoir potential. However, the recognition of erosional shadow remnants (ESR's) (Figure 2.14) associated with mud volcanos, has raised the relevance of processes associated with MTC\_1 for forming stratigraphic traps in deep water margins. Erosional shadow remnants (ESR's), formed by lateral erosion of passing debris flows can be quite large and comprise older turbidites and gravity deposits. They are common in the study area (see previous sections).

## **2.6. CONCLUSIONS**

Enormous MTC's characterize the margin of northeastern South America. Such mass-transport processes and deposits are prevalent in margins around the world. It is clear from the evidence presented here that laminar and turbulent flow can occur simultaneously within these gravity deposits, producing a variety of sedimentary structures. Likewise, a flow can transition as it moves downslope from laminar to turbulent and from confined to unconfined through its interaction with the substrate and surrounding seafloor bathymetry.

The primary mass transport deposit, MTC\_1 is characterized by active slump processes in the upper slope area, enormous scour at its base, and cannibalization of the underlying seafloor and older, deep-marine deposits. Basal scours as much as 2 km wide and 30 m deep attest to the erosive power of the flow. However, the distinct changes in basal-scour types (e.g., mega-scours to cat-claw radial scours) can be used as evidence of flow transition from confined to unconfined. Sharp termination of scour marks can occur

with the transition from non-hydroplaning to hydroplaning flow and the “plucking” of scour tools from the basal surface of the flow.

Large stratigraphic traps, termed here erosional shadow remnants (ESR's) are formed in this setting by the erosive power of the debris flows. In this setting, older, possibly sand-rich levee-channel deposits are preserved on the downslope side of diapirs. These strata are then blanketed by low-permeability and low-porosity deposits of the overlying debris flow. Direct contact of these strata with hydrocarbon migration pathways provided by the mud volcanoes themselves produces a low-uncertainty scenario and high-probability success for traps of this type.

Consistency of mass-transport development processes in this offshore region suggests a higher frequency mechanism at work than sea-level fluctuations alone. High sedimentation rates, gas-hydrate dissolution, high-frequency sea-level fluctuations, and a high occurrence of earthquakes have been identified as the main factors that have generated instabilities in the outer shelf and upper slope area. They have caused episodic gravitational collapses of huge amounts of sediments that have been funneled toward deep-marine environments. As a result, multiple stacked MTC's have been generated, and these units can cover as much as 2017 km<sup>2</sup> in area, reach more than 250 m in thickness, and include several internal subunits, such as rotational slumps in the upper slope area, syndepositional thrust in the downslope confined areas, and hydroplaning debris flows in the distal complex.

Little agreement exists in the geologic community regarding the recognition criteria to differentiate between and the terminology to describe debris flows and turbidites (Shanmugam et al., 1995; Hiscott et al., 1997 and Shanmugam 2000). This lack of agreement has a relevant impact in deep-water reservoir characterization because many deposits originally identified as turbidites have been re-named debris flows

(Shanmugam et al., 1995; Shanmugam 2000) and viceversa (Hiscott et al., 1997). This creates a lack of continuity in the research of these types of phenomena. It is only through additional characterization studies such as the one presented herein that the pertinent observations will be made to resolve many of the disagreements regarding the processes that dominate these complex deposits and the role that they play in the development and fill of continental margin basins.

## 2.7. REFERENCES

- Alvarez, W., A. Montanari, R. Colacicchi, and Anonymous, 1984, Synsedimentary slides and bedding formation in Apennine pelagic limestones: Abstracts with Programs - Geological Society of America, v. 16, p. 429.
- Brami, T. R., C. Pirmez, C. Archie, K. W. Holman, P., R. M. Slatt, J. Coleman, N. C. Rosen, H. Nelson, A. H. Bouma, M. J. Styzen, and D. T. Lawrence, 2000, Late Pleistocene deep-water stratigraphy and depositional processes, offshore Trinidad and Tobago: Deep-Water Reservoirs of the World, p. 104-115.
- Butenko, J., and J. P. Barbot, 1980, Geologic hazards related to offshore drilling and construction in the Orinoco River delta of Venezuela: JPT. Journal of Petroleum Technology, v. 32, p. 764-770.
- Carr-Brown, B., 1972, The Holocene/Pleistocene contact in the offshore area east of Galeota Point, Trinidad, West Indies, Transactions of the Caribbean Geological Conference = Memorias - Conferencia Geologica del Caribe, United States, Queens College Press : Flushing, NY, United States, p. 381.
- Dawson, A. G., P. Lockett, and S. Shi, 2004, Tsunami hazards in Europe: Environment International, v. 30, p. 577-585.
- Fryer, G. J., P. Watts, and L. F. Pratson, 2004, Source of the great tsunami of 1 April 1946; a landslide in the upper Aleutian forearc: Marine Geology, v. 203, p. 201-218.
- Hiscott, R. N., K. T. Pickering, A. H. Bouma, B. M. Hand, B. C. Kneller, G. Postma, and W. Soh, 1997, Basin-floor fans in the North Sea; sequence stratigraphic models vs. sedimentary facies; discussion: AAPG Bulletin, v. 81, p. 662-665.
- Jennette, D. C. G., Timothy R., 1999, The interaction of shelf accommodation, sediment supply and sea level in controlling the facies, architecture and distribution of the Forties and Tay basin-floor fans, central North Sea, AAPG Bulletin, United States, American Association of Petroleum Geologists : Tulsa, OK, United States, p. 1320.

- Klaucke, I., D. G. Masson, N. H. Kenyon, and J. V. Gardner, 2004, Sedimentary processes of the lower Monterey Fan channel and channel-mouth lobe: *Marine Geology*, v. 206, p. 181-198.
- Marr, J. G., P. A. Harff, G. Shanmugam, and G. Parker, 2001, Experiments on subaqueous sandy gravity flows: The role of clay and water content in flow dynamics and depositional structures: *GSA Bulletin*, v. 113, p. 1377-1386.
- Martinez, J. F., J. A. Cartwright, P. M. Burgess, and J. V. Bravo, 2005, 3D seismic interpretation of the Messinian unconformity in the Valencia Basin, Spain: *Memoirs of the Geological Society of London*, v. 29, p. 91-100.
- McGilvery, T. A., D. L. R. Cook, H. H., N. C. Rosen, R. H. Fillon, and J. B. Anderson, 2003, The Influence of local gradients on accommodation space and linked depositional elements across a stepped slope profile, offshore Brunei: *Shelf Margin Deltas and Linked Down Slope Petroleum Systems: Global Significance and Future Exploration Potential*, p. 387-419.
- Mize, K. L., L. J. Wood, and P. Mann, 2004, Controls on the morphology and development of deep-marine channels, eastern offshore Trinidad and Venezuela *AAPG Annual Meeting Program*, v. 13.
- Moiola, R. J., and G. Chanmugam, 1984, Submarine fan sedimentation, Ouachita Mountains, Arkansas and Oklahoma: *Transactions - Gulf Coast Association of Geological Societies*, v. 34, p. 175-182.
- Morris, R. C., 1971, Classification and interpretation of disturbed bedding types in Jackfork flysch rocks (upper Mississippian), Ouachita mountains, Arkansas: *Journal of Sedimentary Research*, v. 41, p. 410-424.
- Moscardelli, L., Wood, L. & Mann, P. (2006) Mass-Transport Complexes and Associated Processes in the Offshore Area of Trinidad and Venezuela. *AAPG Bulletin*, 90, 1059-1088.
- Nisbet, E., and D. J. W. Piper, 1998, Giant submarine landslides: *Nature (London)*, v. 392, p. 329-330.
- Nissen, S. E. H., Norman L., C. T. Steiner, and K. L. Cotterill, 1999, Debris flow outrunner blocks, glide tracks, and pressure ridges identified on the Nigerian continental slope using 3-D seismic coherency, *Leading Edge Tulsa, OK, United States, Society of Exploration Geophysicists* : Tulsa, OK, United States, p. 595.
- Posamentier, H. W., and V. Kolla, 2003, Seismic Geomorphology and Stratigraphy of Depositional Elements in Deep-Water Settings: *Journal of Sedimentary Research*, v. 73, p. 367-388.



- Shanmugam, G., 2000, 50 years of the turbidite paradigm (1950s-1990s); deep-water processes and facies models; a critical perspective: *Marine and Petroleum Geology*, v. 17, p. 285-342.
- Shanmugam, G., R. B. Bloch, S. M. Mitchell, G. W. J. Beamish, R. J. Hodgkinson, J. E. Damuth, T. Staume, S. E. Syvertsen, and K. E. Shields, 1995, Basin-floor fans in the North Sea; sequence stratigraphic models vs. sedimentary facies: *AAPG Bulletin*, v. 79, p. 477-512.
- Shanmugam, G., R. J. Moiola, and J. K. Sales, 1988, Duplex-like structures in submarine fan channels, Ouachita Mountains, Arkansas: *Geology*, v. 16, p. 229-232.
- Shipp, C., J. A. Nott, and J. A. Newlin, 2004, Physical characteristics and impact of mass transport complexes on deepwater jetted conductors and suction anchor piles: *Offshore Technology Conference*, p. 11.
- Sohn, Y. K., 2000, Depositional Processes of Submarine Debris Flows in the Miocene Fan Deltas, Pohang Basin, SE Korea with Special Reference to Flow Transformation: *Journal of Sedimentary Research*, v. 70, p. 491-503.
- Sydow, J. C., J. Finneran, A. P. R. Bowman, H. H., N. C. Rosen, R. H. Fillon, and J. B. Anderson, 2003, Stacked shelf-edge reservoirs of the Columbus Basin, Trinidad, West Indies: Shelf Margin Deltas and Linked Down Slope Petroleum Systems: *Global Significance and Future Exploration Potential*, p. 411-465.

## **Chapter 3: A Genetic Classification of Mass Transport Complexes – Offshore Trinidad**

### **3.1. INTRODUCTION**

Mass transport deposits play a large role in the stratigraphic fill of basins in offshore northeastern South America, as well as along other continental margins around the world. An incredible variety of quaternary-age MTCs have been documented in deep water areas around offshore Trinidad. These deposits provide an opportunity to examine the variety of MTCs that occur in deep water margins, document their architecture and discuss a classification of these deposits based on the similarities and differences between them.

The area of this study is 10,708 km<sup>2</sup> in size and is located in water depths of 300 to 1500 meters along the southeastern margin of the tectonically active Caribbean Plate Boundary Zone (Figure 1.3). Earthquakes up to magnitude 7 are frequent occurrences in the area, and the region is characterized by both compressional and extensional tectonic forces. A variety of faults are found in the area, including, from south-to-north, extensional down-to-the-northeast listric faulting, transpressional south-verging thrusts, and right-lateral strike slip faults (Heppard et al., 1998; Wood 2000; Boettcher et al., 2003). High sediment accumulation rates, dominantly supplied by the Orinoco River and Delta, high frequency Pleistocene sea level fluctuations, abundant gas-hydrate deposits, storm activity, and tectonic instability create a volatile mix of geologic conditions in the study area that are conducive to mass shelf-edge failures and the subsequent deposition of gravity induced deposits (mass transport complexes and turbidites).

This chapter seeks to clarify much of the existing confusing terminology surrounding mass transport deposits by answering the following questions: (1) What are the dimensions and geomorphological characteristics of various mass transport complexes in the deep marine margin of offshore Trinidad? (2) What are the influences on the distribution of gravity induced deposits in the deep marine margin of offshore Trinidad? (3) Can we use seismic geomorphologic character of ancient mass transport deposits to understand the processes active at their time of deposition?

### **Terminology, Dimensions and Relevance of Mass Transport Complexes**

The term mass transport complex (MTC) was originally used by Weimer (1989 and 1990) to describe: “chaotic appearing sediments that occur at the base of deep water stratigraphic sequences and are overlain and/or overlapped by levee/channel complexes”. According to the same author, MTCs commonly overlie an erosional base in updip locations and become mounded downdip. These units were described by Weimer as externally mounded in shape, presenting chaotic reflections with poor continuity and variable amplitude. According to Weimer and Shipp (2004), the term “mass transport complex” can only be applied to features at a scale that can be completely imaged on volumetrically large seismic surveys. However, the same authors pointed out that the term mass transport complex has evolved from its original definition, and it is more recently used in industry and academia to describe a wide spectrum of gravity induced deposits, including slides, slumps and debris flows. This work will show that slides, slumps and debris flows are constituents of MTCs, and these component elements can co-occur in the same event or depositional unit (Galloway and Hobday, 1996).

Mass transport complexes can range up to 10’s of kilometers across, 100’s of kilometers in length, 1000’s of square kilometers in area and 100’s of meters in thickness (Masson et al., 1998; Gee et al., 1999; McAdoo and Orange, 2000; Wynn et al., 2000;

Gee et al., 2001; Imbo et al., 2003; McGilvery et al., 2003; Lee et al., 2004; Newton et al., 2004; Haflidason et al., 2005; Lastras et al., 2005; Moscardelli et al., 2006). Mass transport complexes are believed to comprise more than 70% of the entire stratigraphic column of all continental margins (Maslin et al., 2004; Newton et al., 2004), and they are found in all kind of tectonic settings. Many examples of mass transport complexes that have sea floor expressions have been documented by the use of shallow seismic data and side scan sonar surveys (Table 1 and Figure 3.1). Advances in 3D seismic acquisition and imaging techniques in the past decade have led geoscientists to study and characterize in detail deeply buried, ancient mass transport complexes in most continental margins (Table 1 and Figure 3.1).

The predominance of mass wasting processes in most continental margins around the world, makes MTCs a potentially important component element of any deep water stratigraphic succession. In addition, their influence in the shaping of sea floor bathymetry and continental margin architecture is well documented. The catastrophic erosive nature of these event deposits underscores their potential impact on offshore infrastructures due to their ability to compromise the integrity of underwater equipment such as cables, communication lines and pipelines.

It has been documented that these deep water MTC deposits possess physical characteristics that often differ greatly from deep water submarine fan or slope leveed channel systems (Shipp et al., 2004). The frequent presence of these deposits in deep water basins means that efficient resource exploration and development in such settings hinges on understanding the nature, processes of formation, distribution and relationship that these deposits share with surrounding deep water environments.

## **Seismic Character of Mass Transport Complexes**

Mass transport complexes can take on a variety of plan-form geometries, most influenced by the nature of the depositional basin. In unconstricted basins that receive extra-slope sedimentation, MTC may be elongated. In constricted basins, many of which lack upslope sediment sources, MTC geometries are relatively concentric (Posamentier, 2004; Weimer and Shipp, 2004). In cross sectional seismic lines mass transport complexes are recognizable by the presence of seismic facies that show low amplitude, semitransparent, chaotic reflections (Posamentier and Kolla, 2003). However, internal to the MTC may exist regions of semi-deformed mixtures of low- and high- amplitude reflections, that show thrust and embrication geometries. Internally, mass transport complexes can contain thrust blocks (Weimer and Shipp, 2004) or syndepositional thrusts (Moscardelli et al., 2006) reflecting the ongoing deformation due to the compression associated with spatial variation in the deceleration of the flow. Such deceleration could occur at the terminal end of debris lobes or anywhere the flow is constricted and slows. The presence of bathymetric barriers on the sea floor at the time of deposition, such as mud volcanoes or salt diapirs, can significantly contribute to the reduction of the cross sectional area in regions affected by mass transport complex deposition. This reduction increases the chances of generating syndepositional deformation within the unit. Another distinctive internal characteristic of mass transport complexes is the presence of internally undeformed transported blocks that lay directly or partly submerged into the surrounding chaotic material. These blocks can vary in size from several 100 square meters to several 1000 square meters across and 150 m thick (Lee et al., 2004). Different from these detached and transported olistostromes, there occur intact but buried hoodoos that are surrounded by chaotic MTC material. These features usually form in the shadow of some barrier that inhibits MTC downslope

movement, causing it to flow around the barrier, thus preserving the older strata lying downslope of the barrier. Such deposits, termed erosional shadow remnants by Moscardelli et al., (2006) are closely associated with physiographic barriers such as mud volcanoes and salt diapirs.

The upper and lower boundaries of mass transport complexes tend to be marked by high amplitude seismic reflectors. Their bases often show a variety of erosive features. The largest of these, termed mega-scours by Moscardelli, et al., (2006) can show scour into the substrate that is 10's of meters deep, 100's of meters wide and 100's of kilometers long. (McGilvery et al., 2003; Posamentier and Kolla, 2003; Weimer and Shipp, 2004; Moscardelli et al., 2006), these basal surfaces can also contain particular stratigraphic features termed cat-claw scours (Moscardelli et al., 2006) or monkey fingers (McGilvery et al., 2003) that are composed of a series of shallow smaller radiating scours whose apex is usually close to the downdip termination of individual mega scours. Secondary scours and scratches (Moscardelli et al., 2006) or glide tracks (Nissen et al., 1999) are also common and are associated with outrunner blocks that most likely tooled the scours on the sea-floor.

The upper bounding surface of a mass transport complexes commonly shows erosion associated with processes along the base of overlying levee-channel complexes (Posamentier, 2004). The location of the main depo-axis and the general geometry of the overlying levee-channel complexes are usually controlled by the alterations in bathymetry created by the underlying mass transport complex event (Moscardelli et al., 2006). Mass transport complexes tend to amalgamate, and surfaces between successive mass transport complexes can be obscure and difficult to recognize in seismic (Posamentier, 2004). Lee et al. (2004) working in offshore Morocco identified a prominent seismic reflector that separates the basal and upper cycles of the Tejas A mass

transport complex. This reflector was interpreted as a condensed section, implying a time break between deposition of the basal and upper units. It has also been suggested by the same authors that this condensed section may have acted as the initial sliding surface for the upper mass transport complex unit. In the case of the Morocco MTC (Lee et al., 2004) the prevalence of laminar flow in the basal portions of the upper unit of the Tejas A mass transport complex could contribute to the preservation of the condensed section that was identified between the two units.

### **Physical and Lithological Characteristics of Mass Transport Complexes in Cores and Outcrops**

The availability of core and logs through mass transport deposits is sparse, but has been documented by a few workers (Shipp et al., 2004). Piper et al. (1997) described cores that penetrated mass transport complexes in the Amazon fan in offshore Brazil. The units were composed of clays presenting extensive deformation, dipping beds and blocks of varying sizes. Five lithofacies were defined in the cores: uniform mud with large blocks, variable mud with inferred meter-size blocks, abundant centimeter-to-decimeter size blocks, sand and silt mud, and contorted mud with silty laminae. In general, the sedimentary structures related to mass transport complexes are associated with highly deformed beds, floating clasts within debris flows, and abrupt contacts. Several studies have been performed using well logs that penetrated mass transport complexes. These areas include the Amazon Fan in offshore Brazil (Piper et al., 1997), the Na Kika Basin in the Gulf of Mexico (Pirmez et al., 2004; Shipp et al., 2004) and the offshore area of Trinidad (Shipp et al., 2004). Based on these studies, it is observed that responses within the deposits show an increase in porosity, density, compressional velocity and resistivity. Geotechnical analyses performed in the same areas indicate an increase in shear strength, with a corresponding decrease in void ratio and water content (Shipp et al., 2004).

However, it is important to point out that rheological characteristics of mass transport complex sediments depend on the nature of the original material that failed upslope, and the location of the sediment sample from proximal to distal within the mass transport complex.

Several authors have studied mass transport complexes using outcrop exposures (Figure 3.1). Kleverlaan, 1987 described the Gordo Megabed (Chozas Formation) in the Tabernas basin in Spain and interpreted it as a gravity induced deposit that was triggered by an earthquake during the Miocene. The exposed length and width of the outcrop are 11.5 km and 17 km respectively, the average thickness of the unit is about 40 m, and the total sediment volume was estimated around 6 km<sup>3</sup>. The basal portion of the Gordo Mega bed contains numerous debris flows that are composed of boulder conglomerates supported by a muddy matrix. The character of the lithology on the top portion of the unit suggested numerous transitions from laminar to turbulent flows. Kleverlaan (1987) also pointed out that the recognition of large gravity induced deposits in outcrops can be very difficult because their thicknesses often are in excess of the dimensions of the outcrop. Compaction and erosion are additional factors that need to be taken into consideration when trying to compare outcrop thicknesses of mass transport complexes with “equivalent” measurements collected in modern continental margins using 3D-seismic data.

Macdonald et al. (1993) studied several outcrops that contain slide units in the Mesozoic fore-arc sequence of the Alexander Island in Antarctica (Figure 3.1). There he found slides that reach at least 440 m in thickness, are more than 126 km<sup>2</sup> in area and as much as 300 km<sup>3</sup> in volume. The authors noted that these scales were comparable to deposits documented from modern continental margins. Macdonald et al. (1993) agreed with Kleverlaan (1987), pointing out that the apparent absence of large, ancient slide



deposits or mass transport complexes in outcrops is purely a function of exposure. The units that contain the slides described by Macdonald et al. (1993) in the Alexander Island in Antarctica consist of large sheets of interbedded sandstone and mudstone matrix. The mudstones contains dispersed, randomly oriented, equant, metre-scale blocks of sandstones similar to those described by Lee et al. (2004) in the Tejas A mass transport complex in offshore Morocco. Member B3 of the Ablation Point Formation in Antarctica (Macdonald et al., 1993) is a 100-160 m thick thrust stack with the morphology of an “emergent imbricate fan”, this imbricate pattern is similar to the geometries and dimensions associated with the syndepositional thrusts identified by Moscardelli et al., 2006 in offshore Trinidad. These compressional features are common within mass transport complexes and have been documented by several authors (Martinez et al., 2004; Weimer and Shipp 2004). Shanmugam et al. (1988) also documented similar but smaller scale duplex-like features in an outcrop of the Jackfork Formation of the Ouachita Mountains in Arkansas (Figure 3.1). Dykstra (2005) also reported the presence of imbricate thrusts in outcrops of the Jejenes Formation in the Carboniferous of western Argentina, and similar folds and thrusts faults in the Casaglia Monte della Colonna mass transport complex in the northern Apennines (Italy) (Figure 3.1) where these folds created meter-scale topography. Strachan (2002) also documented multiple internal shear zones and faults in the outcrops of the Little Manly Slump of New Zealand pointing out that the dominance of compressive thrusts structures can be interpreted to result from cessation initiating at the front of the translating slump mass while the rear portion continued to move.

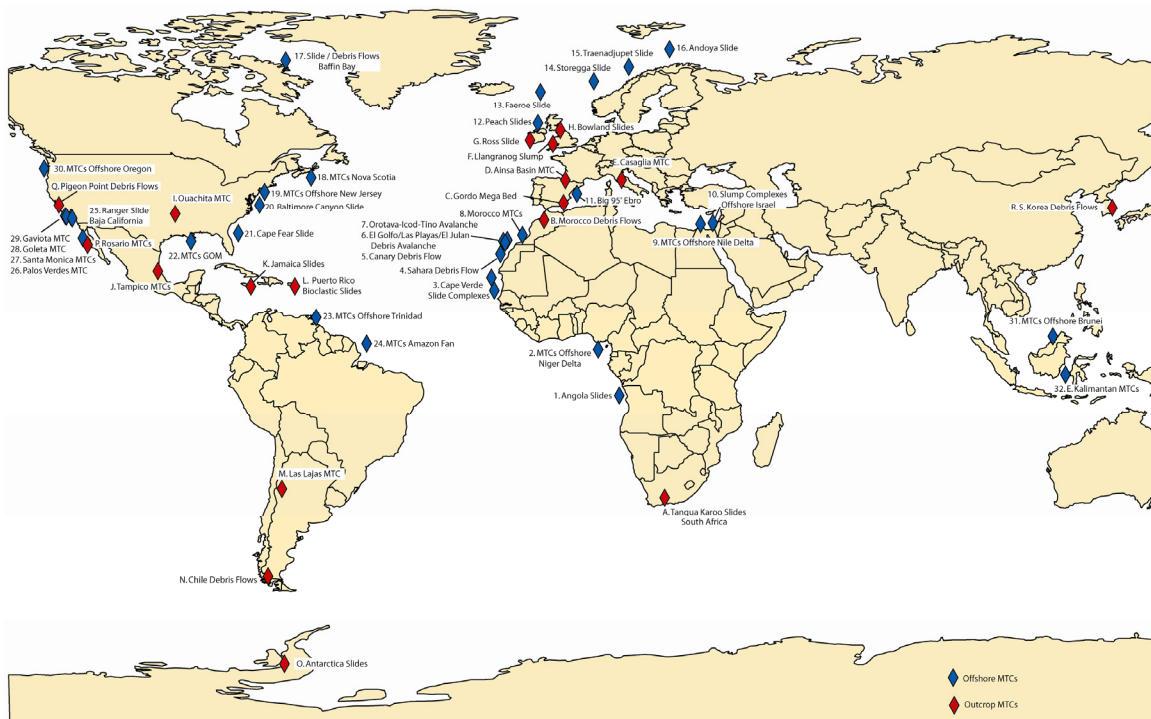


Figure 3.1: Worldwide distribution of mass transport complexes. Numbers indicate the location of modern and ancient offshore MTCs identified in seismic data. Letters indicate the location of ancient MTCs in outcrop. See table I for corresponding locations and references.

Table 3.1: Worldwide Occurrence and Distribution of Offshore Mass Transport Complexes (<sup>(a)</sup>Sea Floor Expression and <sup>(b)</sup>Buried MTCs). Numbers correspond to modern and ancient MTCs identified in offshore seismic. Letters correspond to ancient MTCs identified in outcrop.

No.	Location and Type	Age	Volume (Km <sup>3</sup> )	Reference
1	<sup>b</sup> Angola Slides	Miocene	20	Gee et al. (2006)
2	<sup>a</sup> Niger MTCs	Pliocene	-	Shanmugam et al. (1997) and Nissen et al. (1999)
3	<sup>b</sup> Cape Verde Slides	Pleistocene	-	Wynn et al. (2000)
4	<sup>a</sup> Sahara Debris Flow	Pleistocene	600 – 1.100	Gee et al. (1999)
5	<sup>a</sup> Canary Debris Flows	Pleistocene	400	Masson et al. (1998)
6a	<sup>a</sup> El Golfo Debris Avalanche	Pleistocene	150 - 350	Wynn et al. (2000) and Gee et al. (2001)
6b	<sup>a</sup> El Julian Debris Avalanche	Pleistocene	130	Wynn et al. (2000) and Gee et al. (2001)
6c	<sup>a</sup> Las Playas Debris Avalanche	Pleistocene	30	Wynn et al. (2000) and Gee et al. (2001)
7	<sup>a</sup> Orotava-Icod-Tino Avalanche	Pleistocene	1000	Wynn et al. (2000)
8	<sup>a, b</sup> Morocco MTCs	Tertiary	-	Lee et al. (2004)
9	<sup>a, b</sup> Nile MTCs	Quaternary	670	Newton et al. (2004)
10	<sup>a, b</sup> Israel Slump Complexes	Quaternary	1000	Martinez et al. (2005)
11	<sup>a</sup> Big 95' Debris Flow Ebro Spain	Pleistocene	26	Lastras et al. (2005)
12	<sup>a</sup> Peach Slide	Pleistocene	135	Holmes et al. (1998) and Kuntz et al. (2001)
13	<sup>a, b</sup> Faeroe Slide	Pleistocene	135	Van Weering et al. (1998)
14	<sup>a</sup> Storegga Slide	Holocene	2400 – 3500	Jansen et al. (1987), Evans et al. (1996), Bouriak et al. (2000), Hafliadason et al. (2003)
15	<sup>a</sup> Traenadjupet Slide	Holocene	900	Laberg and Vorren (2000)
16	<sup>a</sup> Andoya Slide	Holocene	485	Laberg and Vorren (2000)
17	<sup>a, b</sup> Baffin Bay Slide/Debris Flow	Plio-Pleistocene	-	Aksu and Hiscott (1989)
18	<sup>a, b</sup> Nova Scotia MTCs	Eocene to Holocene	-	Campbell et al. (2004)
19	<sup>a</sup> New Jersey MTCs	Quaternary	1.7	McAdoo et al. (2000)
20	<sup>a</sup> Baltimore Canyon Slide	Holocene	200	Embley and Jacobi (1986)
21	<sup>a</sup> Cape Fear Slide	Pleistocene	1400	Popenoe et al. (1991)
22	<sup>a, b</sup> Gulf of Mexico MTCs	Tertiary	27.5	McAdoo et al. (2000)
23	<sup>a, b</sup> Trinidad MTCs	Plio-Pleistocene	11.3 - 2017	Moscardelli et al. (2006)
24	<sup>a, b</sup> Amazon Fan MTCs	Pleistocene	1500 - 2000	Piper et al. (1997)
25	<sup>b</sup> Ranger Slide Baja California	Pleistocene	20	Normark (1974)
26	<sup>a</sup> Palos Verdes MTC – California	Holocene	0.34 – 0.72	Lee et al. (2004)
27	<sup>a</sup> Santa Monica MTC – California	Quaternary	0.0002	Lee et al. (2004)
28	<sup>a</sup> Goleta MTC – California	Holocene	0.5	Lee et al. (2004)
29	<sup>a</sup> Gaviota MTC – California	Holocene	0.01 – 0.02	Lee et al. (2004)
30	<sup>a</sup> Oregon MTC	Quaternary	3.8	McAdoo et al. (2000)
31	<sup>a, b</sup> Brunei MTC	Quaternary	80	McGilvery and Cook (2003)
32	<sup>a, b</sup> Eastern Kalimantan MTC	Pleistocene	-	Posamentier and Kolla (2003)

a – MTCs that have sea floor expression

b – Buried MTCs

Pickering and Corregidor (2005) described mass transport complexes in the submarine fans (Eocene) in the outcrops of the Ainsa basin in the Spanish Pyrenees (Figure 3.1). Different types of mass transport complexes were described in the Ainsa submarine fan including: (1) slides derived from the middle-upper slope area that are composed by intra-formational marly and heterolithic sediments that can reach 10's of meters in thickness; (2) local slides associated with collapses in channel margins and that are characterized by the presence of thin intra-formational deformed horizons with folded, attenuated, and partially disaggregated sands contained in a sandy to marly matrix; (3) sediment slides and debris flows whose source area has been associated with collapses of a carbonate platform, as well as with collapse in the upper-middle slope region and that are composed by 16 m thick marl-matrix supported deposits with clasts to cobble and boulder size carbonate platform material; and (4) multiphase granular flows associated with extra-formational material derived from the shelf and from fluvio-deltaic input. These units usually contain well-rounded pebbles, shallow marine shells and abundant reworked nummulites. They can typically range from a few meters to tens of meters thick, and may show cumulative basal erosion of up to tens of meters, the basal portion of these multiphase granular flows are defined by regional erosional surfaces that contain flutes and grooves. This last unit appears to exhibit some of the characteristics described in the basal portions of regional mass transport complexes in offshore Trinidad (Moscardelli et al., 2006), offshore Brunei (McGilvery et al., 2003), and offshore Indonesia (Posamentier and Kolla, 2003).

### **Sequence Stratigraphy, Eustatic Control and Mass Transport Complexes**

According to Posamentier and Kolla (2003), the occurrence of mass transport complexes has been traditionally associated with early stages in cycles of shoreline fall to lowstand, when sedimentation to the shelf edge is at its peak and water overburden

weight is being reduced over shelf regions. The same authors presented a schematic depiction of the traditional relationships that have been defined between relative sea level and dominant mass flow processes. According to this scheme a typical deep water stratigraphic succession comprises: (1) debris flow deposits at the base corresponding to the initial period of relative sea level fall (traditional MTCs associated with shoreline fall to lowstand), (2) frontal splay dominated and then (3) leveed channel-dominated sections corresponding to the subsequent period of late lowstand and early relative sea level rise respectively. However, this scheme has an addition where the succession is ultimately capped by deposition of debris flow and condensed section deposits corresponding to periods of rapid sea level rise and highstand. This relatively new conceptual model suggests that mass transport complexes can be deposited during periods of relative sea level rise and highstand. Observations made by a series of researchers in different continental margins seem to be supporting this idea (McMurtry et al., 2004; Maslin et al., 2005; Moscardelli et al., 2006; Sutter, 2006; Twichell et al., 2006; Wynn, 2006).

On conventional sequence stratigraphic models sediment delivery from the shelf to the deep marine environments dramatically increases during times of lowstand. However, it has been argued that several mechanisms may actually be more effective during highstand or still stand conditions. Sutter (2006) pointed out that under highstand conditions longshore drift can cause the erosion of the shoreline; such a process would stimulate gravitational instabilities in the upper slope area and could potentially end up triggering the genesis of deep water turbidites or mass transport complexes. Maslin et al. (2005), on the basis of detailed biostratigraphic analysis, pointed out that the Eastern and Western Debris Flows in offshore Brazil occurred shortly after 13ka when sea level was rising rapidly. These debris flows were triggered by oversteepening of the continental slope due to an increase of the Amazon Delta sediment discharge and its possible link to a

paleo- Amazon shelf edge delta. Similarly, Moscardelli et al. (2006) placed the timing of mass transport complex MTC\_1 (Plio-Pleistocene) in offshore Trinidad during the early stages of relative sea level rise when still stand conditions were prevalent. This interpretation was based on the aggradational character of the clinoforms that fed the system and that were associated with a paleo- Orinoco shelf edge delta. Twichell et al. (2006) studied the Mississippi fan succession (Plio-Pleistocene) confirming the existence of three phases of development: (1) deposition of turbidites and debris flows derived from the shelf edge during the last lowstand and the initial stage of the Holocene transgression, (2) failures in the Mississippi Canyon that triggered the deposition of the main mass transport complex during the Holocene transgression, and (3) hemipelagic sedimentation that finally covers the fan. Wynn (2006) has used piston coring and geophysical data to extensively study the northwestern African continental margin and the giant mass transport complexes and turbidites that have been deposited during the last 200,000 years. According to these results, the Sahara and the Mauritania slides located on the offshore area of the Western Sahara and in northern Mauritania, occurred during periods of sea level rise and during periods of glacial interglacial transitions. These events of gravity induced deposition took place during late/post-glacial periods of rising sea level. McMurtry et al., (2004) studied the giant submarine slides in Hawaii and found an “intriguing” relationship between the timing of the events and high stands of the sea, the compilation of age estimates for the submarine slides in Hawaii versus the relative sea level curve show that nearly all the events correlate with the onset of warm interglacial periods. They finally concluded that persistent climatic effects during sea-level high stands (warmer and wetter conditions) eventually triggered large failures that originated the giant submarine slides and debris flows that are observed off the coast of Hawaii.

### 3.2. METHODOLOGY AND DATA SETS

The primary data set for study of the deep-water architecture and nature of the offshore Trinidad continental margin is 3-D seismic data. Fortunately, the seismic coverage used for this research initiative is large enough to encompass several entire mass transport complex staging areas and depocenters (Figure 3.2).

The quality of the 3-D data used in this study makes it possible to correlate seismic units with a high degree of confidence. Nine regional horizons were mapped and correlated across the slope into the deep-marine basin. These horizons are shown on Figure 3.3C, a northwest-southeast oriented regional seismic line (see relative location on Figure 3.3A) that shows a strike view across the central region of the study area. The horizons were correlated across several mud volcano provinces. The nine interpreted horizons were named from base to top: P60, P50, P40, P30, P20, P15, P10, P4 and P0 (sea floor) (Sullivan et al., 2004; Garciacaro, 2006; Moscardelli et al., 2006) (Figure 3.3C). Surface P10 defines the base of mass transport complex MTC\_1, this unit was extensively described by Moscardelli et al. (2006). Surface P4 defines the top of MTC\_1 and the erosional base of the youngest levee channel complex in this region (Moscardelli et al., 2006). The latest expression of this channel complex on the modern sea floor and its main geomorphological characteristics were described by Mize et al. (2004) and Sullivan et al. (2004). Surfaces mapped were used to define the gross architecture of the basin and to assess its fill history. Additionally, five isochron maps were generated between the following horizons: P60/P20, P20/P10, P10/P5, P5/P4 and P4/P0 (Figure 3.3C). The isochron maps helped us to understand what the character of the continental margin fill was, as well as to reconstruct the evolution of the basin through time. However, the main focus of this research is concentrated in the description and understanding of mass transport complexes that are contained in the basal portion of the

stratigraphic unit bounded by the P15 and P10 surfaces (Figure 3.3C). In each case, all surfaces were seeded with the picking tool and then interpolated along key amplitude horizons. These surfaces were then adjusted by hand where the picking tool strayed from the horizon.

Mass transport complex architectures were imaged through the use of root-mean-squared (RMS) amplitude extractions. RMS amplitude extractions were taken in successive 20 ms (15 m) time windows above the P15 horizon. The P15 horizon represents the erosional surface that defines the base of the mass transport complexes that are studied in this work (Figure 3.4). The P15 horizon was picked as the “key horizon” that guided the amplitude extractions within the unit of interest because the internal architecture of mass transport complexes is greatly influenced by the initial erosional events that generate their basal surfaces.

Several exploratory wells have been drilled in the study area, but direct access to these data was not available to the authors. Several drop core were collected in the region for geotechnical tests on the near seafloor sediments, but none were deep enough to penetrate the intervals of interest. Data from exploration drilling in the study area were used by Shipp et al. (2004) to document the lithologic and physical characteristics of the northern portion of the shallowest MTC\_1 mass transport complex in the area (Moscardelli et al., 2006). The mass transport complexes that are described in this chapter are slightly older than MTC\_1; however it is believed that their lithologic and physical characteristics are similar.



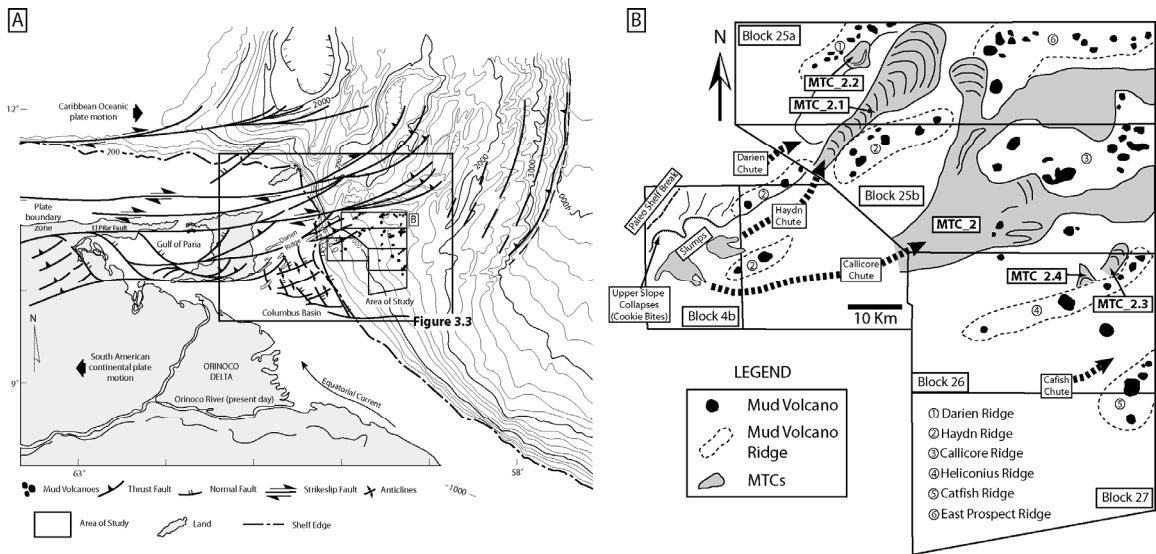


Figure 3.2: A) Map showing the area of study located in the area of northeastern South America along the Caribbean plate boundary zone where the Caribbean plate (to the north) and the South America plate (to the south) meet. The area of 3-D seismic data is outlined in black lines. The shelf break is shown as a heavy black dash and dotted line along the 200 – 300 m (660 – 1000-ft) contour. The Orinoco delta system in Venezuela is the primary supplier of sediments to the eastern shelf and continental slope. B) Seismic surveys in the study area correspond to block names. Shaded areas correspond to the location of mass transport complexes in the P15-P10 stratigraphic interval.

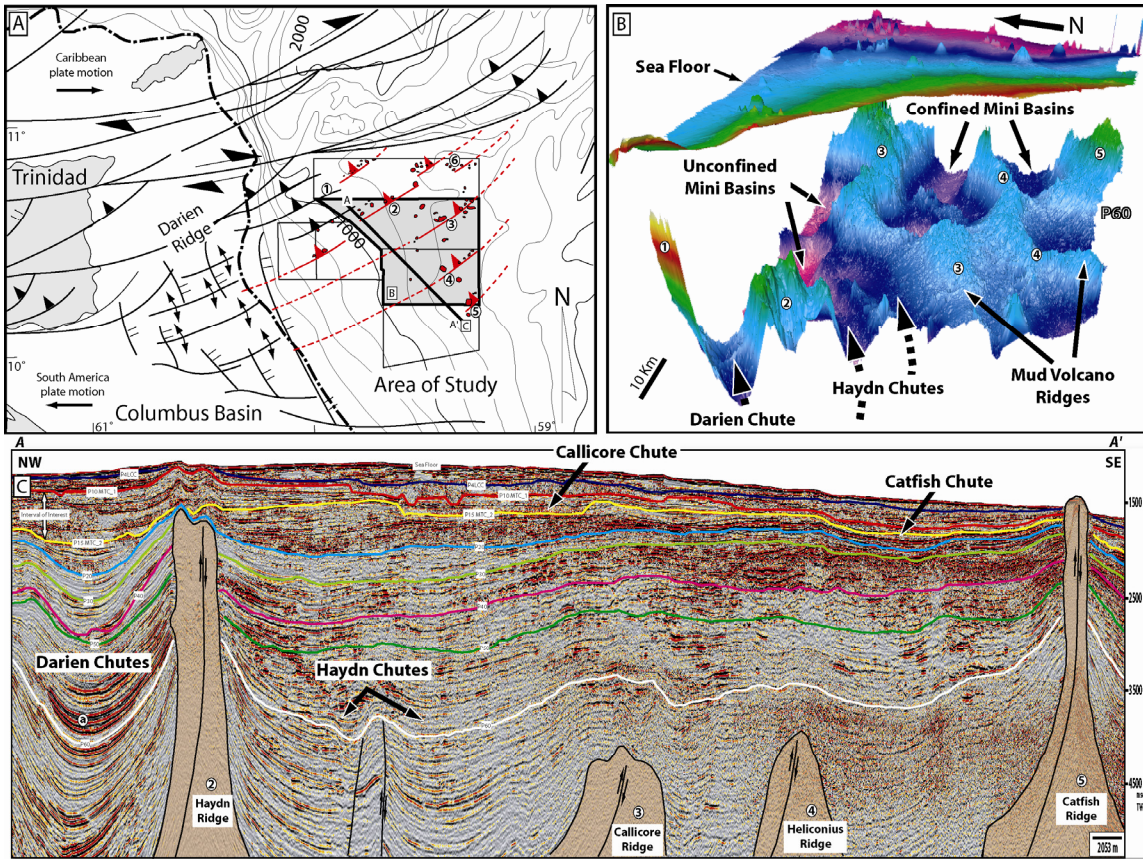


Figure 3.3: A) Map showing the main structures that are present in the study area. Notice the alignment of the mud volcano ridges in the deep marine setting with the northeast-southwest anticlines located in the shelfal portion of the Columbus basin. B) Visualization of the seafloor and the P60 horizon in blocks 26 and 25b (see shadowed area in A for reference). Mud volcano ridges controlled the paleobathymetry during P60 time. In the seafloor mud volcanoes indicate the location of the buried mud masses that have controlled the location of the main sedimentary pathways in this region during the Tertiary. C) Northwest-southeast regional seismic line showing the location of the main mud volcano ridges and chutes across the area. Nine key horizons, including the seafloor, were interpreted in order to understand the architecture of the Tertiary sedimentary infill in the region.

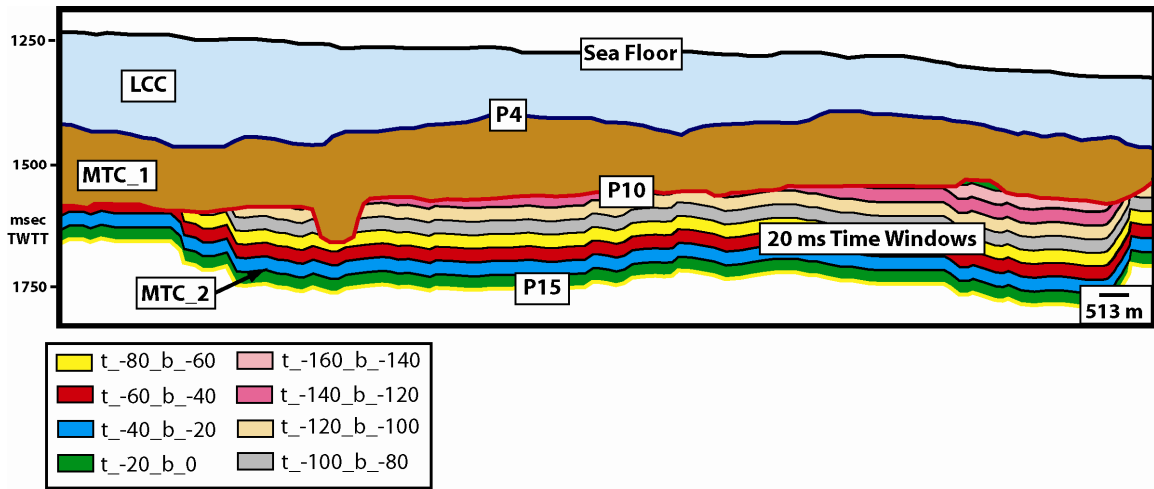


Figure 3.4. Line drawing showing the conceptual method that was used to generate the root-square amplitude extraction maps. Each RMS amplitude extraction over a 20ms interval is represented by the alphanumeric nomenclature shown in the legend.

### **3.3. STRUCTURAL SETTING AND PALEOBATHYMETRY IN OFFSHORE TRINIDAD AND ITS INFLUENCE IN DEEP WATER SEDIMENTATION**

A variety of paleo-bathymetric and structural features have influenced sediment transport and distribution in the proximal and distal parts of the deep marine margin of offshore Trinidad and Venezuela during Pliocene and Pleistocene times (Moscardelli et al., 2006). In the outer shelf / upper slope area, listric normal and counter-normal faults occur. Additionally, normal and inverse faults that define the lateral boundaries of shelf-edge horst and graben paleocanyons funnel sediments from the outer shelf / upper slope area towards the deep marine basin (Figure 3.5) (Moscardelli et al., 2006).

In the distal portions of the basin, mud volcanoes have been an important bathymetric element influencing deep water sedimentation (Figure 3.6). (Sullivan et al., 2004) documented 161 mobile mud-associated structures on the seafloor within the study area. They vary greatly in size, shape, and distribution. Some of these mud diapirs and volcanoes orient in linear “trains” associated with deeper anticlinal structures (Figure 3.6). These “trains” are part of the paleobathymetric highs that bound large sediment pathways or mega-chutes. In western portions of the study area, these “chutes” funnel sediments directly downslope from shelf-edge deltas and from the upper slope collapses towards basinward depo-locations that are relatively unconstrained (unconfined mini-basins). Alternatively, in some areas of the basin and portions of the stratigraphic record, mud ridges act to isolate some portions of the basin from upslope sedimentation (confine mini-basins). Examples of such confinement of basin areas from the shelf and slope sediment sources can be seen in the eastern portions of the study area (Figure 3.3B). For purposes of discussion, from the northwest to the southeast, the ridges associated with these mud volcano trains have been named: (1) the Darien Ridge (2) the Haydn Ridge, (3) the Callicore Ridge, (4) the Heliconius Ridge, and (5) the Catfish Ridge (Figure 3.3).

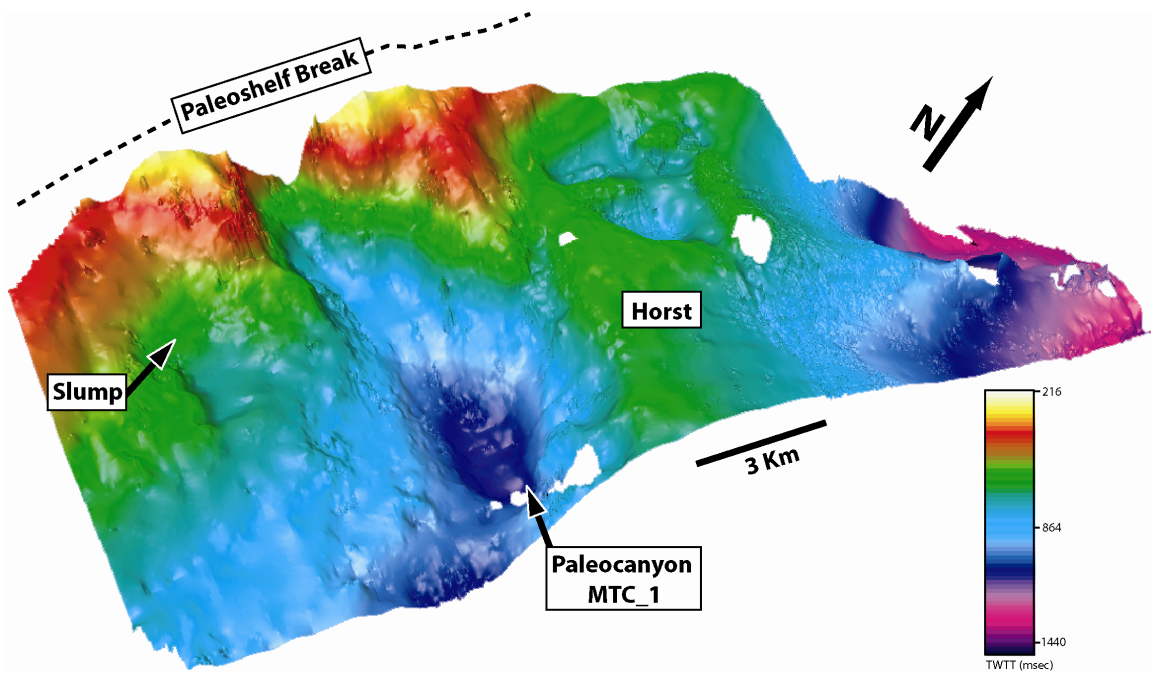


Figure 3.5: Visualization (oblique view looking from the east) of the paleocanyon that funneled sediments from the outer shelf to the deep marine region during the MTC\_1 event. The paleocanyon is bounded along both margins by normal faults, forming a structural depression that is nearly 200 m deep (Moscardelli et al., 2006).

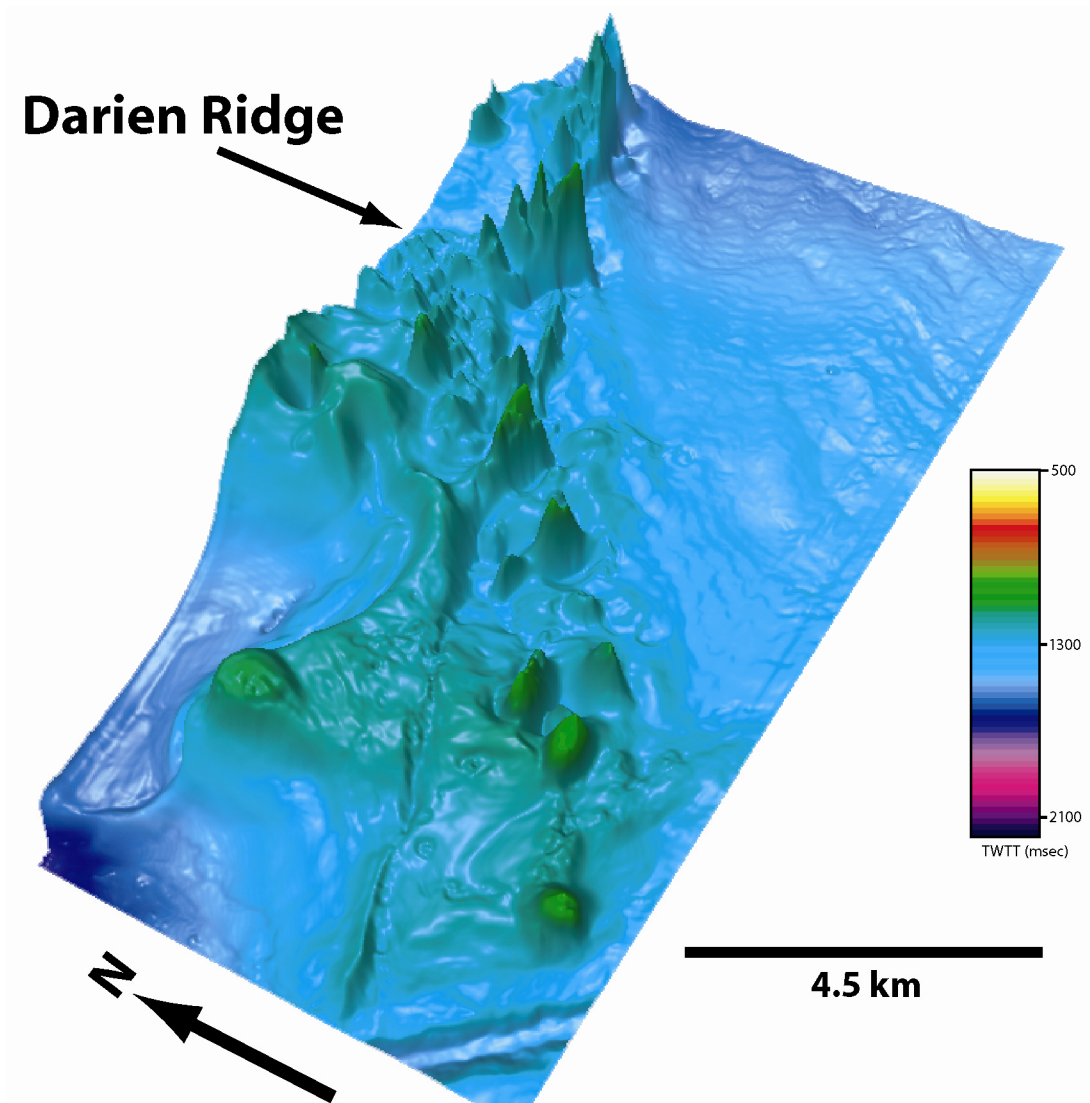


Figure 3.6: Visualization (looking from the west) of the northwestern termination of the Darien Ridge. Mud volcanoes are an important bathymetric element influencing deep water sedimentation. See floor interpreted by Sullivan et al. (2004).

### **3.4. SYNTHESIS OF THE EVOLUTION OF THE DEEP MARINE MARGIN OF OFFSHORE TRINIDAD**

Time structure maps and interval isochron maps (Figure 3.7) document a history of the fill in the study area.

#### **P60-P20 Time Interval**

The isochron map of the P60-P20 time interval (Figure 3.7A) shows several areas where the sedimentary section thickens. In the western portion of the study area, these thicker intervals can reach a maximum of 2400 milliseconds and appear to span from the mapped shelf edge to beyond the data extent to the north. The thicker intervals to the northwest coincide with the location of elongated unconfined mini-basins (Figure 3.3B) where slope- attached systems developed (Figure 3.8). The isochron map of this interval also shows isolated depocenters that are located to the east and southeast and that also present thicker stratigraphic successions (Figure 3.7A); in these localized regions the stratigraphic column is composed by the vertical stacking of multiple episodes of detached mass transport complexes. These detached systems were originated in the flanks of the mud ridges that bounded the confined mini-basins (Figures 3.3B and 3.8).

The isochron map of the entire P60-P20 time interval (Figure 3.7A) shows that sedimentation was active through the entire region in both, confined and unconfined mini-basins during this time period. The P60 time structure map indicates that the Darien and Haydn mega-chutes (Figure 3.3B) were the main sedimentary conduits feeding the northwestern unconfined mini-basins at this time. These unconfined mini-basins were receiving their main sedimentary input from the outer shelf and upper slope area, with occasional contributions from local sources associated with the nearby flanks of the mud volcano ridges. Meanwhile, the Callicore and Heliconius Ridges were acting to isolate

several mini-basins located in the eastern and southeastern portions of the P60 surface from any direct sediments off the outer shelf or upper slope (Figure 3.3B). Spatial confinement on all sides of this mini-basin led to a vertically stacked intercalations of constrained muddy debris flows that cascaded from the ridges, occasional pounded turbidites, and hemipelagic sedimentation filling the basin.

### **P20-P15 Time Interval**

The isochron map of the P20-P15 time period (Figure 3.7B) shows that the thicker intervals are constrained to a relatively elongated region in the northwestern portions of the study area where they can reach in between 400 to 650 milliseconds in thickness. The confined mini-basins that were present on the eastern and southeastern portions of the data base during the P60-P20 time interval are almost non-existent at this time. These observations suggest that during the P20-P15 time interval most of the sedimentation was taking place in the northwestern unconfined mini-basins where shelf- and slope- attached systems were dominating the sedimentation with occasional contributions from the flanks of the mud volcano ridges (detached systems cascading from the Darien and Haydn ridges).

The Haydn mega-chute was the main sedimentary conduit transporting extra-basinal gravity-induced deposits (mass transport complexes and turbidites) towards the deep marine settings (Figure 3.7B). Tectonic loading by ongoing encroachment of the Caribbean Plate from the northwest and transpressive uplift of the Darien Ridge accentuated the subsidence along this main axis of deposition (Figure 3.7B).

### **P15-P10 Time Interval**

The isochron map of the P15-P10 time interval shows a significant reduction in the areal extent of the northwestern depocenter with thicknesses varying from 400 to 600

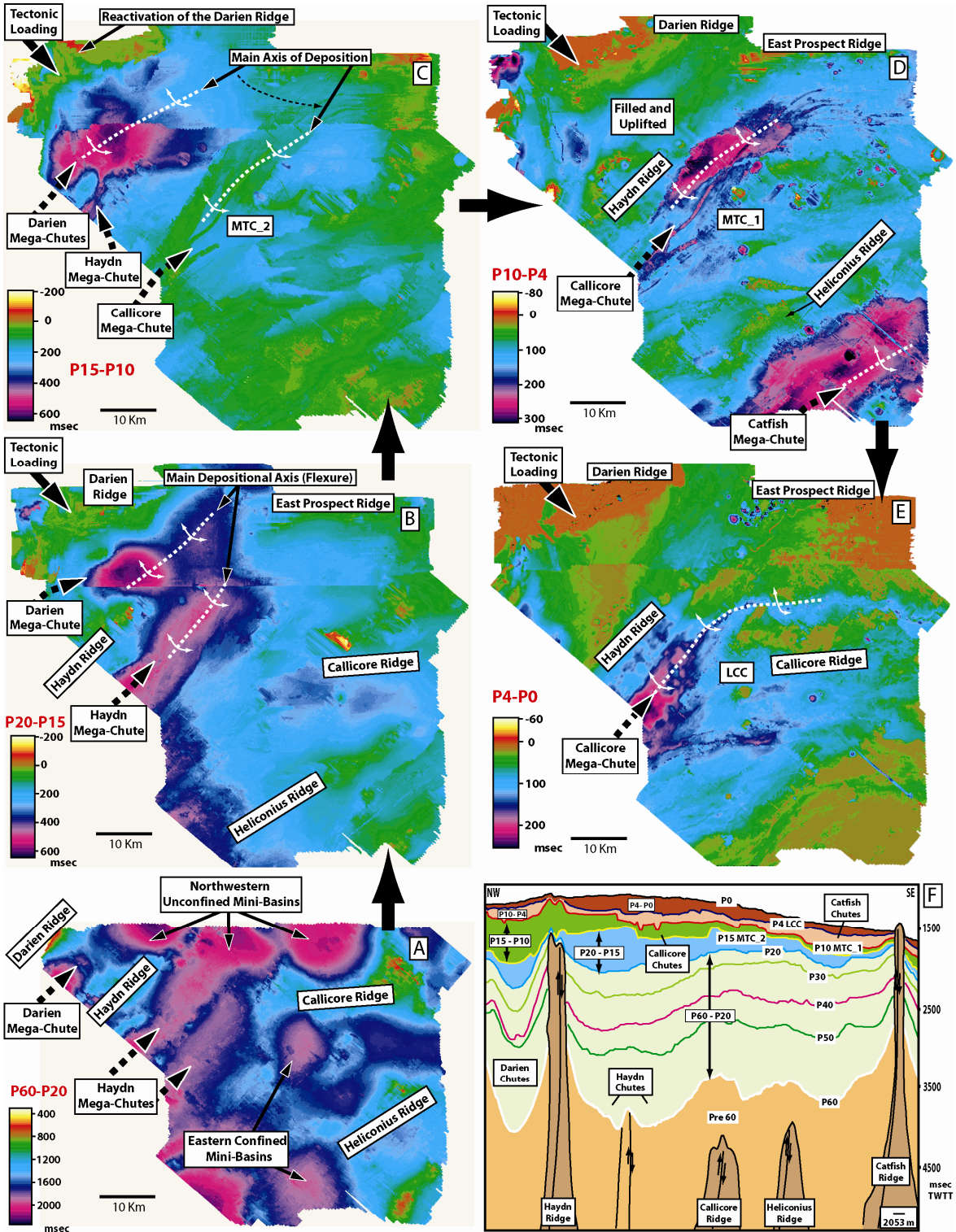


milliseconds (Figure 3.7C). According to approximate time-depth conversions at shallow depths these thicknesses would be equivalent to 300 m and 450 m respectively. By this time, this depocenter was constrained to the west presenting a more concentric geometry, compare to the elongated shape that was observed during the P60-P20 and P20-P15 time intervals. These observations suggest that sedimentation in the northwestern-located, unconfined mini-basin was still active at this time. However, the reduction in the areal extent of the main depocenter also indicates that the sedimentary infilling, mainly composed by extrabasinal slope- attached systems, was in its final stages. The P15-P10 isochron map also shows considerably thinning in the northwestern corner of the data set where the Darien Ridge is located. This thinning is associated with the progressive advance of the deformational front towards the southeast that caused an uplifting episode in the Darien Ridge.

The seismic line in Figures 3.3C shows the vertical incision caused by erosion in the P15 surface between the Haydn and Callicore ridges, this corresponds with the time when the Callicore mega-chute started to feed regional slope- attached systems (MTC\_2) (Figures 3.2B, 3.7C, 3.8 and 3.9) and sedimentation started to shift towards the southeast. During the P15-P10 time interval the mass transport complexes that are the main focus of this study were deposited (MTC\_2, MTC\_2.1, MTC\_2.2, MTC\_2.3 and MTC\_2.4) (see Figure 3.8).

This time period was characterized by an increase in tectonic activity, and the subsequent reactivation and uplifting of the northeastern extension of the Darien Ridge. This period also defined a transitional state that finally led to the shift of sedimentation from the northwest to the central and northeastern portions of the study area (Figures 3.7C and 3.7D).

Figure 3.7: Isochron maps between key stratigraphic surfaces. A) P60-P20 interval - active sedimentation was taking place through all the area. B) P20-P15 interval - sedimentation was concentrated on the northwestern corner of the study area. The Darien and Haydn mega-chutes were active sedimentary pathways. C) P15-P10 interval – sedimentation was constrained to the northwest, the Darien and Haydn mega-chutes were still delivering sediments from the outer shelf / upper slope area (main feeders of MTC\_2.1). The Callicore Ridge started to deliver sediments towards the northeast (main feeder MTC\_2). D) P10-P4 interval – the main axis of deposition was completely shifted towards the northeast. The Callicore and Catfish mega-chutes were the only active sedimentary pathways delivering extrabasinal sediments towards the deep-marine environments. During this time period MTC\_1 was deposited (Moscardelli et al., 2006) E) P4-P0 interval – Last stage of basin infilling, the Callicore mega-chute appears to be the only active sedimentary pathway at this time. The uplifting of the northern region of the study area caused the deflection of the main depositional axis towards the east. This interval was dominated by the deposition of levee-channel complexes (Mize et al., 2004; Moscardelli et al., 2006). F) Northwest-southeast regional section showing the intervals that correspond to the isochron maps.



### **P10-P4 Time Interval**

The location and distribution of the main depocenters in the isochron map of the P10-P4 time interval (Figure 3.7D) greatly differs from the previous configurations of the basin. In this map, the northwestern depocenter is not existent and two new depocenters are observed in the central and southeastern corner of the data set. The central depocenter is located to the south of the Haydn Ridge and it runs parallel to the Callicore Chute. The second depocenter is located in the southeastern corner of the data set, next to the Heliconius Ridge and its axis parallels the Cat Fish Chute (Figure 3.7D). In both depocenters, the thicker intervals vary from 200 to 300 milliseconds (from 150 m to 225 m) and span from the shelf edge (southwest) to beyond the data extent (north/northeast). These depocenters were filled up by the vertical accumulation of sediments associated with slope- and shelf- attached gravity induced deposits.

The P10-P4 isochron map (Figure 3.7D) also shows a general thinning of the stratigraphic succession located in the northwestern corner of the data set, as well as an increase in the areal extension of the relative highs associated with the Darien Ridge. This relative uplifting of the Darien Ridge can be associated with the advances of the deformational front towards the southeast.

During the P10-P4 time period (Figure 3.7D), the bulk of the sedimentation was completely shifted from the northwest to the central and southeastern parts of the study area. The Callicore and Catfish mega-chutes acted as main sedimentary conduits for shelfal sediments to reach the deep water settings. This shift was the result of the reactivation of the deformational front and its migration towards the southeast. The northwestern unconfined mini-basins were completely filled up with sediments and the Darien and Haydn mega-chutes were inactive at this time. During P10 time, mass transport complex MTC\_1 was deposited (Moscardelli et al., 2006). Figure 3.7D clearly

shows that the eastern and southeastern regions of the study area evolved from restricted confined mini-basins (compare to P60-P20 time interval, see Figure 3.7A) to unconfined mini-basins that were receiving active extra basinal sedimentation (shelf- and slope-attached systems).

#### **P4-P0 Time Interval**

During the P4-P0 time interval the bulk of sedimentation was concentrated in the central depocenter located to the south of the Haydn Ridge (Figure 3.7E). The main depositional axis was parallel to the Callicore Chute and the maximum thicknesses reached the 250 milliseconds (equivalent to 188 m).

The P4-P0 interval represents the last stage of infilling of the basin (Figure 3.7E). During this time period, the Callicore mega-chute was the main sedimentary conduit connecting the outer shelf / upper slope area and the deep marine regions. The development of channelized features during this time was dominant in the region (Mize et al., 2004; Moscardelli et al., 2006), the main depositional axis of the levee channel complex was parallel to the Callicore mega-chute (northeast-southwest) (Figure 3.7E). However, the uplifting of the East Prospect ridge caused the abrupt deviation (almost 90 degrees shift) of the main depositional axis of the system towards the east. Additional channel systems were also developed during this time to the south of the Callicore Ridge. The modern seafloor (P0) shows the latest expression of this levee channel complex (Mize et al., 2004).

Today, hemipelagic sedimentation is dominant in the area, as well as local collapses from mud volcano ridges and individual mud volcanoes. Occasional collapses on the shelf edge and upper slope region due to tectonism or gas-hydrate dissociation could trigger the deposition of slope- attached mass transport complexes.

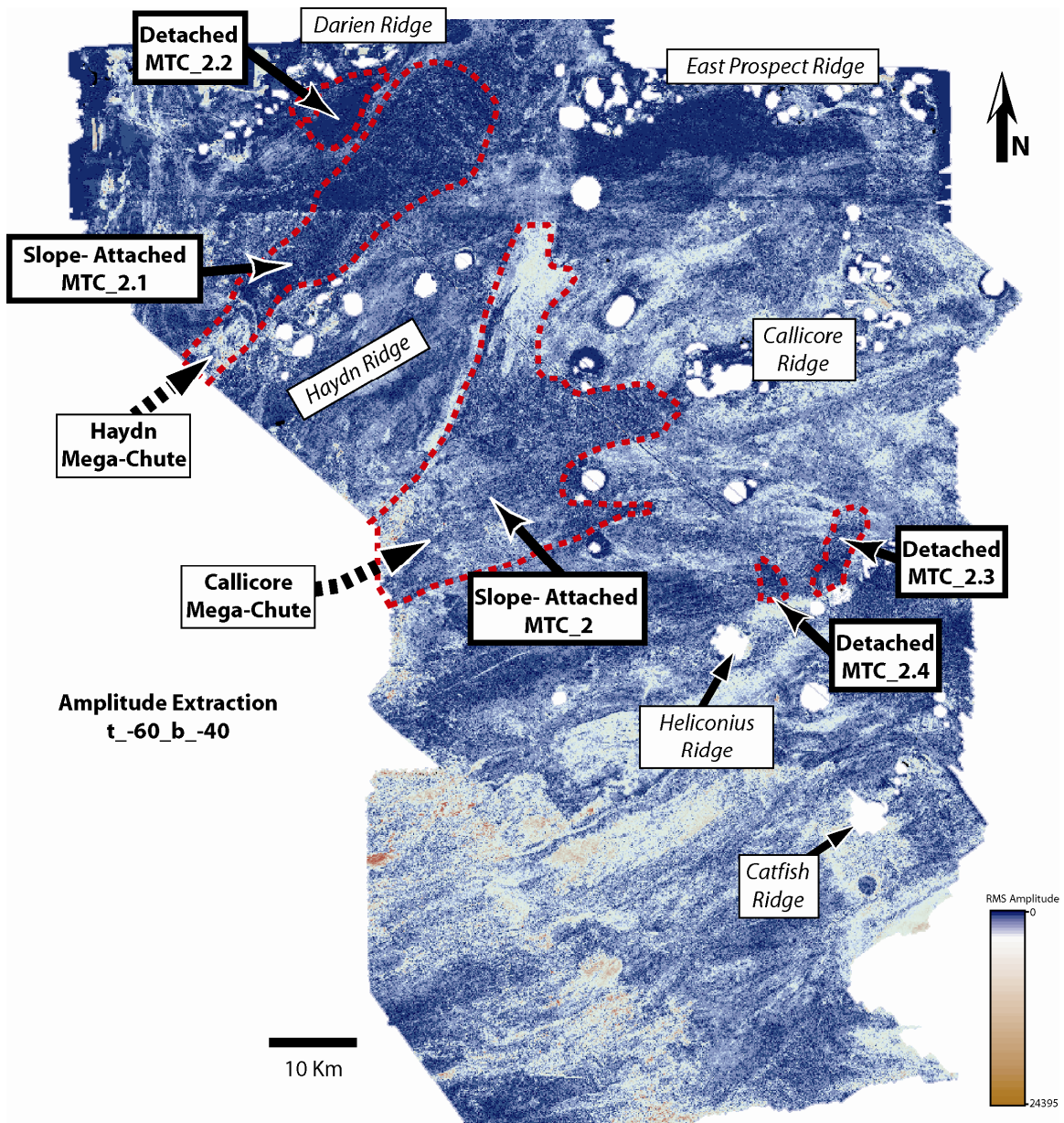


Figure 3.8: RMS amplitude extraction map showing the geomorphological expression in plan view of attached (MTC\_2 and MTC\_2.1) and detached (MTC\_2.2, MTC\_2.3 and MTC\_2.4) mass transport complexes in the study area. The RMS amplitude extraction map is from the basal portion of the P15-P10 stratigraphic interval (see Figure 3.9). Sedimentary sources of attached mass transport complexes are associated with the outer shelf / upper slope area, whereas sedimentary sources for detached mass transport complexes can be linked to the flanks of the mud volcano ridges.

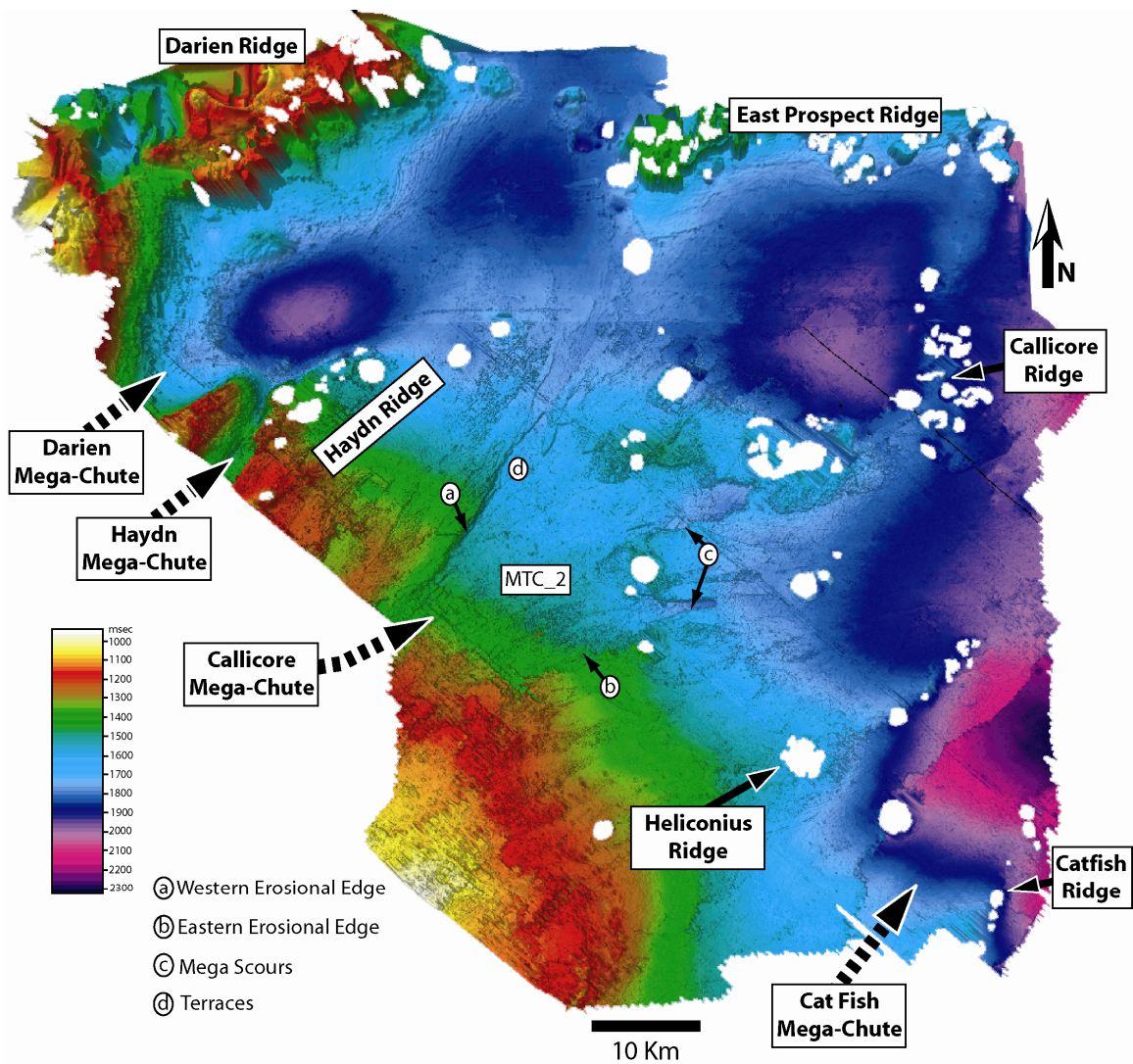


Figure 3.9: Stratigraphic surface P15, this erosional surface defines the base of the stratigraphic interval (P15-P10) that contains the mass transport complexes that are described in this chapter. Slope- attached mass transport complex MTC\_2, located in the central portion of the data set, generated more than 60 m of vertical incision in the basal portion of the P15-P10 stratigraphic interval. Some of the main geomorphological elements that are part of the basal portions of MTC\_2 include (a ,b) east and west erosional edges, (c) mega scours, and (d) several levels of terraces. Colors represent depth in milliseconds (TWTT) with shallower depths in brighter colors and deeper depths in darker colors.

### **3.5. MASS TRANSPORT COMPLEXES IN OFFSHORE TRINIDAD**

Brami et al., (2000) using shallow 3D seismic data, characterized seven principal architectural elements in the most recent deep water sequence of offshore Trinidad. These included; mass transport, confined channel, levee-channel, and distributary channel complexes, slopes with minor channels, undifferentiated slopes, and mud diatremes; mass transport complexes and levee channel complexes seem to be the dominant facies in the basin. Moscardelli et al. (2006) focused on the discussion of processes associated with the most recent mass transport complex in the same offshore area (P10-P0 time frame). In this paper we will concentrated on the description of depositional environments and processes associated with mass transport complexes deposited during the slightly older, P15-P10 time period (Figures 3.2B, 3.3C, 3.8 and 3.9).

Five separate mass transport complexes have been examined within the stratigraphic interval above the P15 surface and below the P10 surface (MTC\_2, MTC\_2.1, MTC\_2.2, MTC\_2.3 and MTC\_2.4). Figure 3.8, a root-mean squared (RMS) amplitude extraction that was obtained from a 20 millisecond window above horizon P15 (see Figure 3.4 and 3.9 for reference), clearly shows the five separate mass transport complexes that are named above, all with very different geomorphological characteristics and dimensions.

Based on the observations presented in the following paragraphs, mass transport complexes have been classified into two categories: attached MTC's and detached MTC's. In addition, attached MTC's have been subdivided into two sub-categories: shelf-attached and slope- attached MTC's (Table 3.2). This classification takes into account a series of factors that include: (1) causal mechanisms, (2) location of the source area, (3) geomorphological and morphometric dimension of the deposits, and (4) the relationship of the deposits to its source area. According to this classification, mass transport complex



MTC\_1 (chapter 2) is classified as a shelf- attached system, mass transport complexes MTC\_2 and MTC\_2.1 (this chapter) are classified as slope- attached systems, and mass transport complexes MTC\_2.2, MTC\_2.3 and MTC\_2.4 (this chapter) are classified as detached systems. Attached mass transport complexes are usually deposited in unconfined mini-basins, whereas detached mass transport complexes are deposited in confined mini-basins (Figure 3.3B).

Table 3.2: Classification, Causal Mechanisms and Source Areas of Mass Transport Complexes

Classification	Causal Mechanisms	Source Area	
<b>ATTACHED MTCs</b>	<b>Shelf- Attached MTC</b>	Relative Sea Level Fluctuations High Sedimentation Rates	Paleo-shelf edge deltas
	<b>Slope- Attached MTC</b>	Tectonism (earthquakes) Gas Hydrate Dissociation Long shore currents Storm activity	Upper slope collapses (mega cookie bites)
<b>DETACHED MTCs</b>	Gravitational instabilities on the flanks of mud volcano ridges / salt masses and levee-channel complexes: Tectonic Pulses Oversteepening Mud volcano activity /methane release	Flanks mud volcano ridges / salt diapirs / Levees	

### Attached Mass Transport Complexes

The term attached mass transport complex refers to systems which sedimentary sources are located in the outer shelf and/or upper slope areas. Attached mass transport complexes can occupied 100's to 1000's sq km in area (Table 3.2) and can transport and remobilized volumetrically significant amounts of sediments towards deep-marine depocenters. Sediments are transported downdip through mega-chutes that connect the upslope systems with unconfined mini-basins in the deep marine regions.

There are two subcategories of attached mass transport complexes, shelf- attached systems (MTC\_1) (chapter 2) and slope- attached systems (MTC\_2 and MTC\_2.1) (this chapter). In terms of their geomorphological expressions and architectural elements, these two types of mass transport complexes are quite similar in their distal areas (down-slope). However, their geomorphological characteristics greatly differ in the staging area near the paleoshelf break (upslope). These differences have been tied to a variety of causal mechanisms and source areas. In this work mass transport complexes that have been linked to sedimentary sources associated with the shelf, such as paleoshelf edge deltas, have been classified as shelf-attached systems. Mass transport complexes that have been linked to upper slope sedimentary sources, such as those associated with catastrophic collapses of the upper slope region, have been classified as slope-attached systems (Table 3.2).

### ***Slope-Attached Mass Transport Complexes (MTC\_2 and MTC\_2.1)***

Moscardelli et al. (2006) described the main geomorphological characteristics of MTC\_2 on the upper slope area near the paleoshelf break (depletion zone). According to this description, at least three consecutive collapse features can be seen along the paleoshelf break. These features, termed “cookie bite features” have a semicircular shape with average diameters of 4.5 km and average areas of 14 km<sup>2</sup>. The sediments that collapsed from the paleoshelf break / upper slope area were by-passed through the Callicore and Haydn mega-chutes as mass transport complexes MTC\_2 and MTC\_2.1 (Figures 3.2B and 3.8). According to Moscardelli et al. (2006) a tectonic event, probably associated with the area’s frequent major earthquake activity, caused the destabilization of a broad area of the upper slope and its subsequent failure.

The slope-attached mass transport complex MTC\_2 is located in the central part of the study area. The Callicore mega-chute was the main feeder of MTC\_2 (Figure 3.8

and 3.10), feeding sediment directly and consistently from the upper slope source into the deep water basin. MTC\_2 covers an approximate area of 626 km<sup>2</sup>; its average length from the upper slope area down to the east boundary of the seismic coverage (deep basin) is 40 km. The unit is likely near its terminus at this eastern point, with evidence of significant thinning and lateral dispersion of the deposit. Its width varies from a minimum of 10 km in the proximal area, widening progressively towards the northeast until it reaches a maximum width of 25 km in the distal parts of the unit. According to the seismic data, the average thickness of MTC\_2 is 60 m, however this is considered to be a minimum value because of the reductions in thickness caused by post-depositional processes such as compaction and erosion. Based on these values, the estimated minimum volume of remobilized sediments calculated for this unit is around 35 km<sup>3</sup>.

Basinward the base of MTC\_2 is defined by an erosional surface that contains a series of distinctive mega-stratigraphic features that are typical of regional mass transport complexes (Figure 3.9). These features include erosional edges, mega scours and multiple levels of terracing. Steep erosional edges that can reach 60 m in relief define the western and eastern lateral boundaries of MTC\_2. The presence of various terrace levels, located in the southern portion of the western erosional edge, suggests that several episodes of incision took place during the emplacement of MTC\_2 (Figure 3.9). Elongated mega scours that are more than 50 m deep and 4 km long surround individual mud volcanoes in the eastern portion of the unit (Figures 3.8, 3.9 and 3.10). These mega scours were formed when passing debris flows were confined by individual mud volcanoes, causing a reduction in the flow's cross sectional area and a short-term increase in the erosive power of the flow. Similar features have been described in several shelf- and slope-attach mass transport complexes around the world (Lee et al., 2004; McGilvery et al., 2004; Posamentier, 2004; Moscardelli et al., 2006).

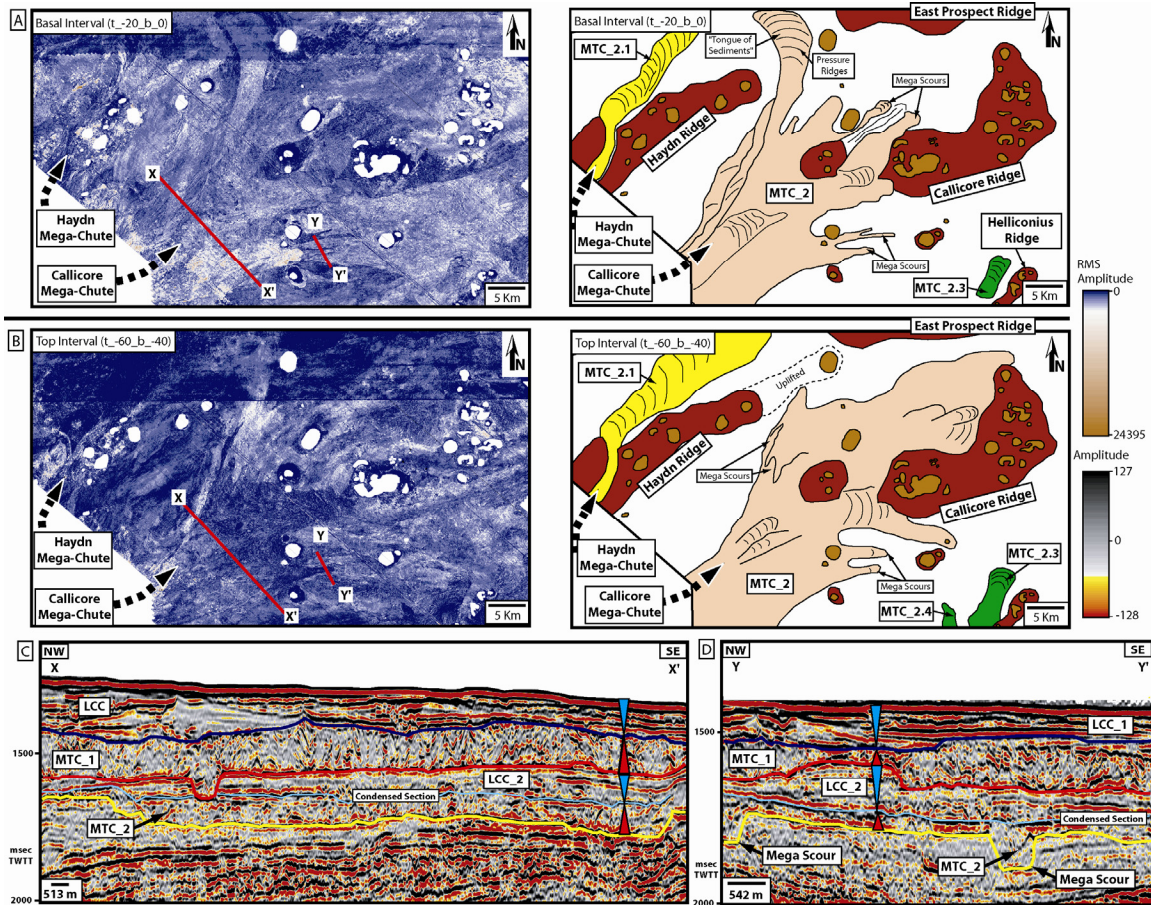


Figure 3.10: A) RMS amplitude extraction map from basal portion of MTC<sub>2</sub>. The geomorphological interpretation on the right shows a series of distinctive architectural elements that are typical of mass transport complexes (erosional edges, mega scours and different levels of terraces). To the northwest a “tongue” of sediments was detached from the main body of MTC<sub>2</sub>. B) RMS amplitude extraction map from the upper portion of MTC<sub>2</sub>. The geomorphological interpretation on the right shows the increment of the areal extension of MTC<sub>2</sub> during this later phase. During this phase sedimentation was diverted towards the northeast occupying areas to the north of the Callicore Ridge. C) Northwest-southeast seismic line showing the main depositional units in the youngest portion of the deep water stratigraphic succession in offshore Trinidad. Notice the incision caused by the MTC<sub>2</sub> event and the erosional edges that define its western and eastern boundaries. D) Northwest-southeast seismic line showing the additional incision generated in areas of scouring.

RMS amplitude extractions that were taken in different stratigraphic levels within MTC\_2 (Figure 3.4), document two main phases of this unit's evolution. Phase 1 (Figure 3.10A) is associated with the initial erosional processes that generated the basal surface of MTC\_2. During this time period of vertical and lateral erosion by the system, several mega-scours were generated around individual mud volcanoes (Figure 3.10A) and successive episodes of incision were responsible for the generation of different levels of terraces in the southwestern margin of the Callicore mega-chute (Figure 3.9). Sediments were transported from the southwest to the northeast, parallel to the main axis of the Haydn and Callicore ridges. The bulk of sediments were deposited between these two major mud volcano ridges (Figures 3.8, 3.9 and 3.10A). However, during Phase 1 a portion of the sediments were diverted towards the northwest through a relative low that was located between the Haydn and East Prospect ridges and that allowed a "tongue" of sediments to spread through this opening (Figure 3.10A). This elongate flow of sediments has a length of 15 km that extends from the western margin of the main body of MTC\_2 to its terminal end to the northwest (Figure 3.10A). Near the main body of MTC\_2, the width of the "tongue" of sediments is 1 km. It widens towards the northwest to a width of 4 km. In the northwestern termination of the "tongue" of sediments a series of pressure ridges can be observed in the RMS amplitude extraction map, these features are typical in terminal lobes of debris flows (Figure 3.10A). Similar pressure ridges have been described in the terminal ends of MTCs in offshore Morocco (Lee et al., 2004), offshore Brunei (McGilvery et al., 2003) and in the Nigerian continental slope (Nissen et al., 1999).

Phase 2 represents the final stages of evolution of MTC\_2. RMS amplitude extractions that were taken through the top portion of MTC\_2 (Figure 3.10B) show an increase in the areal extent occupied by the amplitude anomalies that have been

associated with MTC seismofacies. The RMS amplitude extraction map of this interval (Figure 3.10B) shows high amplitude lineations that diverge from one another as you follow them to the north and northeast, such patterns are interpreted as indicating lateral spreading of the sediments in the northern portions of the Callicore Ridge. The “gateway” that allowed the “tongue” of sediments to move towards the northwest during phase 1 (Figure 3.10A) has become inactive during this time. The interruption of sediment supply towards the northwest through the “sediment gateway” could be originated by a series of factors including: (1) the reactivation of the Haydn ridge and the subsequent uplifting of its northeastern termination, resulting in a closing of the gateway and/or (2) the obstruction of the gateway entrance located between the Haydn and East Prospect ridges by the sediment excess deposited during phase 1. Of these two hypotheses, the reactivation and relative uplifting of the Haydn Ridge due to the migration of the deformational front towards the southeast is most likely to be the cause of this interruption of sediment supply towards the northwest (Figure 3.10B). Therefore, during phase 2 an important portion of the active sedimentation that had taken place in this area shifted towards the northeast where these sediments started to fill up the region located to the north of the Callicore Ridge (Figure 3.10B). Internally, additional mega-scours were formed between the western erosional edge and individual mud volcanoes that were located in the central part of MTC\_2. Similarly to the mega-scours that were described in phase 1, these features were generated due to the reduction in cross sectional area between the erosional edge and the individual mud volcanoes. This reduction caused an increase of the frictional forces that were affecting the basal portions of the flow prompting vertical incision and development of drag marks from the movement of huge chunks of lithified rock in the base of the flow (Figure 3.10C and 3.10D).

The slope- attached mass transport complex (MTC\_2.1) is located in the northwestern corner of the study area, between the Darien and Haydn ridges (Figures 3.8 and 3.11). Similarly to MTC\_2, sediments from the upper slope area were transported from the southwest to the northeast through the Haydn mega-chute into the deep marine settings (Figure 3.2B). The main geomorphological difference between this system (MTC 2.1) and MTC\_2 is that MTC\_2.1 presents a more elongated morphology in plan view (Figure 3.8 and 3.11). The elongated geometry of MTC\_2.1 suggests a major degree of lateral confinement during the time of deposition.

The basal and upper parts of MTC\_2.1 are separated by a seismically prominent reflector that is well preserved in the downslope portions of the basin, but abruptly onlaps the Haydn Ridge and disappears in the upslope direction (Figure 3.12A). This reflector is interpreted to be caused by the presence of a condensed section, similar to that described by Lee et al. (2004) in the Tejas A mass transport complex in offshore Morocco. The presence of the condensed section means that a significant time break occurred between the deposition of the basal and upper portions of MTC\_2.1. According to Lee et al. (2004) these condensed sections have the capacity to provide the initial surfaces across which the mass failure destabilizes and slides. The surfaces are often destroyed by the initial erosional processes associated with mass transport complex development.

RMS amplitude extractions taken from different seismic time intervals within the MTC 2.1 unit reveal two main stages of development. An amplitude extraction taken over the basal portion of MTC 2.1 (phase 1) (Figure 3.11) revealed the geomorphological character of MTC\_2.1 during its first stages of development. Figure 3.11 shows MTC\_2.1 during this phase as a northeast-to-southwest elongated body that internally presents a series of closely-spaced pressure ridges. During this phase the unit was approximately 20 km long, 3 km wide and covered an approximate area of 60 km<sup>2</sup>.

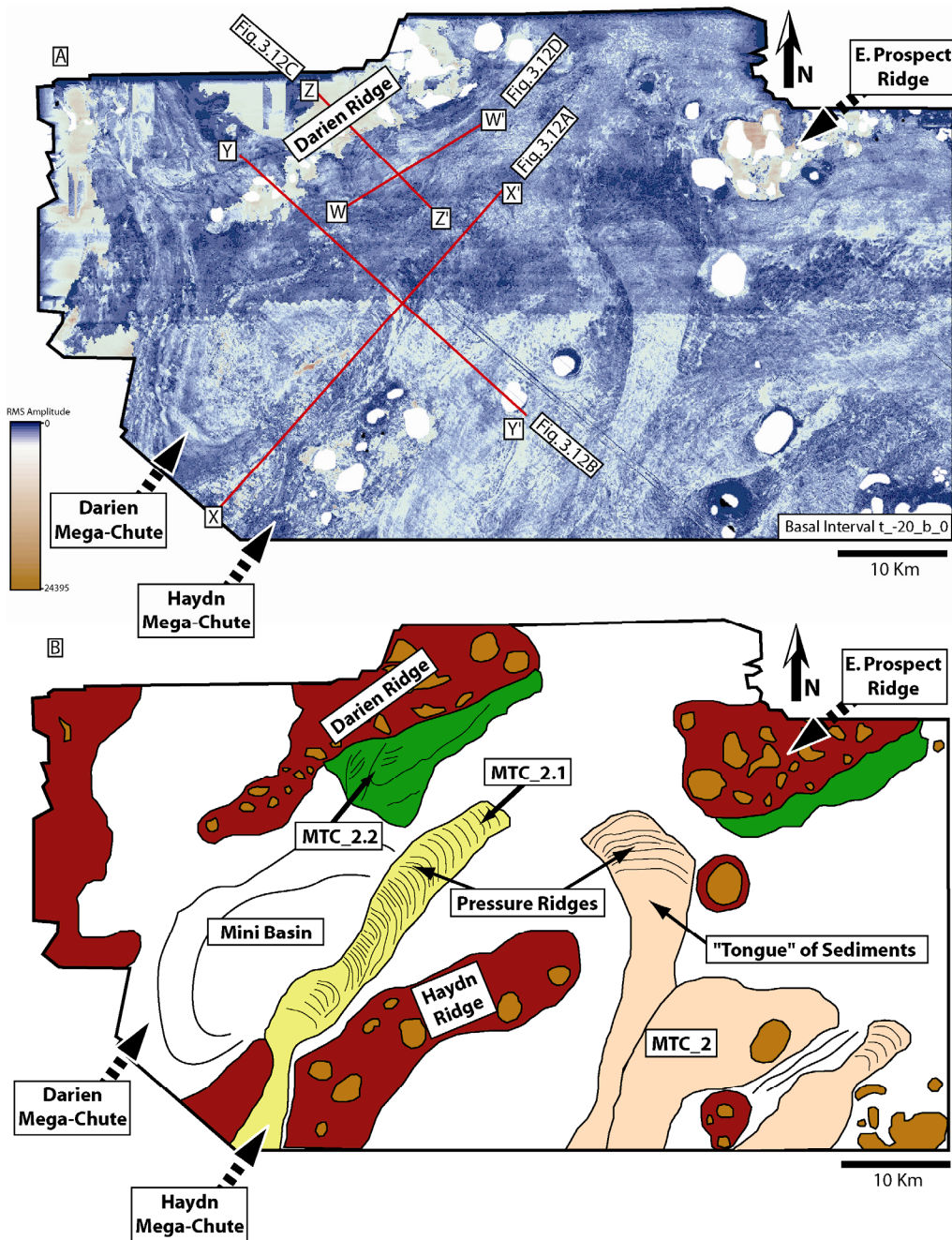
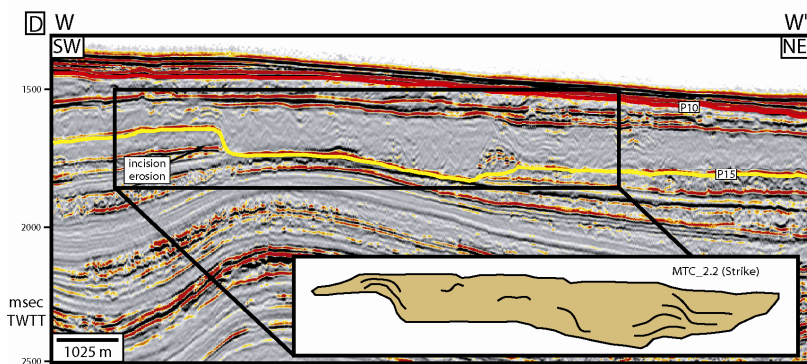
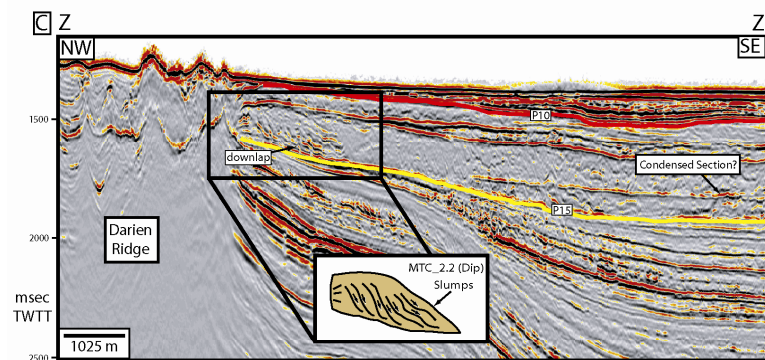
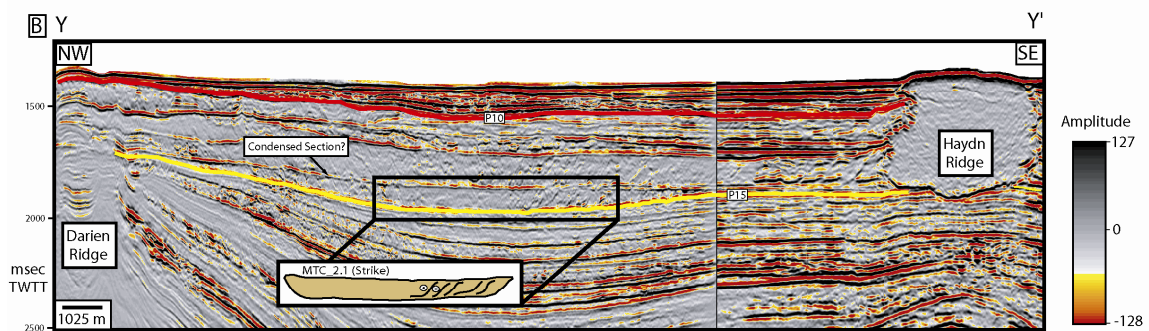
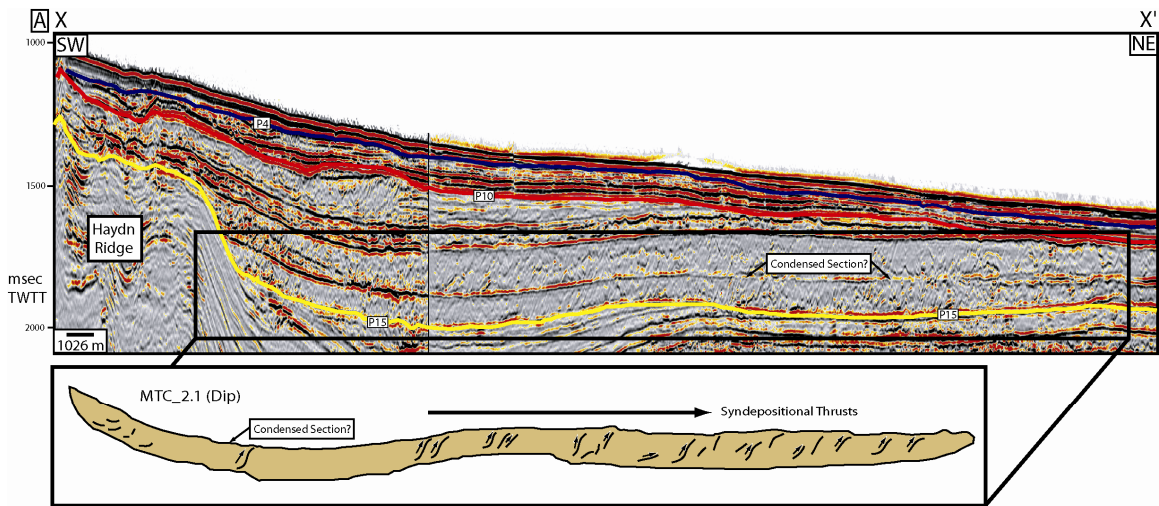


Figure 3.11: A) RMS amplitude extraction map from the basal portion of the P15-P10 stratigraphic interval. B) Geomorphological interpretation of the MTC\_2.1 and MTC\_2.2 mass transport complexes. MTC\_2.1 was fed by extrabasinal sediments that were transported downdip by the Haydn mega-chute. On the other hand, the sedimentary source of MTC\_2.2 was associated with the southern collapsed flank of the Darien Ridge.



Figure 3.12. A) Northeast-southwest seismic line parallel to the depositional dip of MTC\_2.1. The basal and upper parts of MTC\_2.1 are separated by a seismically prominent reflector (condense section) that onlaps against the Haydn Ridge. B) Northwest-southeast seismic line parallel to the depositional strike axis of MTC\_2.1. C) Northwest-southeast seismic line to the depositional dip of MTC\_2.2. The line shows slumped material that failed downslope, the top half of the unit is comprised of low amplitude, chaotic reflectors, but the internal character of the lower half of the unit shows small fragments of continuous high amplitude reflectors that appear to be downsloping onto the P15 basal surface. This seismic character and geometry is typical of slumps. D) Northeast-southwest seismic line parallel to the depositional strike of MTC\_2.2. This line shows vertical incision and erosion affecting the basal surface of MTC\_2.2.



An amplitude extraction near the top of MTC\_2.1 (phase 2) (Figure 3.13) shows the upper deposits to have a slightly different geomorphological character. The upper deposits are more aerially extensive than the lower deposits. Although its elongated geometry is preserved in the proximal (southwest) portions of the deposit, this unit shows a more lobate shape in the distal (northeast) terminal locations (Figure 3.13). The length of the upper unit (phase 2) is 38 km, showing an increase of 18 km compared to the length of the underlying lower unit (phase 1) (Figure 3.11). The width of the upper deposit is 3.5 km in proximal areas and 10 km in distal areas (Figure 3.13). Once again the deposit is widening in its late stages (upper unit, northeastern locations). The total area covered by the upper unit is approximately 100 km<sup>2</sup>, and the total remobilized volume of sediments was estimated on 7 km<sup>3</sup>.

The first stages of infilling for MTC\_2.1 were greatly influenced by the presence of the mud volcano cored, Haydn ridge. This ridge acted as a strong physiographic barrier that constrained the gravity flows to the northwest, within the Haydn mega-chute (Figure 3.11). However, during Phase 2 the flow reached the northeastern terminus of this relative confined mini-basin where more accommodation space was available, thus allowing the lateral spreading of sediments (Figure 3.13).

### ***Shelf- Attached Mass Transport Complex (MTC\_1)***

Mass transport complex MTC\_1 is the shallowest mass transport complex in the study area, it is younger than any of the MTCs described within the P15-P10 time interval and it was described in detail in chapter 2. MTC\_1 was point source fed by a single paleocanyon graben nearly 200 m deep, that was bounded along both margins by normal faults. The paleocanyon, less than 2 km wide on its upper section (updip), widens downslope, reaching more than 10 km on its lower end (toe of the slope). This paleocanyon captured sediments directly from aggradational clinoforms associated with a

paleo-Orinoco shelf edge delta. The aggradational character of the clinoforms was interpreted to reflect the response of the shelf-edge delta to a rising shoreline following lowstand conditions.

MTC\_1 covers an approximate area of 2017 km<sup>2</sup>; its average length from the upper slope area down to the east boundary of the seismic coverage (deep basin) is 140 km. The estimated volume of remobilized sediments is 242 km<sup>3</sup> and the maximum thickness in its core area is 250 m. Similarly to the erosional morphologies described for MTC\_2 and MTC\_2.1 (this chapter), MTC\_1 presents a series of geomorphological features that include an erosional escarpment, deep basal scours, and pressure ridges. In addition, multiple cat-claw scours, erosional shadow remnants (ESRs), smaller scale scratch marks, and imbricated thrust complexes were reported within MTC\_1 (see detailed description in chapter 2).

#### **Detached Mass Transport Complexes (MTC\_2.2, MTC\_2.3 and MTC\_2.4)**

Detached mass transport complexes cover significantly smaller areas than the shelf-attached and slope-attached mass transport complexes (Table 3.3). These systems are fed by localized source areas within the confine mini-basins and do not have a continuous influx of shelf- or slope- derived, extra-basinal sediments (Table 3.2). Detached mass transport complexes are formed when instabilities in the flanks of the confine mini-basin walls trigger partial collapses generating cascading debris flows or slumps (Figures 3.11A and 3.12C). These instabilities can be generated by progressive increases in the steepness of the flanks of the confine mini-basins or by tectonic instabilities. In our specific study area, mud volcano eruptions and regional earthquake forces play a strong role in mini-basin wall failures. Three detached mass transport complexes were identified in the study area (MTC\_2.2, MTC\_2.3 and MTC\_2.4) and their main geomorphological and morphometric characteristics are described below.

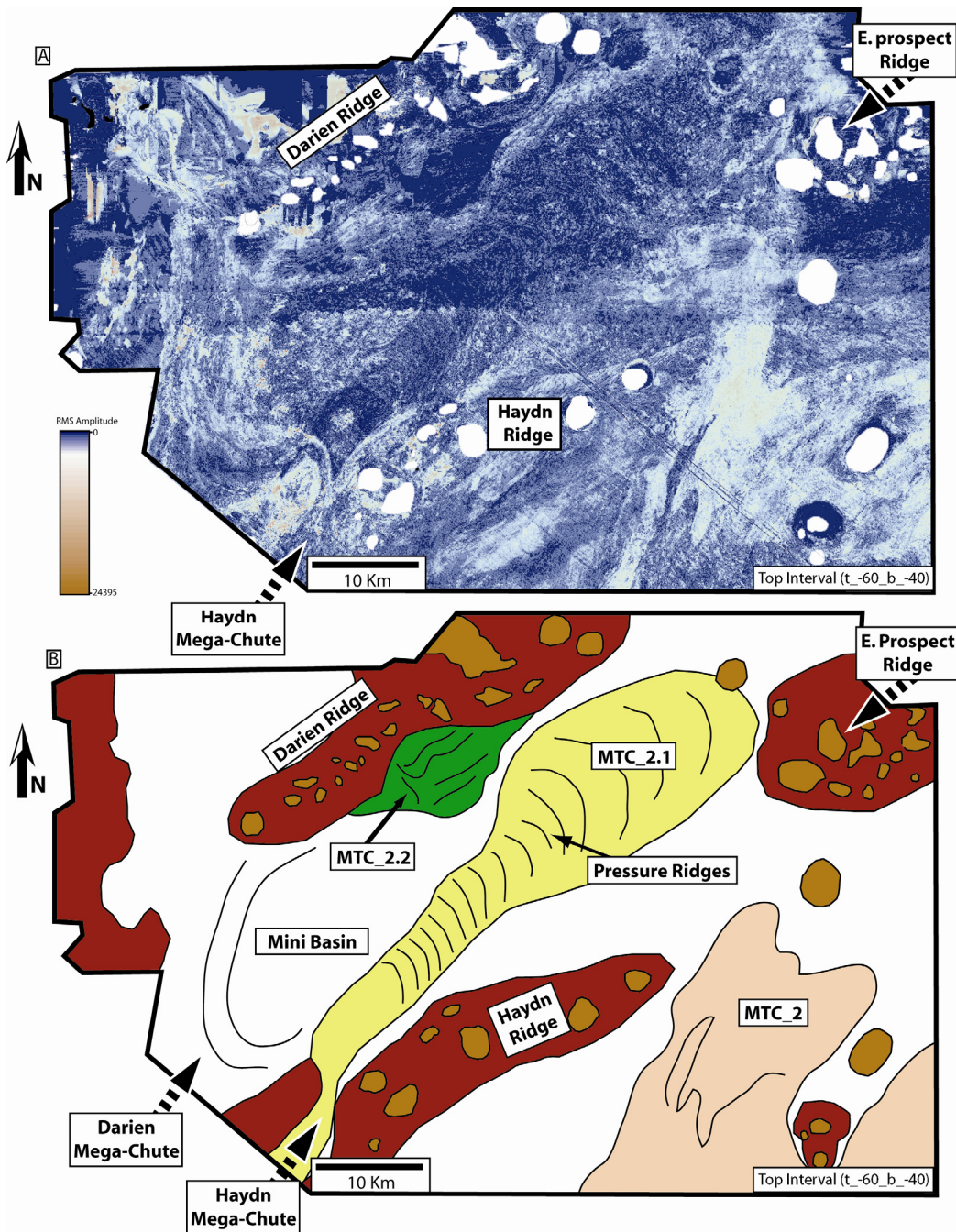


Figure 3.13: A) RMS amplitude extraction map near the top of the MTC\_2.1 mass transport complex. B) Geomorphological interpretation of MTC\_2.1 and MTC\_2.2 mass transport complexes. The upper portion of MTC\_2.1 is more aerially extensive than its lower portion. The elongated geometry of MTC\_2.1 is preserved in the proximal portion of the deposit, but it shows a more lobate shape in its distal termination.

Table 3.3: Classification and Morphometry of Mass Transport Complexes in Offshore Trinidad

Classification	MTC	Area (Km <sup>2</sup> )	Length (Km)	Width (Km)	Thickness (m)	*Volume (Km <sup>3</sup> )	Length / Width
<b>Attached MTCs</b>	<b>Shelf-Attached MTC</b> MTC_1	2017	140	25	< 250	~ 242	<b>5.6</b>
	<b>Slope-Attached MTC</b> MTC_2	626	40	10 - 25	> 60	> 35	<b>4 – 1.6</b>
	MTC_2.1	60 - 100	20 - 38	3 - 10	> 60	> 7	<b>6.6 – 3.8</b>
<b>Detached MTCs</b>	MTC_2.2	22	5.6	5.5	150	3.3	<b>1.08</b>
	MTC_2.3	21.4	8.7	3	136	3	<b>2.9</b>
	MTC_2.4	11.3	5.4	2.5	98	1	<b>2.16</b>

\*Estimated

Figure 3.8 shows the relative location of all the detached mass transport complexes that have been identified in the study area. Detached mass transport complex MTC\_2.2 is located along the southern flank of the Darien Ridge in the northwestern corner of the 3D mega merge (Figures 3.11 and 3.13). MTC\_2.3 and MTC\_2.4 are both located along the northern flank of the Heliconius Ridge (Figure 3.8 and 3.14A) in the southeastern corner of the study area. Based upon closely spaced amplitude extractions (Figure 3.10) MTC\_2.3 appears to be slightly older than MTC\_2.4, with MTC\_2.3 appearing along the flanks of the Heliconius Ridge earlier than MTC\_2.4.

Figure 3.8 also helps to visually appreciate the differences in terms of areal extension and plan view geometries between the detached and attached mass transport complexes. The areas covered by the detached mass transport complexes range from 11 to 22 km<sup>2</sup>, and their thicknesses from 98 to 150 m. The estimated volume of remobilized sediments that collapsed from the flanks of the mud volcano ridges is in between 1 to 3 km<sup>3</sup> (Table 3.3).

RMS amplitude extractions guided by the P15 horizon in the basal portion of the detached mass transport complexes revealed that MTC\_2.2 has a lunate shape in plan view (Figure 3.13), whereas MTC\_2.3 and 2.4 have a more elongated geometry. These units also have a series of common geomorphological characteristics, seismic lines that

are parallel to the depositional strike axis of the detached mass transport complexes (Figures 3.12D, 3.14C and 3.14E) show vertical incision and erosion affecting the basal surfaces of all the detached mass transport complexes. An RMS amplitude extraction map on the top portion of MTC\_2.3 (Figure 3.14A) also shows a series of concentric amplitude anomalies located on the northeastern termination of the MTC\_2.3 lobe. These concentric anomalies are the plan view expression of terminal syndepositional thrusts. A seismic line parallel to the depositional dip axis of MTC\_2.3 shows the cross sectional expression of these thrust structures (Figure 3.14B). The same seismic line shows that the proximal part of MTC\_2.3 is composed of a series of slumps (Figure 3.14B). Similar syndepositional thrusts and slumps have been interpreted in the updip and downdip portions of MTC\_2.2 and MTC\_2.4 (Figures 3.12C and 3.14D).

The sediments that form the detached mass transport complexes are collapsed sediments derived from the mud volcano ridges that were transported down the flanks to the mini-basins. Extensional forces associated with gravitational instabilities that affected the upper portions of the flanks of the mud volcano ridges caused the initial slumping that triggered the formation of the detached mass transport complexes. The collapse materials moved downslope and reached a transitional state where flow transformations started to occur. The decrease in slope angles, the loss of cohesiveness and a lack of space to accommodate the upcoming volume of sediments eventually caused the desacceleration of the flow and the formation of syndepositional thrusts that compensate for the lack of space in the distal ends of the detached mass transport complexes. The flow direction followed by the collapsed sediments that form the detached mass transport complexes is mainly controlled by the geometry and changes in slope gradients that take place in the flanks of the mud volcano ridges.

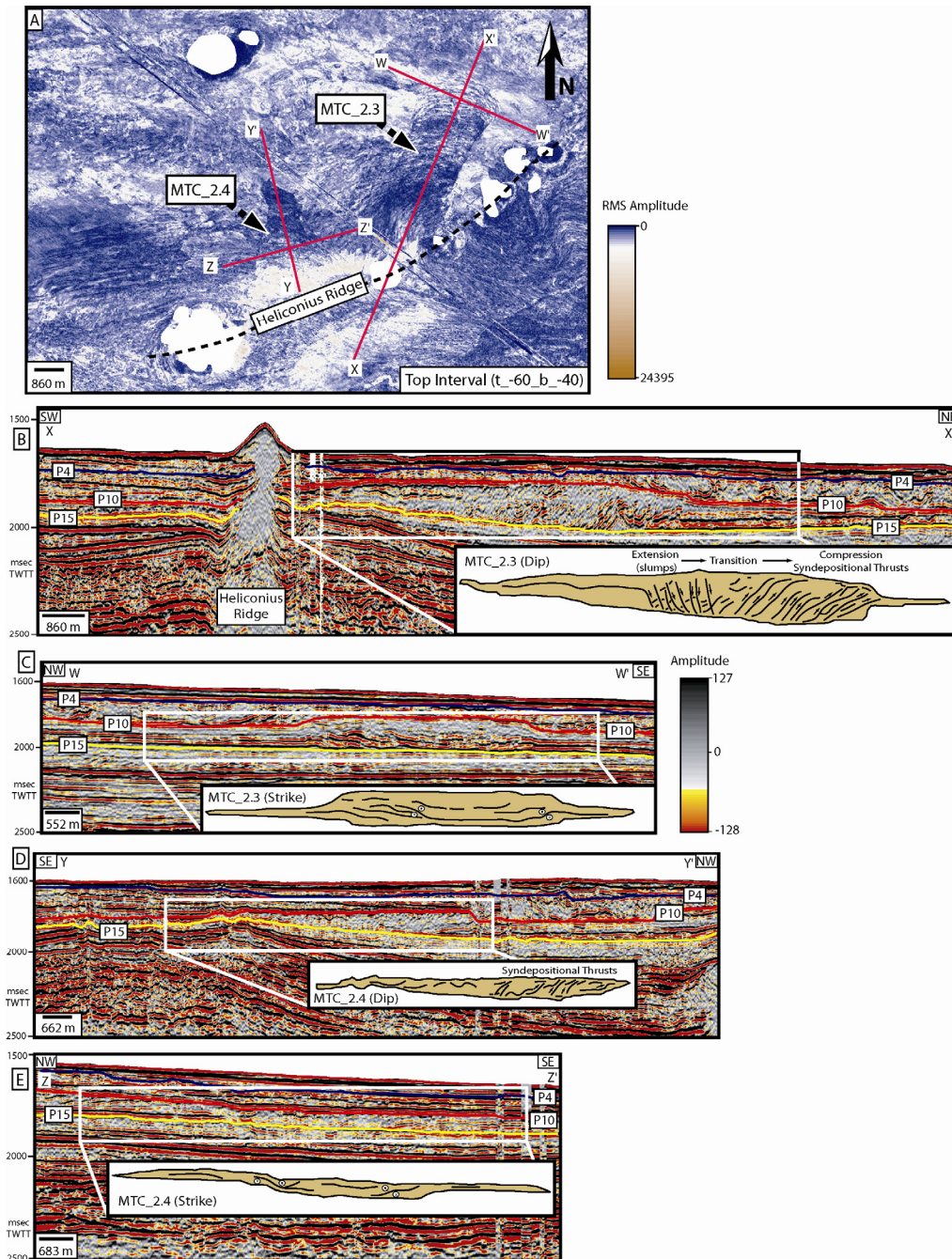


Figure 3.14: A) RMS amplitude extraction map near the top of mass transport complexes MTC\_2.3 and MTC\_2.4. Both detached MTCs are derived from the northern flank of the Heliconius Ridge. B) Northeast-southwest seismic line parallel to the depositional dip of MTC\_2.3. Notice the slumps on the southwestern portion of the mass transport complex and the syndepositional thrusts on its northeastern termination. C) Northwest-southeast seismic line



parallel to the depositional strike of MTC\_2.3. D) Northwest-southeast seismic line parallel to the depositional dip of MTC\_2.4. Syndepositional thrusts can be interpreted on its northwestern termination. (E) Northwest-southeast seismic line parallel to the depositional strike of MTC\_2.4.

### **3.6. MORPHOMETRY OF MASS TRANSPORT COMPLEXES**

Regionally, extensive, attached mass transport complexes can occupy 100's to 1000's of square kilometers in area (A) and 10's of kilometers in length (L). On the other hand, detached mass transport complexes tend to occupy less than 10's of square kilometers in area and only a few kilometers in length (Table 3.3). It is important to point out that the length and the run-out distance of mass transport complexes are not necessarily synonymous terms. In this work, the length is measured based on the area that has been affected by the mass wasting process. However, the run-out distance is defined as the horizontal distance that a single particle within the mass transport complex has traveled through, from its staging area or original location to its final site of deposition (Figure 3.15). In some instances these two parameters can coincide but not always. Therefore, the length measured in both attached and detached mass transport complexes represents a possible maximum value for run-out distance. Due to their areal extension and complexity, different portions of the flow within a single mass transport complex event can present different run-out distances. In order to accurately determine the run-out distances of mass transport complexes; it is necessary to study the geometry of kinematic indicators such as mega scours, rafted blocks and syndepositional thrusts (Figure 3.15). This topic is beyond the scope of this work, but it will be addressed in future research.

The width (W) of mass transport complexes is an important morphometric parameter that needs to be taken into consideration during the analysis of these units. The width values of mass transport complexes can vary from a couple of kilometers to 10's of kilometers. This particular morphometric parameter is highly dependant on the nature of

the deposits (attached versus detached systems), the slope across which it is being moved and deposited, and the relationship with surrounding bathymetry (unconfined versus confined basins). The length / width (L/W) ratio of these deposits can be used to differentiate attached from detached mass transport complexes. According to our data, L/W ratios that are greater than 4 are characteristic of attached mass transport complexes that have been deposited in partially unconfined mini-basins, and L/W ratios that are lower than 4 are indicative of detached mass transport complexes that have been deposited in confined mini-basins (Table 3.3). Likewise the sediment transport relationship with the deposit and the continental shelf has a great influence on the material makeup of the flow deposit.

### **3.7. CLASSIFICATION OF MASS TRANSPORT COMPLEXES AND CAUSAL MECHANISMS**

In terms of causal mechanisms, attached mass transport complexes are triggered by regional events such as a major earthquake, relative sea level fluctuations, gas hydrate dissociation, high sedimentation rates (e.g. shelf edge deltas), and persistent long shore currents. All these elements have in common their capacity to destabilize the outer shelf / upper slope areas causing massive collapses that are responsible for the initiation of mass wasting processes. The sedimentary sources of shelf- attached mass transport complexes are usually associated with shelf edge deltas that are controlled by sea level fluctuations and high sedimentation rates (Table 3.2). Good examples of shelf- attached mass transport complexes are the MTC\_1 event in offshore Trinidad (chapter 2) and the Eastern and Western Debris Flows in offshore Brazil (Maslin et al., 2005). Both of these systems were generated during relative sea level rise or still stand conditions. The increase in the sediment discharge of the paleo- Orinoco and Amazon rivers, necessary condition to boost the sedimentation rates in the paleo- Orinoco and Amazon shelf edge deltas, could have been caused by the deglaciation of the Andes during green-house times

(Thompson et al., 1995; Maslin et al., 2005). Another good example of a shelf- attached mass transport complex was documented in an outcrop by Pickering and Corregidor (2005) in the Ainsa Basin in the Spanish Pyrennes (Figure 3.1), this particular unit was described as a multiphase granular flow associated with extraformational material derived from the shelf and from fluviodeltaic input.

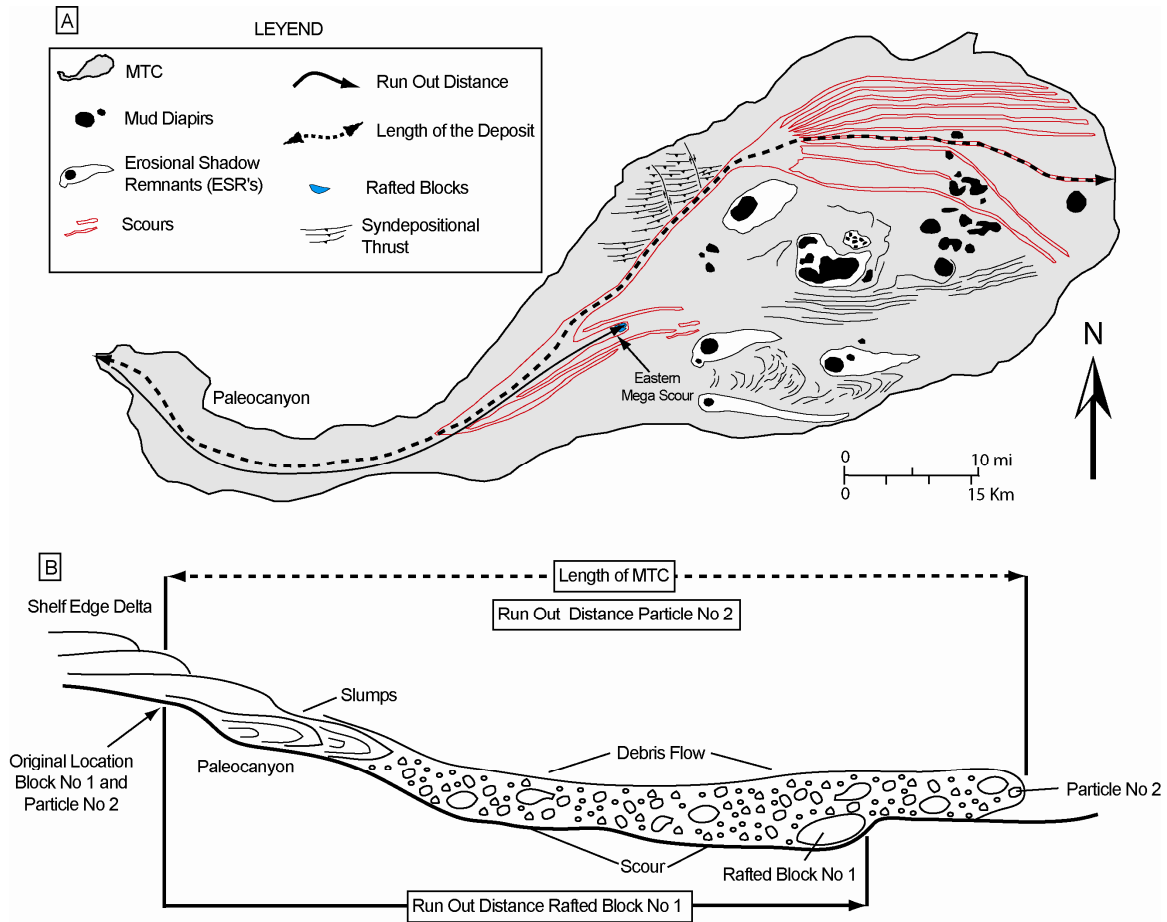


Figure 3.15: A) Geomorphological interpretation of MTC\_1 in offshore Trinidad (Moscardelli et al., 2006). Dotted line represents the length of the deposit and the maximum possible run out distance for a particle. Continuous line parallel to the main axis of the paleocanyon and to the eastern mega scour represents the run out distance of a rafted block B) Schematic cross section showing the difference between length of the deposits and run out.

In contrast to shelf-attached MTCs, the sedimentary sources of slope- attached mass transport complexes are associated with catastrophic collapses of the upper continental slope. Processes associated with upper slope collapses include earthquakes, long shore currents and gas hydrate dissolution. Gas hydrate destabilization can also be caused by rapid episodes of relative sea level fall as was suggested by Maslin et al. (2005) in the continental margin off Brazil. In addition to the slope-attached mass transport complexes that have been documented in this work (MTC\_2 and MTC\_2.1), the glacial mass transport complexes (Deep Earth MTD and Unit R MTD) located in offshore Brazil (Maslin et al., 2005) can also be classified as slope-attached systems. The Deep Earth MTD and Unit R MTD were deposited during periods of rapidly sea level falling that occurred between 35 and 37 ka and between 41 and 45 ka respectively (Shackleton, 1987; Flood et al., 1995). The accelerated rates of relative sea level fall associated with these events reduced the hydrostatic pressure and destabilized the gas-hydrate reservoirs on the continental slope causing the subsequent failure of the North Brazilian margin (Maslin et al., 2005).

Alternatively, triggering mechanisms of localized detached mass transport complexes depend more on local gravitational instabilities that occur on the flanks of mud or salt masses, along the flanks of specifically steep canyons and distal mini-basins, or along the flanks of levees in levee-channel complexes. Attached mass transport complexes tend to be link to paleo-shelf edge deltas and to the outer shelf / upper slope systems. However, in the case of detached mass transport complexes most of the sediments are derived locally within the mini-basin of deposition (Table 3.2). In offshore Trinidad, detached mass transport complexes are derived from the flanks of mud volcano ridges (MTC\_2.2, MTC\_2.3 and MTC\_2.4), but they can be originated from any paleobathymetric high in the sea-floor. In the offshore region of the Gulf of Mexico,

detached mass transport complexes can originate from the flanks of salt masses and from the relative bathymetric highs that define the boundaries of distal mini-basins (Posamentier, 2004; Weimer and Shipp, 2004; Montoya, 2006). Pickering and Corregidor (2005) studying the Ainsa submarine fan, also (Figure 3.1) stratigraphic units composed of local slides that can reach 10's of meters in thickness. These units are associated with collapses in channel margins and are characterized by intraformational material.

### **3.8. CONCLUSIONS**

Three different types of mass transport complexes have been identified in the study area of offshore Trinidad and mapped using an extensive 3D seismic data volume (Figure 3.16). These three types include: (1) Regional, shelf- attached mass transport complexes (MTC\_1) (described in chapter 2), (2) Regional, slope- attached mass transport complexes (MTC\_2 and MTC\_2.1), and (3) Detached mass transport complexes (MTC\_2.2, MTC\_2.3 and MTC\_2.4). Attached mass transport complexes are regional units that can reach 1000's of square kilometers in area and 100's of meters in thickness; their source areas are usually associated with extra-basinal systems such as shelf edge deltas and zones of collapse in the upper slope region. Causal mechanisms associated with regional attached mass transport complexes include large scale earthquakes, relative sea level fluctuations, gas hydrate dissociation, high sedimentation rates and long shore currents, all these elements can potentially destabilize the upper slope area and trigger mass wasting processes. Regional attached mass transport complexes have been subdivided into shelf- attached and slope- attached systems, this classification was made base on differences associated with the geomorphology and morphometric parameters that characterize each system.

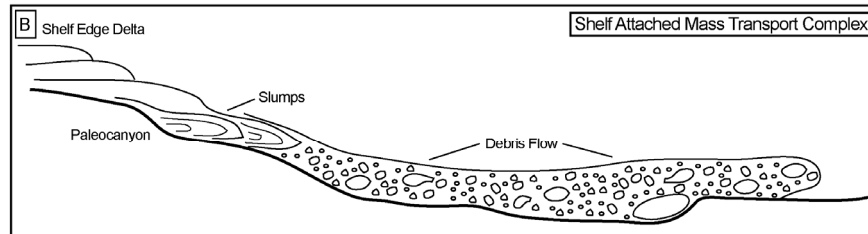
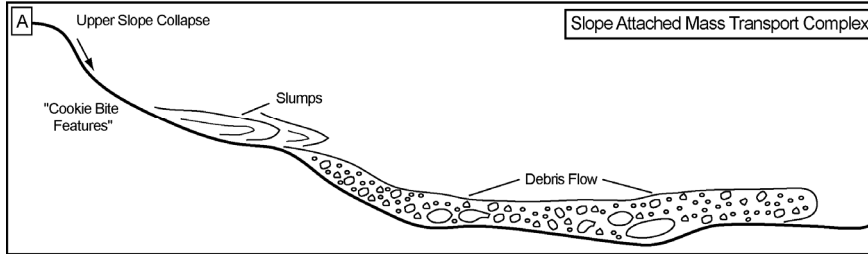
Detached mass transport complexes are smaller; they can occupy 10's of square kilometers in area and the source areas are usually constrain within the margins of the

mini-basin. Collapsed flanks of mud volcano ridges, instable margins of deep water mini basins, and overstep levees in levee-channel complexes are common sources of sediments for detached mass transport complexes. These systems are triggered by local gravitational instabilities that can be associated with small tectonic pulses, oversteepening or mud volcano reactivation.

The length / width ratio ( $L / W$ ) of mass transport complexes is an important morphometric parameter that can be used to determine the level of confinement of mass transport complexes. Length / Width ratios that are greater than 4 are indicative of regional attached mass transport complexes, whereas  $L / W$  ratios that are lower than 4 are characteristic of confined detached mass transport complexes.

Within the study area, large, buckle-fold ridges represent a major control in the definition of sedimentary pathways that are responsible for funneling sediments from the outer shelf / upper slope area to the deep marine basin. These ridges often show mobile muds associated with their core and display significant mud-volcano trains along their crests. In the study area, six ridges have been identified as the main paleobathymetric features that controlled the sedimentation in this region during the Tertiary: (1) Darien Ridge, (2) Haydn Ridge, (3) Callicore Ridge, (4) Heliconius Ridge, (5) Catfish Ridge, and (6) East Prospect Ridge. However, only four major sedimentary pathways associated with these ridges have been identified as main conduits of extra-basinal sediments to the deep marine basin: (1) Darien Mega-chute, (2) Haydn Mega-chute, (3) Callicore Mega-chute, and (4) Catfish Mega-chute. Such ridges and intervening chutes are important components in the deep marine transport systems, affecting the nature of MTC run-out pathways, the thickness of deposits and their linkages to shelf sediment sources.

TYPES OF ATTACHED MASS TRANSPORT COMPLEXES



TYPES OF DETACHED MASS TRANSPORT COMPLEXES

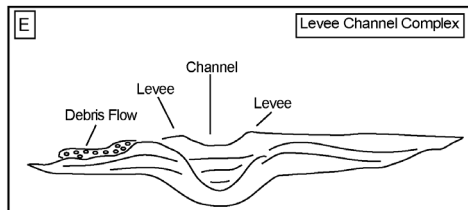
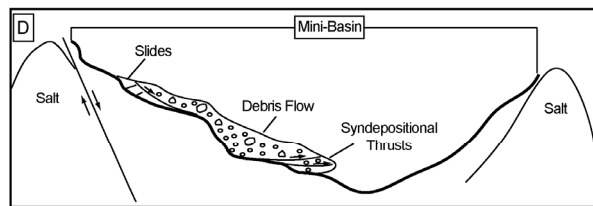
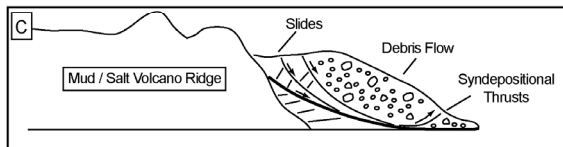


Figure 3.16: Schematic depiction of the different kinds of mass transport complexes and the processes associated with their genesis. A) Slope attached mass transport complex, sediments are derived from the catastrophic collapse of the upper slope area. B) Shelf attached mass transport complex, sediments are provided by shelf edge deltas and dumped into the deep marine basin. C) Detached mass transport complex associated with the collapsing flank of a mud volcano ridge. D) Detached mass transport complex associated with oversteepening of one of the margins of a deep water mini basin. E) Detached mass transport complex associated with a levee-channel complex.

### 3.9. REFERENCES

- Boettcher, S. S., J. L. Jackson, M. J. Quinn, and J. E. Neal, 2003, Lithospheric structure and supracrustal hydrocarbon systems, offshore eastern Trinidad, AAPG Memoir, United States, American Association of Petroleum Geologists : Tulsa, OK, United States, p. 529.
- Dykstra, M., 2005, Dynamics of submarine sediment mass-transport, from the shelf to the deep sea: PhD Thesis thesis, University of California, Santa Barbara, 54 p.
- Flood, R. D., D. J. W. Piper, A. Klaus, S. J. Burns, W. H. Busch, S. M. Cisowski, A. Cramp, J. E. Damuth, M. A. Goni, S. G. Haberle, F. R. Hall, K.-U. Hinrichs, R. N. Hiscott, R. O. Kowsmann, J. D. Kronen, D. Long, M. Lopez, D. K. McDaniel, P. L. Manley, M. A. Maslin, N. Mikkelsen, F. Nanayama, W. R. Normark, C. Pirmez, J. R. dos Santos, R. R. Schneider, W. J. Showers, W. Soh, and J. Thibaut, 1995: Proceedings of the Ocean Drilling Program, Part A: Initial Reports, v. 155.
- Frey Martinez, J., J. Cartwright, and B. Hall, 2005, 3D seismic interpretation of slump complexes: examples from the continental margin of Israel: Basin Research, v. 17, p. 83-108.
- Garciacaro, E. J., 2006, Stratigraphic architecture and basin fill evolution of a plate margin basin, eastern offshore Trinidad and Venezuela: Master thesis, University of Texas, Austin.
- Galloway, W.E. and Hobday, D.K., 1996, Terrigenous Clastic Depositional Systems. Heidelberg, Springer-Verlag.
- Gee, M. J. R., D. G. Masson, A. B. Watts, and P. A. Allen, 1999, The Saharan debris flow; an insight into the mechanics of long runout submarine debris flows, Sedimentology, International, Blackwell : Oxford-Boston, International, p. 317.
- Gee, M. J. R., A. B. Watts, D. G. Masson, and N. C. Mitchell, 2001, Landslides and the evolution of El Hierro in the Canary Islands, Marine Geology, Netherlands, Elsevier : Amsterdam, Netherlands, p. 271-293.
- Grantz, A., R. L. Phillips, M. W. Mullen, S. W. Starratt, G. A. Jones, A. S. Naidu, and B. P. Finney, 1996, Character, paleoenvironment, rate of accumulation, and evidence for seismic triggering of Holocene turbidites, Canada Abyssal Plain, Arctic Ocean: Marine Geology, v. 133, p. 51-73.
- Haflidason, H. L., H. P. Reidar, C. F. Forsberg, and P. Bryn, 2005, The dating and morphometry of the Storegga Slide, Marine and Petroleum Geology, United Kingdom, Elsevier : Oxford, United Kingdom, p. 123.



- Heppard, P. D., H. S. Cander, and E. B. Eggertson, 1998, Abnormal pressure and the occurrence of hydrocarbons in offshore eastern Trinidad, West Indies: AAPG Memoir, v. 70, p. 215-246.
- Imbo, Y. D. B., M. Canals, M. J. Prieto, and J. Baraza, 2003, The Gebra Slide; a submarine slide on the Trinity Peninsula margin, Antarctica, Marine Geology, Netherlands, Elsevier : Amsterdam, Netherlands, p. 235.
- Kleverlaan, K., 1987, Gordo megabed; a possible seismite in a Tortonian submarine fan, Tabernas Basin, Province Almeria, Southeast Spain, Sedimentary Geology, Netherlands, Elsevier : Amsterdam, Netherlands, p. 165.
- Knutz, P. C., W. E. N. Austin, and E. J. Jones, 2001, Millennial-scale depositional cycles related to British Ice Sheet variability and North Atlantic paleocirculation since 45 kyr B.P., Barra Fan, U.K. margin: Paleoceanography, v. 16, p. 53-64.
- Lastras, G. D. B., F. Vittorio, M. Canals, and A. Elverhoi, 2005, Conceptual and numerical modeling of the Big'95 debris flow, western Mediterranean Sea, Journal of Sedimentary Research, United States, Society of Economic Paleontologists and Mineralogists : Tulsa, OK, United States, p. 784.
- Lee, C., J. A. Nott, F. B. Keller, and A. R. Parrish, 2004, Seismic expression of the Cenozoic mass transport complexes, deepwater Tarfaya-Agadir Basin, offshore Morocco: Offshore Technology Conference, p. 18, OTC 16741.
- Macdonald, D. I. M., A. Moncrieff, and P. J. Butterworth, 1993, Giant slide deposits from a Mesozoic fore-arc basin, Alexander Island, Antarctica, Geology Boulder, United States, Geological Society of America (GSA) : Boulder, CO, United States, p. 1047.
- Martinez, J. F., J. A. Cartwright, P. M. Burgess, and J. V. Bravo, 2004, 3D seismic interpretation of the Messinian unconformity in the Valencia Basin, Spain: Memoirs of the Geological Society of London, v. 29, p. 91-100.
- Maslin, M., M. Owen, S. Day, and D. Long, 2004, Linking continental-slope failures and climate change: Testing the clathrate gun hypothesis: Geology, v. 32, p. 53-56.
- Maslin, M., C. Vilela, N. Mikkelsen, and P. Grootes, 2005, Causes of catastrophic sediment failures of the Amazon Fan: Quaternary Science Reviews, v. 24, p. 2180-2193.
- Masson, D. G., M. Canals, B. Alonso, R. Urgeles, and V. Huhnerbach, 1998, The Canary debris flow; source area morphology and failure mechanisms, Sedimentology, International, Blackwell : Oxford-Boston, International, p. 411.

- McAdoo, B. G., L. F. Pratson, and D. L. Orange, 2000, Submarine landslide geomorphology, US continental slope, *Marine Geology*, Netherlands, Elsevier : Amsterdam, Netherlands, p. 103.
- McGilvery, T. A., D. L. R. Cook, H. H., N. C. Rosen, R. H. Fillon, and J. B. Anderson, 2003, The Influence of local gradients on accommodation space and linked depositional elements across a stepped slope profile, offshore Brunei: Shelf Margin Deltas and Linked Down Slope Petroleum Systems: Global Significance and Future Exploration Potential, p. 387-419.
- McGilvery, T. A., G. Haddad, and D. L. Cook, 2004, Seafloor and shallow subsurface examples of mass transport complexes, offshore Brunei: Offshore Technology Conference, p. 13, OTC 16780.
- McMurtry, G. M., P. Watts, G. J. Fryer, J. R. Smith, and F. Imamura, 2004, Giant landslides, mega-tsunamis, and paleo-sea level in the Hawaiian Islands: *Marine Geology*, v. 203, p. 219-233.
- Mize, K. L., L. J. Wood, and P. Mann, 2004, Controls on the morphology and development of deep-marine channels, eastern offshore Trinidad and Venezuela AAPG Annual Meeting Program, v. 13.
- Montoya, P., 2006, Salt tectonics and Sequence-Stratigraphic History of Minibasins near the Sigsbee Escarpment, Gulf of Mexico PhD Thesis thesis, University of Texas at Austin, Austin, 276 p.
- Moscardelli, L., L. Wood, and P. Mann, 2006, Mass-transport complexes and associated processes in the offshore area of Trinidad and Venezuela: *AAPG Bulletin*, v. 90, p. 1059-1088.
- Newton, C. S., R. C. Shipp, D. C. Mosher, and G. D. Wach, 2004, Importance of mass transport complexes in the Quaternary development of the Nile Fan, Egypt: Offshore Technology Conference, p. 10, OTC 16742.
- Nissen, S. E., H. Norman, C. T. Steiner, and K. L. Coterill, 1999, Debris flow outrunner blocks, glide tracks, and pressure ridges identified on the Nigerian continental slope using 3-D seismic coherency, Leading Edge Tulsa, OK, United States, Society of Exploration Geophysicists : Tulsa, OK, United States, p. 595.
- Pickering, K. T., and J. Corregidor, 2005, Mass-transport complexes (MTCs) and tectonic control on basin-floor submarine fans, middle Eocene, south Spanish Pyrenees, *Journal of Sedimentary Research*, United States, Society of Economic Paleontologists and Mineralogists : Tulsa, OK, United States, p. 761.

- Pirmez, C., J. Marr, C. Shipp, and F. Kopp, 2004, Observations and numerical modeling of debris flows in the Na Kika Basin, Gulf of Mexico: Offshore Technology Conference, p. 13, OTC 16749.
- Popenoe, P., E. A. Schmuck, and W. P. Dillon, 1993, The Cape Fear landslide; slope failure associated with salt diapirism and gas hydrate decomposition: U. S. Geological Survey Bulletin, p. 40-53.
- Posamentier, H., 2004, Stratigraphy and geomorphology of deep-water mass transport complexes based on 3D seismic data: Offshore Technology Conference, p. 7, OTC 16740.
- Posamentier, H. W., and V. Kolla, 2003, Seismic Geomorphology and Stratigraphy of Depositional Elements in Deep-Water Settings: Journal of Sedimentary Research, v. 73, p. 367-388.
- Shackleton, N. J., 1987, Oxygen isotopes, ice volume and sea level: Quaternary Science Reviews, v. 6, p. 183-190.
- Shanmugam, G., R. J. Moiola, and J. K. Sales, 1988, Duplex-like structures in submarine fan channels, Ouachita Mountains, Arkansas: Geology, v. 16, p. 229-232.
- Shipp, C., J. A. Nott, and J. A. Newlin, 2004, Physical characteristics and impact of mass transport complexes on deepwater jetted conductors and suction anchor piles: Offshore Technology Conference, p. 11, OTC 16751.
- Strachan, L. J., 2002, Geometry to Genesis: A Comparative Field Study of Slump Deposits and Their Modes of Formation: PhD Dissertation thesis, Cardiff University, Cardiff, 412 p.
- Sullivan, S., L. J. Wood, and P. Mann, 2004, Distribution, nature and origin of Mobile mud features offshore Trinidad: Salt-Sediment Interactions and Hydrocarbon Prospectivity: Concepts, Applications, and Case Studies for the 21st Century, p. 840-867.
- Sutter, J. R., 2006, Shelf margin systems: Interface between shallow water sediment sources and deep water sinks: External Controls on Deep Water Depositional Systems: Climate, Sea-Level and Sediment Flux, p. 78.
- Thompson, L. G., E. Mosley-Thompson, M. E. Davis, P. N. Lin, K. A. Henderson, J. Cole-Dai, J. F. Bolzan, and K. B. Liu, 1995, Late Glacial Stage and Holocene tropical ice core records from Huscaran, Peru: Science, v. 269, p. 46-50.
- Twichell, D. C., W. C. Schwab, C. H. Nelson, and N. H. Kenyon, 2006, The effects of submarine canyon and proximal fan processes on the depositional systems of the

- distal Mississippi Fan: External Controls on Deep Water Depositional Systems: Climate, Sea-Level and Sediment Flux, p. 81.
- Weimer, P., 1989, Sequence stratigraphy of the Mississippi Fan (Plio-Pleistocene), Gulf of Mexico: *Geo-Marine Letters*, v. 9, p. 185 - 272.
- Weimer, P., 1990, Sequence stratigraphy, seismic geometries, and depositional history of the Mississippi Fan, deep Gulf of Mexico: *AAPG Bulletin*, v. 74, p. 425-453.
- Weimer, P., and C. Shipp, 2004, Mass transport complex: Musing on the past uses and suggestions for future directions: *Offshore Technology Conference*, p. 10, OTC 16752.
- Wood, L. J., 2000, Chronostratigraphy and Tectonostratigraphy of the Columbus Basin, Eastern Offshore Trinidad: *AAPG Bulletin*, v. 84, p. 1905-1928.
- Wynn, R. B., 2006, Timing and relation to climate/sea-level of giant landslides and turbidity currents on the Northwest African continental margin, from Morocco to Senegal: *External Controls on Deep Water Depositional Systems: Climate, Sea-Level and Sediment Flux*, p. 87.
- Wynn, R. B., D. G. Masson, D. A. Stow, and P. P. Weaver, 2000, The Northwest African slope apron: a modern analogue for deep-water systems with complex seafloor topography: *Marine and Petroleum Geology*, v. 17, p. 253-265.

## **Chapter 4: A New Insight into the Morphometry of Mass Transport Complexes and its Significance**

### **4.1. INTRODUCTION**

#### **Quantitative data from Worldwide Mass Transport Deposits**

A large data set on the area, length, thickness and volume of 186 mass transport deposits were compiled from peer-reviewed literature. These deposits were from a wide variety of basin types and siliciclastic sedimentary settings from around the world. In addition to literature derived data, data from several mass transport deposits currently under study by the author in offshore Trinidad were included in the compilation. Observation of most of the mass transport complexes reported in this compilation were characterized on the basis of bathymetric, towed ocean bottom instruments (TOBI), side scan, and seismic data. The Trinidad deposits were documented in a large 3D seismic data volume (chapters 2 and 3). These data provide the means to analyze and compare the geometry of deposits from various geologic settings and margin types around the world.

In any literature compilation, there is danger in comparing data which have been collected by different means, or using different imaging techniques such that it may skew the compilation. For this study, great care was taken to quality control the data that were used. Only measurements that met the following criteria were included in this study: 1) morphometric measurements were only included when they encompass the entire area affected by the mass transport deposits (including source areas and depolocations), and 2) the deposits should have been clearly identified as generated by mass wasting processes (slides, slumps, and debris flows), this specifically excludes any kind of channelized feature (e.g. levee-channel complexes, slope channels, etc.). In some instances authors

did not included specific values of area, or length into the text of the articles, only describing the deposits qualitatively. In such cases, direct measurements were taken from the maps of the deposits that were provided in the papers. Some authors documented the area, length, and volume of a deposit, but failed to document the thicknesses of the unit. In these cases the thickness was calculated by this author based on the volume and area of the deposit. The resulting data compiled for this study are shown in appendix 4.1.

### **Can we predict sediment nature from deposit geometry?**

Several authors have suggested a link between mass transport deposit geometry and sediment character. Haflidason et al. (2005) collected a series of measurements in the Storegga slide in the Ormen Lange Field area, which were used to carry out statistical analyses of the slide. These authors arrived at the conclusion that the good correlation between area, length, and volume of the slide demonstrated that the rheological characteristics of the sediments that failed in the different slide units were uniform, and that scaling of these parameters should be possible. Hühnerbach and Masson (2004), also analyzed morphometric parameters of several mass transport complexes in the North Atlantic continental margins. They observed that contrary to common belief, slope angle does not influence the occurrence of mass transport complexes. They further observed that most of the source areas of these units (headwalls) occurred at water depths between 1,000 and 1,300 m. According to these authors this consistent headwall water depth suggests the prevalence of a specific sediment rheology, as well as gas hydrate dissociation as a possible mass failure triggering mechanism. The same authors documented the correlation between length, and width of the deposits, and briefly mentioned that these correlations may be used to predictive slide behavior. Issler et al. (2005) reported that the strong geometric similarity between mass transport complexes of different sizes could be indicating that the soil strength grows linearly with depth. Despite

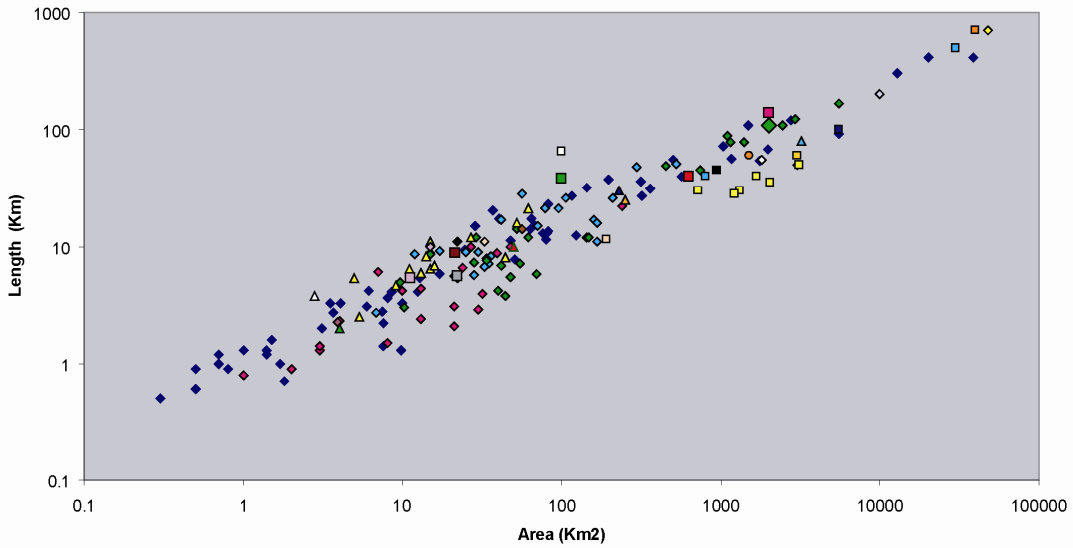
the fact that several authors have associated rheological characteristics of mass transport complexes to these morphometric correlations, the involvement of causal mechanisms as a possible controlling factor in the scaling behavior and geometry of these deposits has not been explored.

The main objectives of this work are to analyze the geometry of mass transport complexes to better understand their causal mechanisms, and to establish whether systematic morphometric parameters characterize these deposits along different continental margins around the world. Through these comparative studies we hope to 1) gain insight into the relationship between setting and deposit geometry, 2) deduce the ability to predict sediment character in a mass transport complex from examination of its geometry and 3) derive relationships that allow us to predict the extended nature of mass transport complexes from sometimes limited imaged dimensions.

#### **4.2. MORPHOMETRY OF MASS TRANSPORT COMPLEXES**

Quantitative measurements were compiled on the geometry of 186 mass transport complexes located in different continental margins, and tectonic settings (Appendix 4.1). Figure 4.1 is a log-log plot that shows the exponential relationship between area (A) and length (L) of the mass transport complexes that were presented in appendix 4.1. This log-log plot demonstrates a geometric relationship between these two variables that is independent of lobe size (Haflidason et al., 2005). The distribution of data points along a straight line in the figure 4.2A log-log plot suggests that the area (A) and length (L) of mass transport complexes respond to a power law of the form:

$$L = 1.1351 A^{0.5661} \quad (1)$$



- ◆ Storegga Individual Slides (Hafliðason et al., 2005)
- Saguenay Fjord< Canada (Syvinski and Schafer, 1996)
- ◇ California USA (McAdoo et al.,2000)
- ▲ New Jersey (McAdoo et al.,2000)
- El Hierro El Golfo (Gee et al.,2001)
- El Hierro Las Playas 2 (Gee et al.,2001)
- MTC\_2 Trinidad (Moscardelli et al., 2006)
- ◇ Amazon (WMTD) (Piper et al., 1997)
- Brunei (min) (McGilvery and Cook,2003)
- ◇ Tejas A Offshore Morocco (Lee et al.,2004)
- ▲ Offshore Nova Scotia, Canada (Campbell et al.,2004)
- MTC\_2.1 Trinidad (Moscardelli et al., 2007)
- MTC\_2.3 Trinidad (Moscardelli et al., 2007)
- ▲ Brunei Cohesive Slump 1
- ▲ Brunei Cohesive Slump 3 (old)
- ◆ Goleta E. / S. Barbara (Lee et al.,2004)
- ◆ Goleta W. / S. Barbara (Lee et al.,2004)
- ◇ Palos Verdes MTC / S. Pedro (Lee et al.,2004)
- Cape Verde Slide Complex (Wynn et al.,2000)
- MTC\_1 Trinidad (Moscardelli et al., 2006)
- ◆ Oregon USA (McAdoo et al.,2000)
- ◆ GOM (McAdoo et al.,2000)
- Canary Debris Flow (Masson et al.,1998)
- ◇ El Hierro El Julian (Gee et al.,2001)
- ◆ Ebro Spain BIG 95' (Lastras et al.,2005)
- ▲ Gebra Slide Antarctica (Imbo et al., 2003)
- Gordo Megabed Unit I Spain (Kleverlaan, 1987)
- ▲ Brunei (max) (McGilvery and Cook,2003)
- Tejas B Offshore Morocco
- Nile Fan, Egypt (Newton et al.,2004)
- MTC\_2.2 Trinidad (Moscardelli et al., 2007)
- MTC\_2.4 Trinidad (Moscardelli et al., 2007)
- ▲ Brunei Cohesive Slump 2
- ◆ Gaviota S. Barbara CA (Lee et al.,2004)
- ◆ Goleta C. / S. Barbara (Lee et al.,2004)
- ◆ Buried MTC S. Monica (Lee et al.,2004)
- ◆ Sahara Debris Flow (Gee et al.,1999)
- Oratava\_lcod\_Tino debris avalanche (Wynn et al.,2000)

Figure 4.1: Log-log plot showing the relationship between area (A) and length (L) of mass transport complexes around the world.



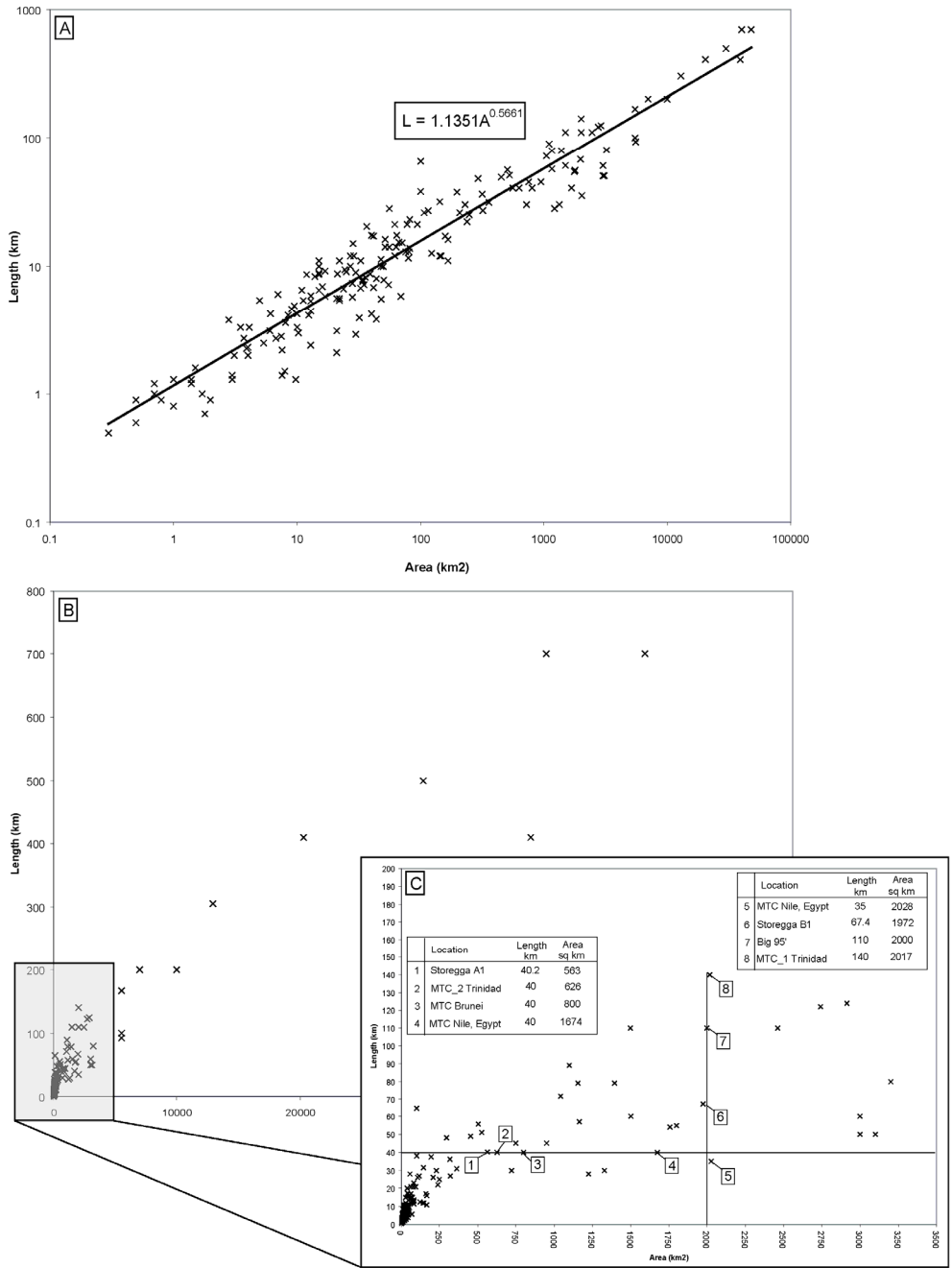


Figure 4.2: (A) Log-log plot showing the relationship between area and length of MTCs, and the power function that defines this relationship (B) Linear plot of the same data showing scatter distribution of points (C) Inset from plot B showing that the area occupied by mass transport complexes does not necessarily increase with an increase in length and vice versa.

This geometric relationship can also be expressed in the following form:

$$A = 1.1426 L^{1.6187} \quad (2)$$

However, it is important to keep in mind that the length (L) of a mass transport complex is defined as “the horizontal distance measure in the downslope direction based on the total area that has been affected by the mass wasting process” (chapter 3). This measurement is completely different from the concept of run-out distance (R) which is understood as “the horizontal distance that a single particle within the mass transport complex has travel through, from its staging area or original location to its final site of deposition” (chapter 3) (Figure 4.3). It is important to highlight this difference due to its practical implications, the length (L) of a mass transport complex is a simple morphometric parameter that can be obtain from a rough outline of the area affected by a mass transport complex. In contrast, the run-out distance is a more process-oriented parameter that needs an exhaustive analysis of internal kinematic indicators such as scours, rafted blocks, and depositional thrusts (Figure 4.3). Moreover, the run-out (R) distance of mass transport complexes is impossible to express as a single number. Rather the possible numeric values are nearly infinite, since different particles within the deposit can reach different distances depending upon the presence of pre-existing bathymetric constrains, and the successive changes in the rheology of the flow as it moves downslope (Figure 4.3).

Figure 4.4 is a log-log plot that shows the relationship between area (A) and volume (V) of the same deposits that are shown in figures 4.1 and 4.2. Figure 4.5 shows that there is also an exponential relationship between these two morphometric

parameters. This additional relationship between area (A) and volume (V) responds to a power law of the following form:

$$V = 0.0379 A^{1.0652} \quad (3)$$

Or

$$A = 23.125 V^{0.874} \quad (4)$$

It is important to point out, that the volume values that are shown in these plots (figures 4.4 and 4.5) account for both, the sediments that were transported from the source area, as well as for the sediments that were remobilized on the pre-existing substratum, and subsequently incorporated into the flow through basal erosion.

The relationships illustrated in the previous graphs may be useful under conditions of limited data extents to estimate the nature of large MTCs. For example, if the available data (seismic, sonar, etc) is not large enough to encompass the entire area affected by a mass transport complex event, but the total length of the same deposit is a known parameter, then the length can be used as an input parameter to estimate the area (equation 1) (Figure 4.6). The combination of equations (2) and (3) would allow an estimation of volume based on the length (L) of the deposits (equation 5) (Figure 4.6).

$$V = 0.0471 L^{1.6939} \quad (5)$$

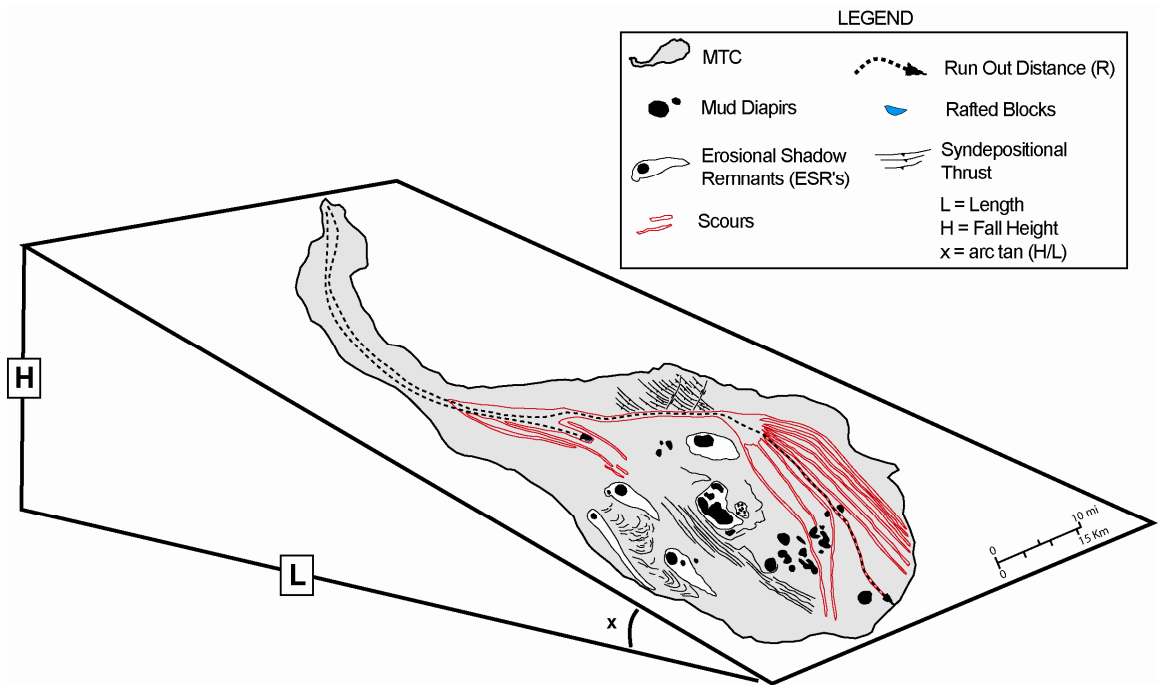
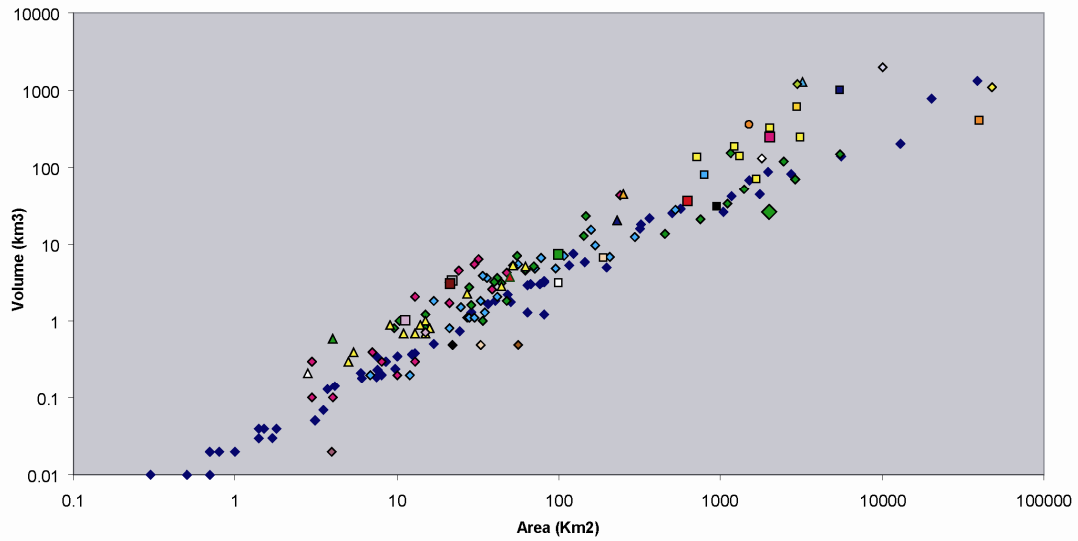


Figure 4.3: Schematic illustration showing the difference between the concepts of run-out (R), and length (L) (Modified from Issler et al., 2005)



- ◆ Storegga Individual Slides (Hafidason et al., 2005)
- Saguenay Fjord< Canada (Syvinski and Schafer, 1996)
- ◇ California USA (McAdoo et al.,2000)
- ▲ New Jersey (McAdoo et al.,2000)
- El Hierro El Golfo (Gee et al.,2001)
- El Hierro Las Playas 2 (Gee et al.,2001)
- MTC\_2 Trinidad (Moscardelli et al., 2006)
- ◇ Amazon (WMTD) (Piper et al., 1997)
- Brunei (min) (McGilvery and Cook,2003)
- ◇ Tejas A Offshore Morocco (Lee et al.,2004)
- ▲ Offshore Nova Scotia, Canada (Campbell et al.,2004)
- MTC\_2.1 Trinidad (Moscardelli et al., 2007)
- MTC\_2.3 Trinidad (Moscardelli et al., 2007)
- ▲ Brunei Cohesive Slump 1
- ▲ Brunei Cohesive Slump 3 (old)
- ◆ Goleta E. / S. Barbara (Lee et al.,2004)
- ◆ Goleta W. / S. Barbara (Lee et al.,2004)
- ◇ Palos Verdes MTC / S. Pedro (Lee et al.,2004)
- Oratava\_lcod\_Tino debris avalanche (Wynn et al.,2000)
- MTC\_1 Trinidad (Moscardelli et al., 2006)
- ◇ Oregon USA (McAdoo et al.,2000)
- ◇ GOM (McAdoo et al.,2000)
- Canary Debris Flow (Masson et al.,1998)
- ◇ El Hierro El Julian (Gee et al.,2001)
- ◇ Ebro Spain BIG 95' (Lastras et al.,2005)
- ▲ Gebra Slide Antarctica (Imbo et al., 2003)
- Gordo Megabed Unit I Spain (Kleverlaan, 1987)
- ▲ Brunei (max) (McGilvery and Cook,2003)
- Tejas B Offshore Morocco
- Nile Fan, Egypt (Newton et al.,2004)
- MTC\_2.2 Trinidad (Moscardelli et al., 2007)
- MTC\_2.4 Trinidad (Moscardelli et al., 2007)
- △ Brunei Cohesive Slump 2
- ◇ Gaviota S. Barbara CA (Lee et al.,2004)
- ◇ Goleta C. / S. Barbara (Lee et al.,2004)
- ◇ Buried MTC S. Monica (Lee et al.,2004)
- ◇ Sahara Debris Flow (Gee et al.,1999)

Figure 4.4: Log-log plot showing the relationship between area (A) and volume (V) of mass transport complexes around the world.

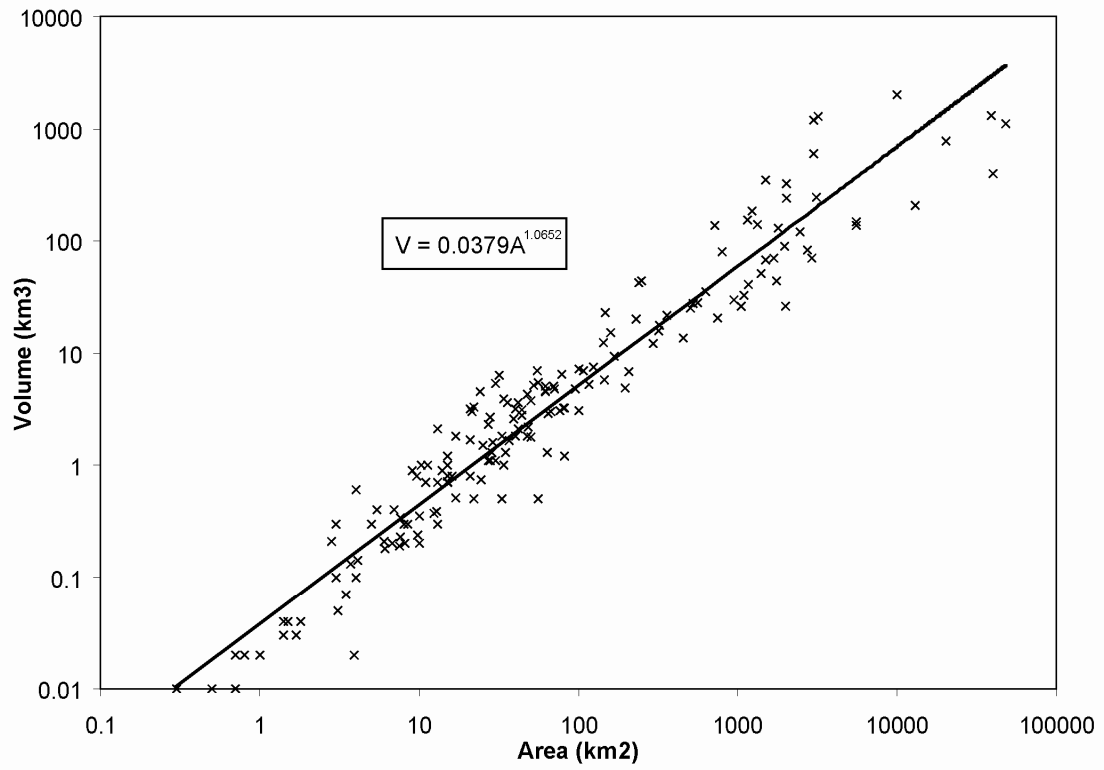


Figure 4.5: Log-log plot showing the relationship between area and volume of MTC's, and the power function that better defines this relationship.

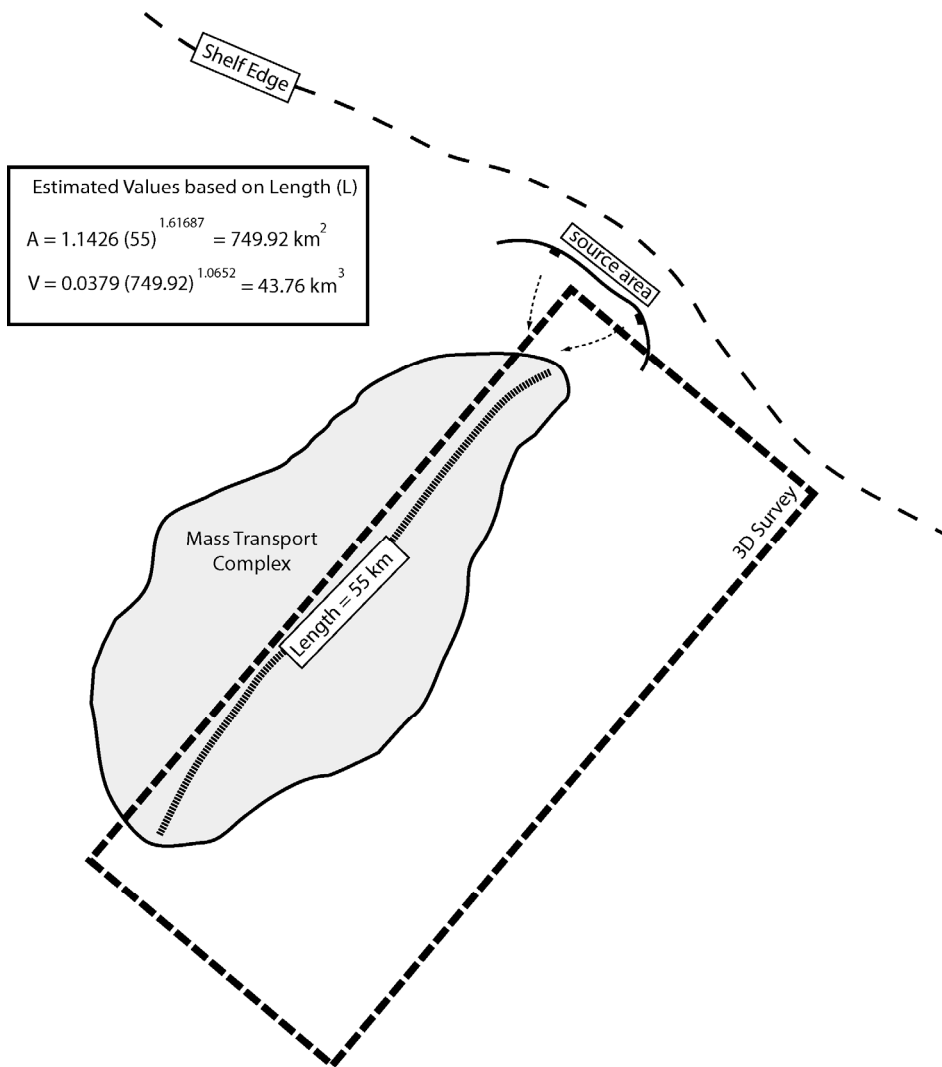


Figure 4.6: The 3D seismic volume does not cover the entire area affected by the MTC. However, an estimation of the area and volume of the deposit is possible using the known length of the unit.

### 4.3. THE SCALE AND GEOMETRY OF MASS TRANSPORT COMPLEXES

Some authors have mentioned that the plot shown in figure 4.2A is illustrating an “obvious” relationship between area (A) and length (L) of the deposits, where an increase in area implies an “expected” and “logical” increase in length and vice versa (Huhnerbach and Masson, 2004). In our opinion, this is not the case and the log-log plot is instead showing that this relationship between area (A) and length (L) is purely exponential (see equation 1 and Figure 4.2A). To further clarify this point, the same data points are displayed in figures 4.2B and 4.2C as a linear plot. In this new display we can observe that the distribution of points is not uniform, and that the relationship between the variables is definitely not linear. For instance, we can see that several mass transport complexes within the same length range can affect areas that differ in several orders of magnitude and vice versa (Figure 4.2C). For example, figure 4.2C shows some mass transport complexes that are in the 40 km long range (L) and that can cover areas (A) that vary from 500 to 1,600 sq km, and some others that have areas (A) around 2,000 sq km and can have lengths (L) that vary from 35 to 140 km. In order to advance in the understanding of the geometry of mass transport complexes, it is crucial to highlight that an increase in length does not necessarily imply an increase in the area of these deposits and vice versa.

The relationship between area (A) and length (L) in mass transport complexes seems to be scale-invariant; however what the log-log plot is doing is providing valuable information in relation to the geometry, and shape of these deposits. To better illustrate this point, a series of ideal geometric relationships involving different types, and sizes of rectangles have been superimposed in the mass transport complex area (A) versus length (L) plot shown in Figure 4.7. In this new plot, each line represents a series of rectangles



that have a fixed length:width ratio that varies from 0.1 to 10. Two fields have been defined in this plot, the lower field where the length:width ratios are greater or equal than 0.1, and lower or equal to 1 ( $0.1 \leq L:W \leq 1$ ); and the upper field where the length:width ratios are greater than 1, and lower or equal to 10 ( $1 < L:W \leq 10$ ) (see Figure 4.7). Figure 4.7 shows that only 20% of the collected data points fell into the lower field of the log-log plot. Furthermore, most of the mass transport complexes contained in the lower field (except for the Nile deposits) covered areas that are less than 200 sq km, and have lengths that range from 0.3 to 11.5 km. The lower field mass transport complexes are wider than they are longer, and they are relatively smaller than their counterparts in the upper field (except for the Nile deposits) (Figure 4.7). Mass transport complexes contained in the lower field mainly correspond to small slide debris events associated with the Storegga region (Haflidason et al., 2005), as well as to smaller submarine slides within salt withdrawal basins of the Gulf of Mexico. In addition, some events in the Sigsbee Escarpment, and almost all the slides identified in the offshore Oregon region are also located in the lower field (except for one) (McAdoo et al., 2000).

The remaining 80% of the data points in the set are located in the upper field of the log-log plot (Figure 4.7). These mass transport complexes cover a wide spectrum of areas (A) that can reach a maximum of 48,000 sq km, and lengths that range from a minimum of 0.5 km to a maximum of 600 km. However, 70% of the data points contained in the upper field cover areas that are greater than 100 sq km, and have lengths that are greater than 11 km. The upper field mass transport complexes are characterized by an elongated appearance (they are longer than they are wide). The biggest mass transport complexes that plot in the upper field are associated with events located in the offshore area of western Africa (Canary and Sahara debris flows, and Cape Verde and Oratava\_Icod\_Tino slide complexes) (Masson et al., 1998; Gee et al., 1999, and Wynn et

al., 2000), in offshore Norway (main lobes of the Storegga event) (Haflidason et al., 2005), in the Gulf of Mexico adjacent to the Mississippi Canyon (McAdoo et al., 2000), in the Mediterranean sea (Big 95' event) (Lastras et al., 2005), and in offshore Trinidad (Moscardelli et al., 2006).

#### **4.4. THE MISSING LINK BETWEEN THE MORPHOMETRY OF MASS TRANSPORT COMPLEXES AND THEIR CAUSAL MECHANISMS**

The term attached mass transport complexes is defined as systems whose sedimentary sources are located in the outer shelf and/or upper slope areas, and that can occupied 100's to 1000's sq km in area. These systems are capable to transport, and remobilized volumetrically significant amounts of sediments towards deep-marine depocenters. Causal mechanisms associated with attached mass transport complexes include relative sea level fluctuations, and changes in sedimentation rates (shelf- attached systems), as well as gravitational instabilities due to tectonism, gas hydrate dissociation, and long shore currents among others (slope- attached systems). In contrast, detached mass transport complexes are smaller than their attached counterparts. These systems are fed by localize source areas that usually are confined areas, such as mini-basins, or the flanks of mud/salt ridges, and anticlines. Detached mass transport complexes are generated by localized instabilities. For instance, in the offshore areas of Trinidad, they are high frequency events, produced by progressive increases in the steepness of the flanks of confine mini-basins.

To test the hypothesis that attached and detached MTCs are a genetically valid classification based on common characteristics shared by these MTC types, all of the mass transport complexes shown in appendix 4.2 were re-classified according to the new criteria (attached versus detached systems)(Chapter 3). The main aspect that was considered into the re-classification process was the triggering mechanism associated

with the deposits. Figures 4.8 and 4.9 show an area (A) versus length (L) and an area (A) versus volume (V) log-log plots that are similar to the plots that were used and analyzed in the previous section (Figures 4.2A and 4.5), however in these new plots the data points were qualitatively regrouped into two series: (1) attached mass transport complexes, and (2) detached mass transport complexes. The new display shows that the majority of the data points associated with the attached mass transport complexes are constrained to the right hand side of the area (A) versus length (L) log-log plot ( $A > 100$  sq km and  $L > 11$  km) (Figure 4.8), and to the previously defined upper field ( $1 < L:W \leq 10$ ) (Figure 4.7). According to this distribution, attached mass transport complexes tend to be longer than wider; they can cover areas between 100 to 50,000 sq km, and their lengths vary from 11 to 700 km. Figure 4.9 also shows that the total volume of sediments remobilized by attached mass transport complexes can range from 5 to 2,000 cubic kilometers. It is interesting to notice that the field occupied by attached mass transport complexes in figure 4.8 coincides pretty well with the relationships observed by Hühnerbach and Masson (2004) in their “Eastern Atlantic” series (see their Figure7a).

The data show that attached mass transport complexes tend to group in specific clusters in the log-log plots (upper/right hand side) (Figures 4.8 and 4.9). The causal mechanisms associated with this kind of deposits are highly variable (Figure 4.10), but related to:

- (1) Flank failures in volcanic islands (e.g. Canary and Sahara debris flows, El Hierro landslides, Orot/Icod/Tino debris avalanche).

- (2) Successive advances and retreats of glaciers in continental margins (e.g. Storegga, Nova Scotia, and Gebra slides).

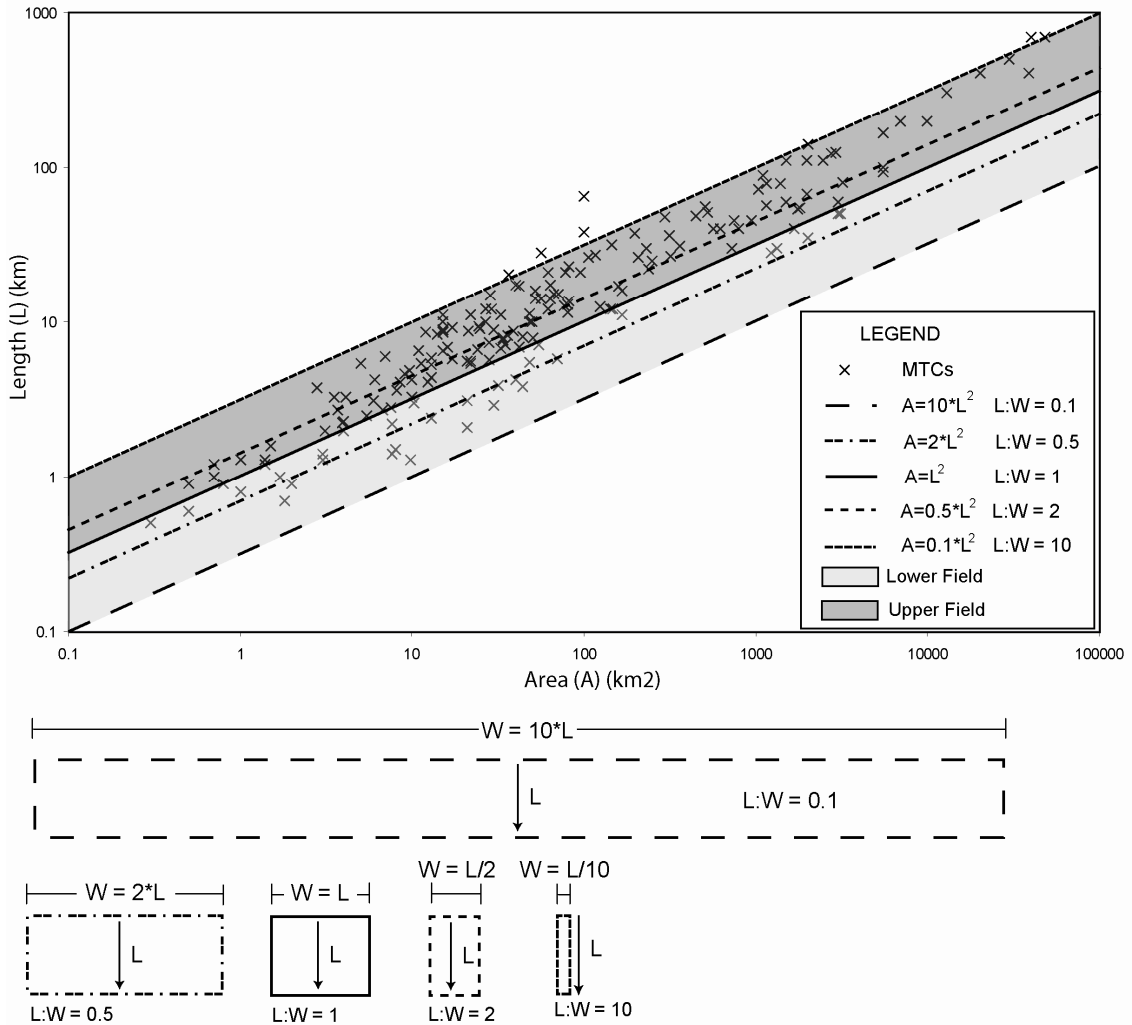
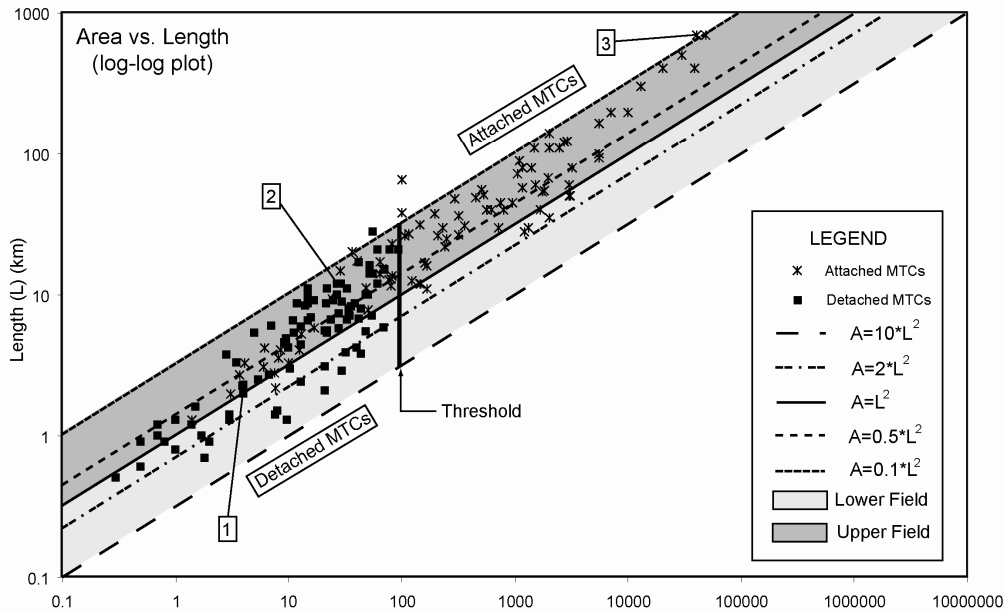
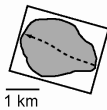


Figure 4.7: Geometric relationships of rectangles associated with a variety of scales and types of mass transport complexes. The lower and upper fields are shaded in this plot.

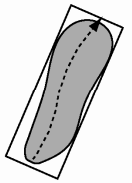


1 Cohesive Slump Complex  
Brunei (McGilvery and Cook, 2003)



Area = 4 km<sup>2</sup>  
Length = 2 km

2 Detached MTC - Trinidad  
(Moscardelli & Wood, 2007  
in review)



Area = 21.4 km<sup>2</sup>  
Length = 8.7 km

Area (A) (km<sup>2</sup>)

3 Canary debris flow - West Africa  
(Masson et al., 1998)

Area = 40000 km<sup>2</sup>  
Length = 700 km

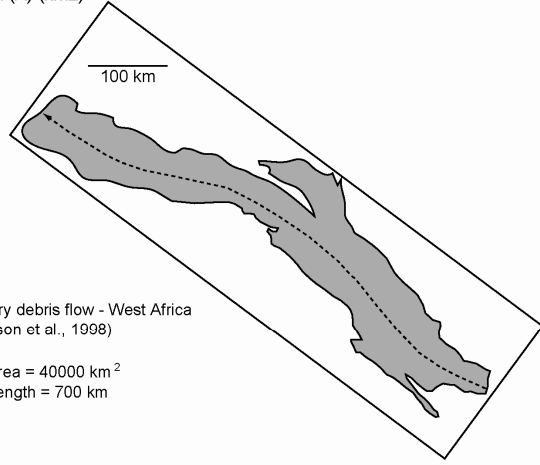


Figure 4.8: Area versus length log-log plot showing the distribution of attached mass transport complexes and detached mass transport complexes, as well as the geometric relationships and scaling associated with each series.

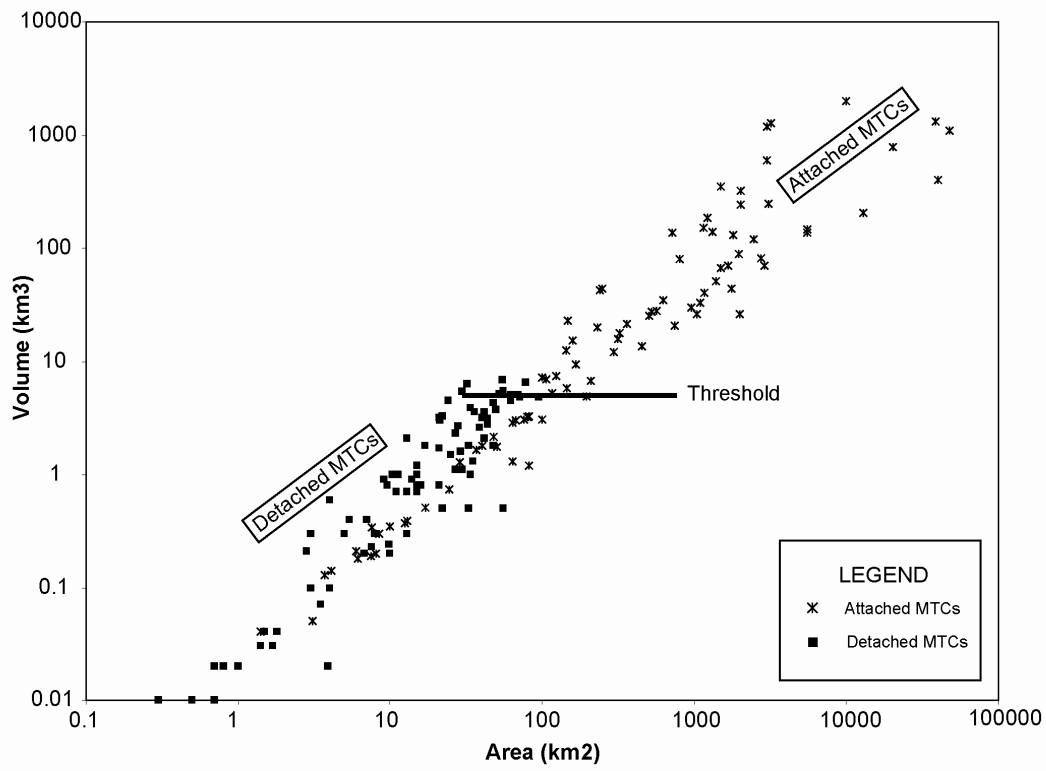


Figure 4.9: Log-log plot showing the relationship between area and volume. This plot also shows the distribution of two different types of mass transport complexes; detached MTC's on the lower left corner, and attached MTC's on the upper right corner of the plot.

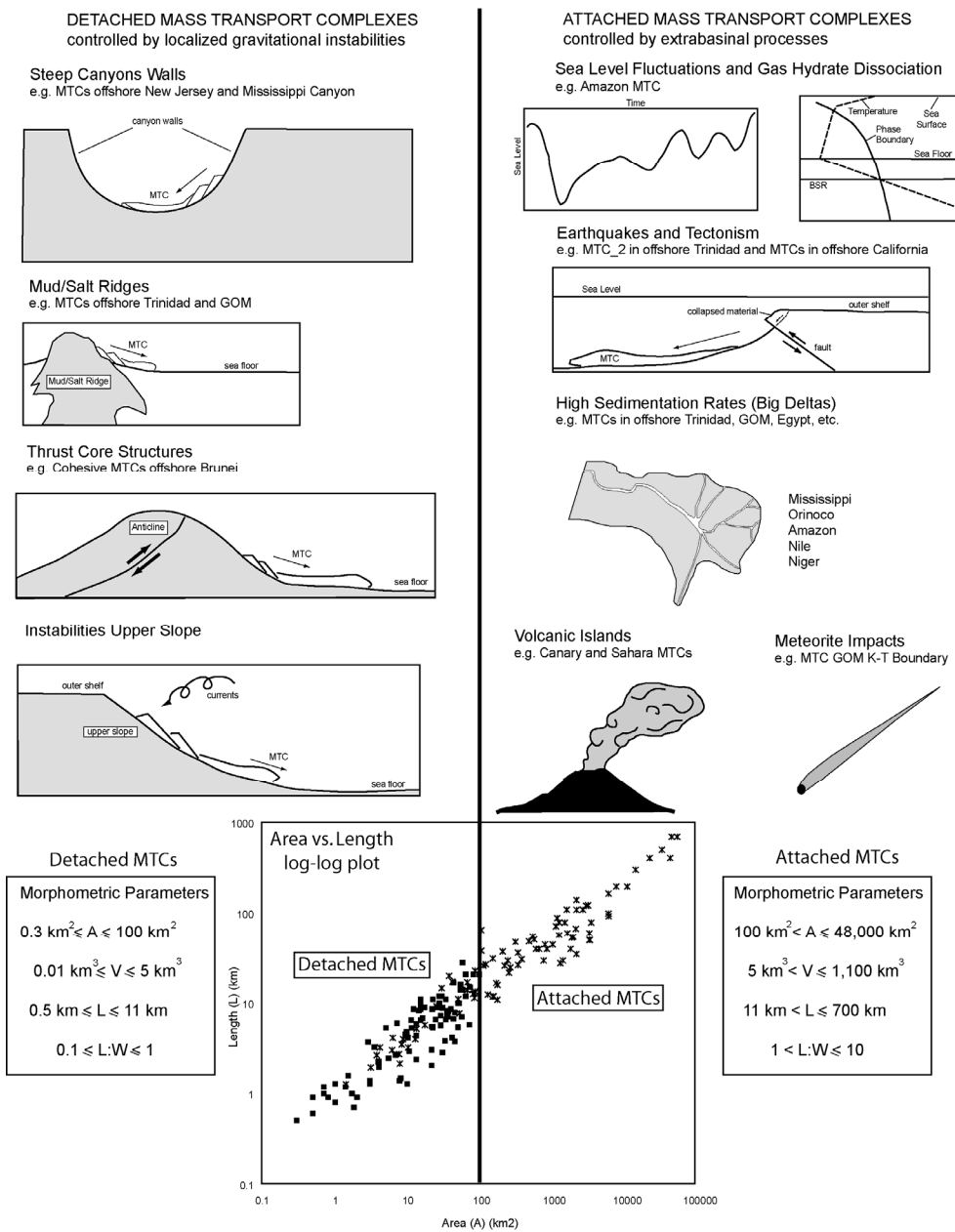


Figure 4.10: Relationship between causal mechanisms and morphometry of mass transport complexes.

(3) High sedimentation rates associated with big deltas (e.g. large mass transport complexes in the Gulf of Mexico, Amazon mass transport complexes in offshore Brazil, and MTC\_1 in offshore Trinidad).

(4) Destabilization of the upper slope area due to earthquakes trigger by tectonism, volcanism, or gas hydrate dissociation (e.g. Big 95' event in the western Mediterranean region, MTC\_2 in offshore Trinidad, and Saguenay Fjord Collapse in Canada).

(5) Big meteorite impacts (regional mass transport complexes in offshore Morocco).

(6) Failure of the upper slope region due to an increase in gravitational load (mass transport complexes in offshore Egypt, and Cape Verde slide in offshore western Africa).

Detached mass transport complexes are constrained to the left hand side of the log-log plots (Figures 4.8 and 4.9), but they are distributed in both the lower and upper fields (Figure 4.8). These systems cover areas from 0.3 to 100 sq km, and their lengths can vary from 0.5 to 28 km (Figure 4.8); they come in a variety of shapes but smaller, detached mass transport complexes tend to be wider than longer (lower field MTCs) (Figure 4.8). The volume of sediments mobilized by detached mass transport complexes can range from 0.01 to around 5 cubic kilometers (Figure 4.9). In offshore Trinidad the areal extent of detached mass transport complexes is controlled by the orientation, height and geometry of mud volcano ridges (Chapter 3). Similarly localized cohesive slump complexes described by McGilvery et al. (2004) in offshore Brunei are controlled by the geometry of the flanks of deep-seated structures (anticlines). Hühnerbach and Masson (2004) also observed that localized submarine slides that develop in fjords are influenced, and limited by the geometry and paleobathymetry of the area where they occur. The field occupied by detached mass transport complexes in our area versus length plot also



coincides with submarine slides that were plotted in a similar graph, and that were grouped by Hühnerbach and Masson (2004) in two distinctive series identified as “Western Atlantic” mass transport complexes, and slides that were developed in “Fjords and others” (see their Figure 7a). In the Gulf of Mexico, detached mass transport complexes occur in the steep flanks of salt withdrawal mini basins, and at the base of the Sigsbee Escarpment (McAdoo et al., 2000). Post Storegga small slides, and geometrically similar deposits in offshore California, New Jersey, and Oregon are also classified as detached mass transport complexes, these systems are triggered by gravitational instabilities in steep slopes that usually are associated with canyon walls. These instabilities can be triggered by a variety of factors, including earthquakes, downslope sediment flows, and the action of submarine currents (McAdoo et al., 2000 and Haflidason et al., 2005) (Figure 4.10).

#### **4.5. THE THICKNESS OF MASS TRANSPORT COMPLEXES**

Figure 4.11 is an area (A) versus thickness (T) plot that shows the relationship between these two parameters in mass transport complexes from different continental margins around the world. It is important to keep in mind that these deposits are composed of a variety of lithologies. In this plot the values in the x-axis are displayed in a logarithmic scale in order to better appreciate the scatter of the data points. This particular graph is quite useful to establish comparisons regarding the flow efficiency of different events. Figure 4.11A shows that despite the fact that the Canary and Sahara debris flows are the events with major areal extension (~ 40,000 sq km), their thicknesses (<50 m) are relatively small when compare with the rest of the data points. This suggests that a relatively small amount of sediments were mobilized by the initial mass failure, however the flow that finally embedded these sediments must have been highly competent in order to cover such a broad area of the seafloor. This observation is consistent with the

lithological and rheological descriptions provided by Masson et al. (1998) and Gee et al. (1999). These authors pointed out that the flows that originated the Canary and Sahara debris flows were highly fluid, and that the nature of the volcanoclastic material that failed contributed to decrease the basal friction of the flow, and to significantly increase its competence. A different scenario is presented for the Brunei and Morocco mass transport complexes (Figure 4.11A); the thick character of these units (~ 400 m) suggests that these deposits were generated by successive failures, and not by isolated events. McGilvery et al. (2004) and Lee et al. (2004) pointed out that the Brunei and Morocco mass transport complexes were characterized by multiple events of deposition; some intervals were dominated by long distance fluidized debris flows that were similar to those observed in the Sahara and Canary deposits, however the presence of huge rafted blocks, that can reach 1 km across and 150 m in thickness, and that are embedded in some intervals within these mass transport complexes, suggests that local cohesive flow processes also played an important role in the genesis of these units. The alternation between fluidized and cohesive flows within the Brunei and Morocco mass transport complexes, can explain why greater volumes of sediment are occupying less area, when compare to the areal extension that is occupied by the Sahara and Canary debris flows where highly fluidized flows were dominant through the entire depositional process. For the Storegga slide event, we can observe that despite the fact that the range of areas that are covered by individual lobes is enormous (0.3 to 38,740 sq km); the thicknesses are quite constant (~ 33 m). Haflidason et al. (2005) noticed that the morphometric relationships in the Storegga slide are independent of lobe size and thicknesses; therefore they suggested that these relationships can be used to develop a scaled flow model using only the morphometric values of one lobe, these values would be capable of honoring the behavior of the entire Storegga slide failure.

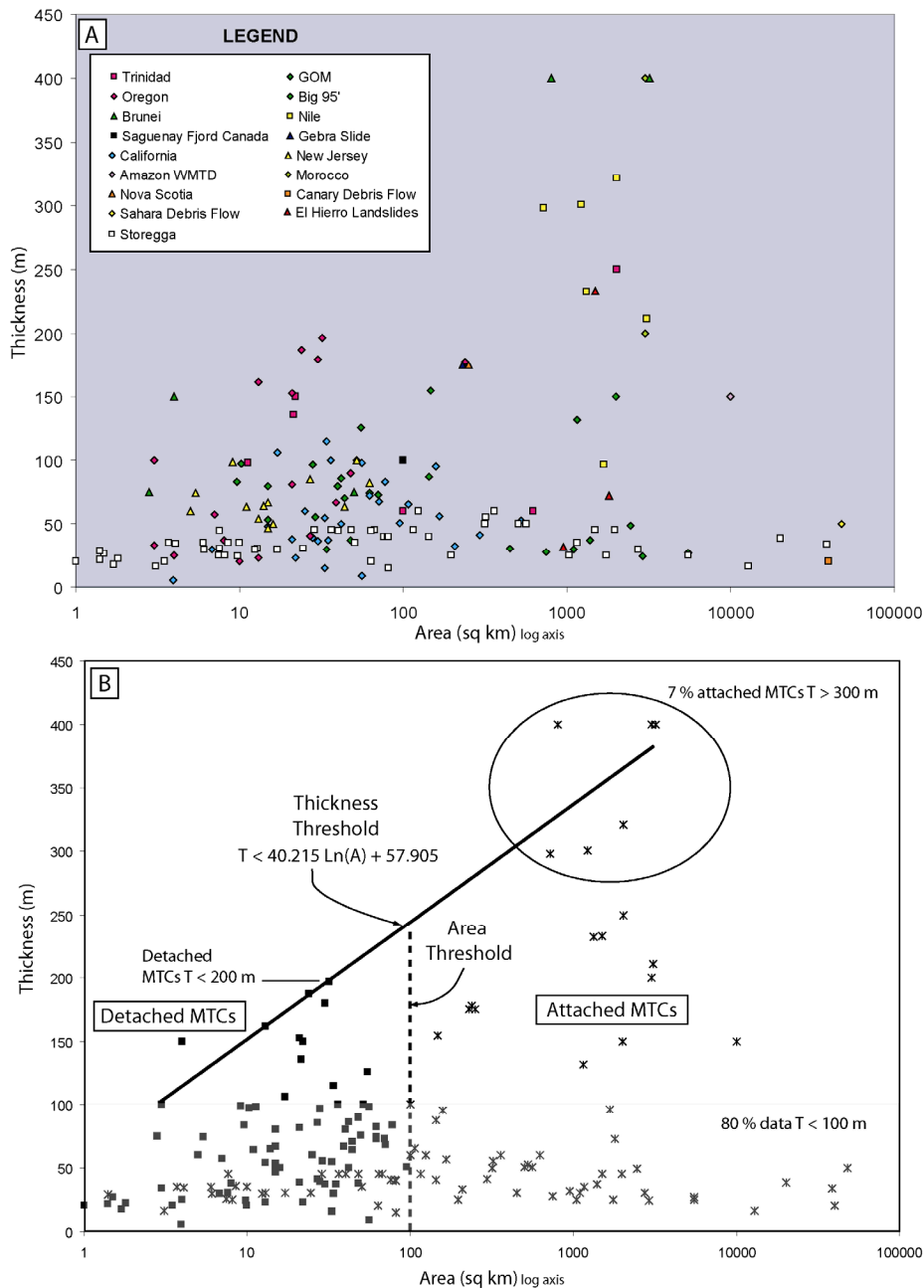


Figure 4.11: (A) Area versus thickness plot showing a variety of mass transport complexes from different continental margins around the world. (B) Area versus thickness plot showing the distribution of attached and detached mass transport complexes. The x-axis is displaying values in a logarithmic scale.

Despite the trends already observed in the plots that described the other morphometric relationships (area (A) versus length (L), and area (A) versus volume (V)), the area (A) versus thickness (T) plot shown in figure 4.11 does not respond to an exponential relationship. However, it seems to be that there is a “thickness threshold” that can be defined in the following form (see figure 4.11B), where T = thickness, A = Area, and Ln = natural logarithm:

$$T < 40.215 \ln(A) + 57.905 \quad (6)$$

The area versus thickness plot also shows that around 80% of the total data points have thicknesses that are less than 100 m; that the detached mass transport complexes usually do not reach thicknesses that are greater than 200 m, and that only 7% of the attached mass transport complexes have thicknesses that are greater than 300 m (typically due to superimposition of several events) (Figure 4.11B). This plot also suggests that the thickness (T) of MTCs is not a function of the release volume (V).

#### **4.6. CONCLUSIONS**

Analysis of the relationships between different morphometric parameters of mass transport complexes have been performed before by other authors (Issler et al., 2004; Haflidason et al., 2004, and Hühnerbach and Masson, 2004). Most of these authors have accurately suggested that the systematic collection of morphometric parameters of mass transport complexes, and the study of their relationships could lead to a better understanding of the rheology of the pre- and post- failed sediments. However, until now the involvement of triggering mechanisms has been mostly excluded in these discussions (Hühnerbach and Masson, 2004). We believe that there is a clear relationship between morphometric parameters of mass transport complexes, and their causal mechanisms.

The relationship between area (A), length (L), and volume (V) of mass transport complexes is scale-invariant, and responds to simple exponential relationships that can be expressed using power laws. An increase in length (L) does not necessarily imply an increase in the area (A) of the deposits or vice versa; instead the relationship between these two variables provides valuable information in terms of the geometry, and shape of mass transport complexes. Two main fields can be defined based on the geometric relationships that were observed between the area (A) and length (L) of the studied deposits. The upper field contains 80% of the data points that were collected in this study, whereas the lower field only contains the remaining 20% of the measurements. The mass transport complexes contained in the lower field tend to be wider than longer, and relatively smaller than their counterparts in the upper field. The upper field mass transport complexes are more elongated, and come in a wide range of sizes and scales.

It is clear for us that mass transport complexes that have been triggered by major events such as, sea level fluctuations and gas hydrate dissociation, high sedimentation rates, gravitational instabilities due to tectonism or volcanism, and major meteorite impacts are more likely to generate regional elongated deposits, with areas that can range in the order of 100's to 10,000's sq km, and lengths that vary from 10's to 100's of km (attached mass transport complexes). On the other hand, mass transport complexes that have been triggered by local gravitational instabilities in steep canyon walls, steep sidewalls of salt withdrawal basins, steep flanks of mud volcano ridges and thrust core structures, or that have been generated by submarine currents affecting the upper slope area, or similar intra-basinal events, are more likely to form deposits with areas ranging from 0.1 to 100's of sq km, and lengths that vary from 0.1 to 10's of km. Their shapes are more variable since the geometry of the final deposits is controlled by the space available in the environment in which they occur.

The majority of mass transport complexes (80%) have thicknesses that do not exceeded 100 m; detached mass transport complexes rarely exceed 200 m in thickness, and attached mass transport complexes which total thickness exceeds 300 m are extremely rare.

#### **4.7. REFERENCES**

- Campbell, D. C., J. W. Shimeld, D. C. Mosher, and D. J. W. Piper, 2004, Relationships between sediment mass-failure modes and magnitudes in the evolution of the Scotian slope, offshore Nova Scotia: Offshore Technology Conference, p. 14, OTC 16743.
- Gee, M. J. M., D. G., A. B. Watts, and P. A. Allen, 1999, The Saharan debris flow; an insight into the mechanics of long runout submarine debris flows, *Sedimentology, International*, Blackwell : Oxford-Boston, International, p. 317.
- Gee, M. J. R., A. B. Watts, D. G. Masson, and N. C. Mitchell, 2001, Landslides and the evolution of El Hierro in the Canary Islands, *Marine Geology, Netherlands*, Elsevier : Amsterdam, Netherlands, p. 271-293.
- Hafliðason, H., R. Lien, H. P. Sejrup, C. F. Forsberg, and P. Bryn, 2005, The dating and morphometry of the Storegga Slide, *Marine and Petroleum Geology, United Kingdom*, Elsevier : Oxford, United Kingdom, p. 123.
- Huhnerbach, V., and D. G. Masson, 2004, Landslides in the North Atlantic and its adjacent seas: an analysis of their morphology, setting and behaviour: *Marine Geology*, v. 213, p. 343-362.
- Imbo, Y., M. De Batist, M. Canals, M. J. Prieto, and J. Baraza, 2003, The Gebra Slide; a submarine slide on the Trinity Peninsula margin, Antarctica, *Marine Geology, Netherlands*, Elsevier : Amsterdam, Netherlands, p. 235.
- Kleverlaan, K., 1987, Gordo megabed; a possible seismite in a Tortonian submarine fan, Tabernas Basin, Province Almeria, Southeast Spain, *Sedimentary Geology, Netherlands*, Elsevier : Amsterdam, Netherlands, p. 165.
- Kvalstad, T. J., P. Gauer, A. M. Kaynia, and F. Nadim, 2002, Slope stability at Ormen Lange.: *Proceedings Offshore Site Investigation and Geotechnics: diversity and sustainability*, p. 233 - 250.
- Lastras, G., F. V. De Blasio, M. Canals, and A. Elverhoi, 2005, Conceptual and numerical modeling of the Big'95 debris flow, western Mediterranean Sea, *Journal of*

- Sedimentary Research, United States, Society of Economic Paleontologists and Mineralogists : Tulsa, OK, United States, p. 784.
- Lee, C., J. A. Nott, F. B. Keller, and A. R. Parrish, 2004a, Seismic expression of the Cenozoic mass transport complexes, deepwater Tarfaya-Agadir Basin, offshore Morocco: Offshore Technology Conference, p. 18, OTC 16741.
- Lee, H. J., W. R. Normark, M. A. Fisher, G. Greene, B. D. Edwards, and J. Locat, 2004b, Timing and extent of submarine landslides in southern California: Offshore Technology Conference, p. 11, OTC 16744.
- Maslin, M., C. Vilela, N. Mikkelsen, and P. Grootes, 2005, Causes of catastrophic sediment failures of the Amazon Fan: Quaternary Science Reviews, v. 24, p. 2180-2193.
- Masson, D. G., M. Canals, B. Alonso, R. Urgeles, and V. Huhnerbach, 1998, The Canary debris flow; source area morphology and failure mechanisms, Sedimentology, International, Blackwell : Oxford-Boston, International, p. 411.
- McAdoo, B. G., L. F. Pratson, and D. L. Orange, 2000, Submarine landslide geomorphology, US continental slope, Marine Geology, Netherlands, Elsevier : Amsterdam, Netherlands, p. 103.
- McGilvery, T. A., D. L. Cook, H. H. Roberts, N. C. Rosen, R. H. Fillon, and J. B. Anderson, 2003, The Influence of local gradients on accommodation space and linked depositional elements across a stepped slope profile, offshore Brunei: Shelf Margin Deltas and Linked Down Slope Petroleum Systems: Global Significance and Future Exploration Potential, p. 387-419.
- McGilvery, T. A., G. Haddad, and D. L. Cook, 2004, Seafloor and shallow subsurface examples of mass transport complexes, offshore Brunei: Offshore Technology Conference, p. 13, OTC 16780.
- Moscardelli, L., L. Wood, and P. Mann, 2006, Mass-transport complexes and associated processes in the offshore area of Trinidad and Venezuela: AAPG Bulletin, v. 90, p. 1059-1088.
- Newton, C. S., R. C. Shipp, D. C. Mosher, and G. D. Wach, 2004, Importance of mass transport complexes in the Quaternary development of the Nile Fan, Egypt: Offshore Technology Conference, p. 10, OTC 16742.
- Piper, D. J. W., C. Pirmez, P. L. Manley, D. Long, R. D. Flood, W. R. Normark, W. J. Showers, R. D. Flood, D. J. W. Piper, A. Klaus, S. J. Burns, W. H. Busch, S. M. Cisowski, A. Cramp, J. E. Damuth, M. A. Goni, S. G. Haberle, F. R. Hall, K.-U. Hinrichs, R. N. Hiscott, R. O. Kowsmann, J. D. Kronen, D. Long, M. Lopez, D. K. McDaniel, P. L. Manley, M. A. Maslin, N. Mikkelsen, F. Nanayama, W. R.

- Normark, C. Pirmez, J. R. dos Santos, R. R. Schneider, W. J. Showers, W. Soh, and J. Thibaut, 1997, Mass-transport deposits of the Amazon Fan: Proceedings of the Ocean Drilling Program, Scientific Results, v. 155, p. 109-146.
- Syvitski, J., and C. Schafer, 1996, Evidence for an earthquake-triggered basin collapse in Saguenay Fjord, Canada, *Sedimentary Geology*, Netherlands, Elsevier: Amsterdam, Netherlands, p. 127.
- Urgeles, R., G. Lastras, M. Canals, V. Willmott, A. Moreno, D. Casas, J. Baraza, and S. Berne, 2003, The BIG'95 debris flow and adjacent unfailed sediments in the NW Mediterranean Sea: geotechnical-sedimentological properties, and dating: *Advances in natural and technological hazards research*: Dordrecht, The Netherlands, Kluwer, 479 - 490 p.
- Wynn, R. B., D. G. Masson, D. A. Stow, and P. P. Weaver, 2000, The Northwest African slope apron: a modern analogue for deep-water systems with complex seafloor topography: *Marine and Petroleum Geology*, v. 17, p. 253-265.



# Appendices

## APPENDIX 1. DATA BASE OF BASIC MORPHOMETRIC PARAMETERS OF MASS TRANSPORT COMPLEXES AROUND THE WORLD

	Location and Event	Area (Km2)	Length (Km)	Thickness** (m)	Volume (Km3)	Source	
1	Offshore Trinidad(1)					(Moscardelli, L. et al., 2006; Moscardelli, L. & Wood, L. J., 2007)	
2	MTC_1	2017	140	250	242		
3	MTC_2	626	40	> 60	35		
4	MTC_2.1	100	38	> 60	7.27		
5	MTC_2.2	22	5.6	150	3.3		
6	MTC_2.3	21.4	8.7	136	3		
7	Storegga Slide(2)					(Haflidason, H. et al., 2005)	
8	Lobe 1	38740	410	34	~ 1050 – 1310		
9	Lobe 2	20278	410	38	~ 530 – 780		
10	Lobe 3	12900	305	16	~ 145 – 205		
11	Lobe 4	5530	93	25	~ 83 – 138.3		
12	Lobe 5	2742	122	30	~ 54.8 – 82.3		
13	A1	563	40.2	50	~ 22.5 – 28.2		
14	A2	1043	71.8	25	~ 15.6 – 26.1		
15	B1	1972	67.4	45	~ 59.2 – 88.7		
16	B2	1163	57	35	~ 29.1 – 40.7		
17	B3	196.4	37.6	25	~ 2.9 – 4.9		
18	B4	1756	54	25	~ 26.3 – 43.9		
19	B5	63.7	14	20	~ 1 – 1.3		
20	B6	81.8	23	15	~ 0.8 – 1.2		
21	C1	1497.7	110	45	~ 52.4 – 67.4		
22	C2	505	55.8	50	~ 17.7 – 25.3		
23	C3	360.5	31	60	~ 16.2 – 21.6		
24	C4	144.6	31.6	40	~ 4.3 – 5.8		
25	D1	321	26.8	55	~ 14.4 – 17.7		
26	D2	316.8	26.2	50	~ 12.7 – 15.8		
27	E1a	48.1	11.3	45	~ 1.92 – 2.17		
28	E1b	36.7	20.2	45	~ 1.47 – 1.65		
29	E1c	28.7	14.9	45	~ 1.15 – 1.29		
30	E1d	67.2	15.2	45	~ 2.69 – 3.02		
31	E1e	7.6	2.2	45	~ 0.3 – 0.34		
32	E2	76.3	12.8	40	~ 2.67 – 3.05		
33	E3	80.3	11.5	40	~ 2.81 – 3.21		
34	E4	80.9	12.9	40	~ 2.83 – 3.24		
35	E5	81.6	13.6	40	~ 2.85 – 3.26		
36	E6	40.3	17.3	45	~ 1.41 – 1.81		
37	E7	64.1	17.2	45	~ 1.92 – 2.88		
38	E8	115.9	26.9	45	~ 4.06 – 5.22		
39	F1	6.1	4.2	30	~ 0.15 – 0.18		
40	F2	12.9	5.3	30	~ 0.32 – 0.39		
41	F3	17	5.8	30	~ 0.43 – 0.51		
42	F4	24.5	9.4	30	~ 0.61 – 0.74		
43	F5	12.4	4.1	30	~ 0.31 – 0.37		
44	F6	6	3.1	35	~ 0.18 – 0.21		
45	F7	8.5	4.1	35	~ 0.25 – 0.3		
46	F8	4.1	3.3	34	~ 0.1 – 0.14		
47	F9	3.7	2.7	35	~ 0.11 – 0.13		
48	F10	7.5	2.8	25	~ 0.15 – 0.19		
49	F11	8.1	3.6	25	~ 0.16 – 0.2		
50	F12	10	3.3	35	~ 0.3 – 0.35		
51	G1	1.4	1.2	21	~ 0.02 – 0.03		
52	G2	1.8	0.7	22	~ 0.03 – 0.04		
53	G3	0.7	1.2	14	~ 0.01 – 0.01		
54	G4	3.5	3.3	20	~ 0.05 – 0.07		
55	G5	0.5	0.6	20	~ 0.01 – 0.01		
56	G6	1.5	1.6	27	~ 0.03 – 0.04		
57	G7	0.5	0.9	20	~ 0.01 – 0.01		
58	G8	0.7	1	29	~ 0.01 – 0.02		
59	G9	0.7	1	14	~ 0.01 – 0.01		
60	G10	1	1.3	20	~ 0.02 – 0.02		
61	G11	0.7	1	14	~ 0.01 – 0.01		
62	G12	0.3	0.5	33	~ 0.01 – 0.01		
63	G13	0.8	0.9	25	~ 0.01 – 0.02		
64	G14	1.7	1	18	~ 0.03 – 0.03		
65	G15	9.8	1.3	24	~ 0.17 – 0.24		
66	G16	7.6	1.4	30	~ 0.15 – 0.23		
67	I	123.8	12.5	60	~ 6.19 – 7.43		
68	II	50.5	7.8	35	~ 1.52 – 1.77		
69	III	1.4	1.3	29	~ 0.03 – 0.04		
70	IV	3.1	2	16	~ 0.03 – 0.05		
70	Saguenay Fjord, Canada(3)	100	65	100	3.06		(Syvitski, J. & Schafer, C., 1996)
71	US Continental Slope Oregon(4)	10	4.2	20	~ 0.2		(McAdoo, B. G. et al., 2000)
72		1	0.8	-	-		
73		3	1.3	33	~ 0.1		
74		8	1.5	38	~ 0.2 – 0.3		
75		2	0.9	-	-		
76		32	3.9	197	~ 1.2 – 6.3		
77		3	1.4	100	~ 0.2 – 0.3		
78		27	10	41	~ 0.7 – 1.1		
79		4	2.3	25	~ 0.1		
80		7	6	57	~ 0.2 – 0.4		
81		21	3.1	81	~ 1.2 – 1.7		

	Location and Event	Area (Km2)	Length (Km)	Thickness** (m)	Volume (Km3)	Source	
82	California(4)	48	10	90	~2.8-4.3	(McAdoo, B. G. et al., 2000)	
83		30	2.9	180	~3.6-5.4		
84		21	2.1	152	~2.1-3.2		
85		39	8.7	67	~1.7-2.6		
86		239	22	177	~28.1-42.5		
87		13	4.4	162	~1.4-2.1		
88		13	2.4	23	~0.2-0.3		
89		24	6.6	188	~2.9-4.5		
90		71	15	68	~3.2-4.8		
91		21	5.6	38	~0.6-0.8		
92		6.8	2.7	29	~0.2		
93		78	21	83	~4.3-6.5		
94		159	17	96	~10-15.2		
95		36	8.2	100	~2.4-3.6		
96	208	26	33	~4.5-6.8			
97	34	7.9	115	~2.6-3.9			
98	22	5.4	23	~0.3-0.5			
99	28	5.7	39	~0.7-1.1			
100	95	21	51	~3.2-4.8			
101	35	7.1	37	~0.9-1.3			
102	25	9	60	~1-1.5			
103	62	12	73	~3-4.5			
104	30	8.9	37	~0.7-1.1			
105	42	17	50	~1.4-2.1			
106	107	26	65	~4.6-7			
107	56	28	98	~3.7-5.5			
108	17	9.1	106	~1.2-1.8			
109	33	6.7	55	~1.2-1.8			
110	167	11	56	~6.2-9.4			
111	12	8.6	17	~0.1-0.2			
112	295	48	41	~8-12.1			
113	167	16	56	~6.2-9.4			
114	525	51	53	~18.2-27.6	(Lee, H. J. et al., 2004)		
115	Gaviota	3.93	2.25	5	~0.02	(Lee, H. J. et al., 2004)	
116	Goleta East	22	11	23	~0.5		
117	Goleta Central	33	11	15	~0.5		
118	Goleta West	56	14	9	~0.5		
119	Santa Monica Basin / Buried MTC(5)	0.06	0.3	~3	~0.0002		
120	San Pedro Basin / Palos Verdes Debris Avalanche(5)	15	10	48	~0.72	(McAdoo, B. G. et al., 2000)	
121	Gulf of Mexico(4)	452	49	30	~8.9-13.6		
122		44	3.8	70	~2-3.1		
123		29	12	55	~1.1-1.6		
124		62	12	74	~3-4.6		
125		48	5.5	37	~1.2-1.8		
126		52	14	100	~3.4-5.2		
127		15	8.8	80	~0.8-1.2		
128		15	8.6	53	~0.5-0.8		
129		10.3	3	97	~0.7-1		
130		1156	79	132	~100.4-152.2		
131		9.6	4.9	83	~0.5-0.8		
132		34	7.6	29	~0.7-1		
133		143	12	87	~8.3-12.5		
134		28	7.3	96	~1.8-2.7		
135		42	6.8	85	~2.4-3.6		
136		70	5.8	72	~3.4-5.1		
137		148	12	155	~15.1-22.9		
138		55	7.1	125	~4.6-6.9		
139		40	4.2	80	~2.1-3.2		
140		748	45	28	~13.6-20.6		
141		5509	167	27	~97.7-148		
142		1394	79	37	~33.9-51.4		
143		2913	124	24	~46.5-70.4		
144		2460	110	49	~79.1-119.9		
145		1098	89	30	~13.1-32.9		
146	New Jersey(4)	62	21	82	~3.3-5.1	(McAdoo, B. G. et al., 2000)	
147		52	16	100	~3.4-5.2		
148		27	12	85	~1.5-2.3		
149		44	8	63	~1.8-2.8		
150		15	6.5	66	~0.7-1		
151		5	5.4	60	~0.2-0.3		
152		15	11	46	~0.5-0.7		
153		16	6.9	50	~0.5-0.8		
154		14	8.3	64	~0.6-0.9		
155		11	6.5	63	~0.5-0.7		
156	5.4	2.5	74	~0.2-0.4			
157	9.1	4.6	99	~0.6-0.9			
158	13	5.9	54	~0.5-0.7			
159	Canary Debris Flow(6)	40000	600	20	~400	(Masson, D. G. et al., 1998)	
160	Sahara Debris Flow(7)	48000	700	50	~1100	(Gee, M. J. M., D. G. et al., 1999)	
161	El Hierro(8)	1500	60	233	~150-180	(Wynn, R. B. et al., 2000; Gee, M. J. R. et al., 2001)	
162		El Golfo	1800	55	72		~130
163		Las Playas 2	950	45	32		~30
164	Big 95° Ebro Spain(9)	2000	110	150	~26	(Urgeles, R. et al., 2003; Lastras, G. et al., 2005)	
165	Gebra Slide / Shetland Island / Antarctica(10)	160	-	-	~20	(Imbo, Y. et al., 2003)	
166		230	30	175	~20		
167	Amazon (11)					(Piper, D. J. W. et al., 1997)	
167	Amazon Fan (WMTD)	10000	200	150	~2000		
168	Buried MTC(URMTD)	11000	-	-	~610		
169	Buried MTC(BMTD)	7000	200	-	-		
170	Offshore Brunei (12)					(McGilvery, T. A. et al., 2003; McGilvery, T. A. et al., 2004)	
170	MTC-Regional Minimum estimates	800	40	400	~80		
171	MTC-Regional Maximum estimates	3200	80	400	~1280		
172	Brunei Cohesive Slump 1	50	10	75	~3.75		

	Location and Event	Area (Km <sup>2</sup> )	Length (Km)	Thickness** (m)	Volume (Km <sup>3</sup> )	Source
173	Brunei Cohesive Slump 2	2.81	3.75	75	~ 0.21	(McGilvery, T. A. et al., 2003; McGilvery, T. A. et al., 2004)
174	Brunei Cohesive Slump 3	4	2	150	~ 0.6	
175	Tarfaya Agadir Basin Morocco(13)					(Lee, C. et al., 2004)
176	Tejas A Tejas B	3000 3000	50 60	400 200	~150 – 1200 ~ 600	
177	Nova Scotia, Canada(14)	250	25	175	~ 44	(Newton, C. S. et al., 2004)
	Nile Fan Quaternary, Egypt(15)					
178	Red	1674	40	96	~ 70	
179	Blue	3101	50	211	~ 246	
180	Yellow	1328	30	232	~ 139	
181	light blue	721	30	298	~ 137	
182	Orange	2028	35	321	~ 322	
183	Green	1223	28	301	~ 185	
184	Cape Verde Slide Complex(16)	30000	500	-	-	
185	Oratava_lcod_Tino debris avalanche Tenerife(16)	5500	100	~ 181	~ 1000	
186	Gordo Mega Bed Spain(17) (a)	190	11.5	~ 35	~ 6.58	(Kleverlaan, K., 1987)

(a) Ancient event

\*\* T = (V/A)\*1000 (m)

## APPENDIX 2. CLASSIFICATION OF MASS TRANSPORT COMPLEXES

Attached Mass Transport Complexes (Upper Field MTCs)		
Event	Triggering Mechanism(s)	Source
Big 95' Event Western Mediterranean Age: 11500 BP	Under-consolidated material that failed on the upper slope area due to local uplifting, and volcanic activity.	(Urgeles, R. et al., 2003; Lastras, G. et al., 2005)
Main Storegga Slides Norwegian Margin Age: 7250±250 to 8100±250 BP	Regular advances of glaciers to the shelf break. Tectonic activity and gas hydrate dissociation.	(Kvalstad, T. J. et al., 2002; Hafflidason, H. et al., 2005)
Gulf of Mexico (large MTCs)	The very largest MTCs occur adjacent to the Mississippi Canyon, suggesting that high sedimentation rates associated with the Mississippi Delta played an important role in the genesis of these large MTCs.	(McAdoo, B. G. et al., 2000)
Amazon Fan MTDs Offshore Brazil Age: 45 ka to 13 ka	MTDs were originated in the upper slope area, where gas hydrates occur. Changes in sedimentation rates also played an important role.	(Maslin, M. et al., 2005)
Tejas A and Tejas B MTCs Offshore Morocco – Agadir Basin K-T Boundary (interpretative)	Tectonism associated with a step margin, and narrow shelf. Cretaceous-Tertiary impact event in the Yucatan Peninsula could have triggered slope failures in the Moroccan Atlantic margin.	(Lee, C. et al., 2004)
Brunei MTCs Late Tertiary to Recent	Triggered catastrophically by deep seismic events, or by over-steepening of the seafloor due to thrust-driven folding	(McGilvery, T. A. et al., 2004)
MTC_1, MTC_2 and MTC_2.1 Offshore Trinidad Age: Plio-Pleistocene	High sedimentation rates and over-steepening associated with the paleo Orinoco River, and gravitational instabilities in the upper slope area due to tectonism.	(Moscardelli, L. & Wood, L. J., 2007)
Nile Fan MTCs Age: Quaternary	The deposits likely sourced from failure of turbidite channels in the upslope portions of the basin.	(Newton, C. S. et al., 2004)
Offshore Nova Scotia MTCs Age: Cenozoic	Passive margin earthquakes, increase in sediment load due to deglaciation, gas hydrate dissociation, surface and subsurface groundwater flow. Progressive lateral spreading leading to catastrophic failures, salt tectonics, or tectonics related to isostatic adjustments.	(Campbell, D. C. et al., 2004)
Canary Debris Flow	Flank failure due to cumulative gravitational stresses arising from oversteepening of the island flanks related to volcanic and intrusive igneous processes.	(Masson, D. G. et al., 1998)
El Hierro Landslides Age: 15 to >200 ka		(Gee, M. J. R. et al., 2001)
Saharan Debris Flow Age: 60 ka		(Gee, M. J. M., D. G. et al., 1999)
Orota/lcod/Tino debris Avalanche W. Africa Offshore West Africa		(Wynn, R. B. et al., 2000)
Saguenay Fjord Collapse Canada Age: 1663 A.D.		Landslides and submarine slides were triggered by an earthquake (magnitude: Mercalli IX)

<b>Attached Mass Transport Complexes (Upper Field MTCs)</b>		
<b>Event</b>	<b>Triggering Mechanism(s)</b>	<b>Source</b>
Gebra Slide Antarctica Peninsula Age: Holocene	Combination of factors including high sedimentation rates during the last glacial period, unloading effects due to the retreat of the ice sheet during deglaciation, and high seismicity.	(Imbo, Y. et al., 2003)
California Landslides Age: Holocene	All occur on the sidewall of large canyons where erosion and sedimentation are more active. Sediment weakening is also possible due to gas/fluid melting. Earthquakes can also play an important role in slope destabilization.	(McAdoo, B. G. et al., 2000)
Oregon Landslides (one event >100 sq km) Age: Holocene	Earthquake caused destabilization of the steep slope.	(McAdoo, B. G. et al., 2000)
Cape Verde Slide Complex Offshore West Africa	Destabilization upper slope area (sea level fluctuations, tectonism?)	(Wynn, R. B. et al., 2000)
<b>Detached Mass Transport Complexes (Lower Field MTCs)</b>		
<b>Event</b>	<b>Triggering Mechanism(s)</b>	<b>Source</b>
Post-Storegga Small Slides Norwegian Margin Age: 5700 to 2200 BP	Gravitational instabilities due to steep slopes, and the action of submarine currents.	(Hafidason, H. et al., 2005)
Gulf of Mexico (small slides)	Commonly occur on the steep sidewalls of the salt withdrawal basins, and at the base of the Sigsbee Escarpment.	(McAdoo, B. G. et al., 2000)
Brunei Cohesive Slumps Late Tertiary to Recent	Commonly developed along the margins of thrust cored structures.	(McGilvery et al., 2004)
MTC_2.2, MTC_2.3 and MTC_2.4 Offshore Trinidad Age: Plio-Pleistocene	Gravitational instabilities on the flanks of mud volcano ridges.	(this work)
Small scale MTCs Offshore California Gaviota, Goleta, Palos Verdes Age: 300 to 164000 yrs.	Steep slopes susceptible to destabilization due to earthquakes. Downslope mud transport by episodic high-concentration storm advections.	(Lee et al., 2004)
New Jersey Landslides Age: Holocene	Failure could be influence by intercanyon down-slope sediment flows that lead to oversteepening, and subsequent failure.	(McAdoo, B. G. et al., 2000)
Oregon Landslides Age Holocene	Failures occur in steep local slopes associated with the Cascadia accretionary prism.	(McAdoo, B. G. et al., 2000)

## References

- Alvarez, W., A. Montanari, R. Colacicchi, and Anonymous, 1984, Synsedimentary slides and bedding formation in Apennine pelagic limestones: Abstracts with Programs - Geological Society of America, v. 16, p. 429.
- Anderson, J. B., J. Wellner, K. Abdulah, S. R. Sarzalejo, H. H., N. C. Rosen, R. H. Fillon, and J. B. Anderson, 2003, Late Quaternary shelf-margin delta and slope-fan complexes of the East Texas-western Louisiana margin: variable response to eustasy and sediment supply: Shelf Margin Deltas and Linked Down Slope Petroleum Systems: Global Significance and Future Exploration Potential, p. 67-78.
- Armentrout, J. M. R., H. H., N. C. Rosen, R. H. Fillon, and J. B. Anderson, 2003, Timing of Late Pleistocene shelf-margin deltaic depositional and mass-transport events, East Breaks 160-161 shelf-edge minibasin, Gulf of Mexico: Shelf Margin Deltas and Linked Down Slope Petroleum Systems: Global Significance and Future Exploration Potential, p. 91-114.
- Aslan, A., W. A. White, A. G. Warne, and E. H. Guevara, 2003, Holocene evolution of the western Orinoco Delta, Venezuela: GSA Bulletin, v. 115, p. 479-498.
- Beaubouef, R. T. V. W., J. C., and N. L. Adair, 2003, Ultra-high resolution 3-D characterization of deep-water deposits; Part II; Insights into the evolution of a submarine fan and comparisons with river deltas, Annual Meeting Expanded Abstracts - American Association of Petroleum Geologists, United States, American Association of Petroleum Geologists and Society of Economic Paleontologists and Mineralogists (AAPG) : Tulsa, OK, United States, p. 10.
- Beaubouef, R. T., S. J. W. Friedmann, P., R. M. Slatt, J. Coleman, N. C. Rosen, H. Nelson, A. H. Bouma, M. J. Styzen, and D. T. Lawrence, 2000, High resolution seismic/sequence stratigraphic framework for the evolution of Pleistocene intra slope basins, western Gulf of Mexico: depositional models and reservoir analogs: Deep-Water Reservoirs of the World.
- Beaubouef, R. T., V. Abreu, J. C. R. Van Wagoner, H. H., N. C. Rosen, R. H. Fillon, and J. B. Anderson, 2003, Basin 4 of the Brazos-Trinity slope system, western Gulf of Mexico: the terminal portion of a late Pleistocene lowstand systems tract: Shelf Margin Deltas and Linked Down Slope Petroleum Systems: Global Significance and Future Exploration Potential, p. 45-47.
- Belderson, R. H. K., N. H., A. H. Stride, and C. D. Pelton, 1984, A 'braided' distributary system on the Orinoco deep-sea fan, Marine Geology, Netherlands, Elsevier : Amsterdam, Netherlands, p. 195.

- Boettcher, S. S. J., J. L., M. J. Quinn, and J. E. Neal, 2003, Lithospheric structure and supracrustal hydrocarbon systems, offshore eastern Trinidad, AAPG Memoir, United States, American Association of Petroleum Geologists : Tulsa, OK, United States, p. 529.
- Brami, T. R., C. Pirmez, C. Archie, K. W. Holman, P., R. M. Slatt, J. Coleman, N. C. Rosen, H. Nelson, A. H. Bouma, M. J. Styzen, and D. T. Lawrence, 2000, Late Pleistocene deep-water stratigraphy and depositional processes, offshore Trinidad and Tobago: Deep-Water Reservoirs of the World, p. 104-115.
- Butenko, J., and J. P. Barbot, 1980, Geologic hazards related to offshore drilling and construction in the Orinoco River delta of Venezuela: JPT. Journal of Petroleum Technology, v. 32, p. 764-770.
- Campbell, D. C., J. W. Shimeld, D. C. Mosher, and D. J. W. Piper, 2004, Relationships between sediment mass-failure modes and magnitudes in the evolution of the Scotian slope, offshore Nova Scotia: Offshore Technology Conference, p. 14, OTC 16743.
- Carr-Brown, B., 1972, The Holocene/Pleistocene contact in the offshore area east of Galeota Point, Trinidad, West Indies, Transactions of the Caribbean Geological Conference = Memorias - Conferencia Geologica del Caribe, United States, Queens College Press : Flushing, NY, United States, p. 381.
- Damuth, J. E., R. D. Flood, R. O. Kowsmann, R. H. Belderson, and M. A. Gorini, 1988, Anatomy and growth pattern of Amazon deep-sea fan as revealed by long-range side-scan sonar (GLORIA) and high-resolution seismic studies: AAPG Bulletin, v. 72, p. 885-911.
- Dawson, A. G., P. Lockett, and S. Shi, 2004, Tsunami hazards in Europe: Environment International, v. 30, p. 577-585.
- Deville, E., A. Battani, R. Griboulard, S. Guerlais, J. P. Herbin, J. P. Houzay, C. Muller, and A. Prinzhofer, 2003a, The origin and processes of mud volcanism; new insights from Trinidad: Geological Society Special Publications, v. 216, p. 475-490.
- Deville, E., A. Mascle, S. H. Guerlais, C. Decalf, and B. Colletta, 2003b, Lateral changes of frontal accretion and mud volcanism processes in the Barbados accretionary prism and some implications: AAPG Memoir, v. 79, p. 656-674.
- Diaz de Gamero, M. L., 1996, The changing course of the Orinoco River during the Neogene: a review: Palaeogeography, Palaeoclimatology, Palaeoecology, v. 123, p. 385-402.

- Dykstra, M., 2005, Dynamics of submarine sediment mass-transport, from the shelf to the deep sea: PhD Thesis thesis, University of California, Santa Barbara, 54 p.
- Ercilla, G., B. Alonso, J. W. Baraza, P., R. M. Slatt, J. Coleman, N. C. Rosen, H. Nelson, A. H. Bouma, M. J. Styzen, and D. T. Lawrence, 2000, High resolution morpho-sedimentary characteristics of the distal Orinoco turbidite system: Deep-Water Reservoirs of the World, p. 374-388.
- Flood, R. D., D. J. W. Piper, A. Klaus, S. J. Burns, W. H. Busch, S. M. Cisowski, A. Cramp, J. E. Damuth, M. A. Goni, S. G. Haberle, F. R. Hall, K.-U. Hinrichs, R. N. Hiscott, R. O. Kowsmann, J. D. Kronen, D. Long, M. Lopez, D. K. McDaniel, P. L. Manley, M. A. Maslin, N. Mikkelsen, F. Nanayama, W. R. Normark, C. Pirmez, J. R. dos Santos, R. R. Schneider, W. J. Showers, W. Soh, and J. Thibald, 1995: Proceedings of the Ocean Drilling Program, Part A: Initial Reports, v. 155.
- Frey Martinez, J., J. Cartwright, and B. Hall, 2005, 3D seismic interpretation of slump complexes: examples from the continental margin of Israel: Basin Research, v. 17, p. 83-108.
- Fryer, G. J., P. Watts, and L. F. Pratson, 2004, Source of the great tsunami of 1 April 1946: a landslide in the upper Aleutian forearc: Marine Geology, v. 203, p. 201-218.
- Galloway, W.E. and Hobday, D.K., 1996, Terrigenous Clastic Depositional Systems. Heidelberg, Springer-Verlag.
- Garciacono, E. J., 2006, Stratigraphic architecture and basin fill evolution of a plate margin basin, eastern offshore Trinidad and Venezuela: Master thesis, University of Texas, Austin.
- Gee, M. J. R. M., D. G., A. B. Watts, and P. A. Allen, 1999, The Saharan debris flow; an insight into the mechanics of long runout submarine debris flows, Sedimentology, International, Blackwell : Oxford-Boston, International, p. 317.
- Gee, M. J. R., A. B. Watts, D. G. Masson, and N. C. Mitchell, 2001, Landslides and the evolution of El Hierro in the Canary Islands, Marine Geology, Netherlands, Elsevier : Amsterdam, Netherlands, p. 271-293.
- Gee, M. J. R., D. G. Masson, A. B. Watts, and N. C. Mitchell, 2001, Passage of debris flows and turbidity currents through a topographic constriction; seafloor erosion and deflection of flow pathways: Sedimentology, v. 48, p. 1389-1409.
- Grantz, A., R. L. Phillips, M. W. Mullen, S. W. Starratt, G. A. Jones, A. S. Naidu, and B. P. Finney, 1996, Character, paleoenvironment, rate of accumulation, and evidence for seismic triggering of Holocene turbidites, Canada Abyssal Plain, Arctic Ocean: Marine Geology, v. 133, p. 51-73.

- Haflidason, H., R. Lien, H. P. Sejrup, C. F. Forsberg, and P. Bryn, 2005, The dating and morphometry of the Storegga Slide, *Marine and Petroleum Geology*, United Kingdom, Elsevier : Oxford, United Kingdom, p. 123.
- Haq, B. U., 1993, Deep sea response to eustatic changes and significance of gas hydrates for continental margin stratigraphy: *International Association of Sedimentologists Special Publication*, v. 18, p. 93-106.
- Haq, B. U., 1995, Growth and decay of gas hydrates: a forcing mechanism for abrupt climate change and sediment wasting on ocean margins?: *Akademie Wetenschap*, v. 44, p. 191-203.
- Hearne, M. E., N. R. Grindlay, and P. Mann, 2003, Landslide deposits, cookie bites, and crescentic fracturing along the northern Puerto Rico-Virgin Islands margin: implications for potential tsunamigenesis: *Eos Transactions American Geophysical Union*, v. 84, p. 46.
- Heppard, P. D., H. S. Cander, and E. B. Eggertson, 1998, Abnormal pressure and the occurrence of hydrocarbons in offshore eastern Trinidad, West Indies: *AAPG Memoir*, v. 70, p. 215-246.
- Herrera, L., G. Febres, and R. Avila, 1981, Las mareas en aguas Venezolanas y su amplificacion en la region del delta del Orinoco: *Acta Cientifica Venezolana*, v. 32, p. 299-306.
- Hiscott, R. N., K. T. Pickering, A. H. Bouma, B. M. Hand, B. C. Kneller, G. Postma, and W. Soh, 1997, Basin-floor fans in the North Sea; sequence stratigraphic models vs. sedimentary facies; discussion: *AAPG Bulletin*, v. 81, p. 662-665.
- Hoffman, J. S., M. J. Kaluza, R. Griffiths, G. McCullough, J. Hall, and T. Nguyen, 2004, Addressing the challenges in the placement of seafloor infrastructure on the East Breaks slide—a case study: the Falcon Field (EB 579/623): *Northwestern Gulf of Mexico: Offshore Technology Conference*, p. 17.
- Huhnerbach, V., and D. G. Masson, 2004, Landslides in the North Atlantic and its adjacent seas: an analysis of their morphology, setting and behaviour: *Marine Geology*, v. 213, p. 343-362.
- Imbo, Y. D. B., M. Canals, M. J. Prieto, and J. Baraza, 2003, The Gebra Slide; a submarine slide on the Trinity Peninsula margin, Antarctica, *Marine Geology*, Netherlands, Elsevier : Amsterdam, Netherlands, p. 235.
- Jennette, D. C. G., Timothy R., 1999, The interaction of shelf accommodation, sediment supply and sea level in controlling the facies, architecture and distribution of the Forties and Tay basin-floor fans, central North Sea, *AAPG Bulletin*, United States,



- American Association of Petroleum Geologists : Tulsa, OK, United States, p. 1320.
- Klaucke, I., D. G. Masson, N. H. Kenyon, and J. V. Gardner, 2004, Sedimentary processes of the lower Monterey Fan channel and channel-mouth lobe: *Marine Geology*, v. 206, p. 181-198.
- Kleverlaan, K., 1987, Gordo megabed; a possible seismite in a Tortonian submarine fan, Tabernas Basin, Province Almeria, Southeast Spain, *Sedimentary Geology*, Netherlands, Elsevier : Amsterdam, Netherlands, p. 165.
- Knapp, J. H., C. C. Diaconescu, and Anonymous, 2000, Evidence for buried gas hydrates and their role in seafloor instability in the South Caspian Sea, Azerbaijan: *Abstracts with Programs - Geological Society of America*, v. 32, p. 102.
- Knutz, P. C., W. E. N. Austin, and E. J. Jones, 2001, Millennial-scale depositional cycles related to British Ice Sheet variability and North Atlantic paleocirculation since 45 kyr B.P., Barra Fan, U.K. margin: *Paleoceanography*, v. 16, p. 53-64.
- Kvalstad, T. J., P. Gauer, A. M. Kaynia, and F. Nadim, 2002, Slope stability at Ormen Lange.: *Proceedings Offshore Site Investigation and Geotechnics: diversity and sustainability*, p. 233 - 250.
- Kvenvolden, K. A., 1993, Gas hydrates, geological perspective and global change: *Reviews of Geophysics*, v. 31, p. 173-187.
- Lastras, G. D. B., F. Vittorio, M. Canals, and A. Elverhoi, 2005, Conceptual and numerical modeling of the Big'95 debris flow, western Mediterranean Sea, *Journal of Sedimentary Research*, United States, Society of Economic Paleontologists and Mineralogists : Tulsa, OK, United States, p. 784.
- Lee, C., J. A. Nott, F. B. Keller, and A. R. Parrish, 2004, Seismic expression of the Cenozoic mass transport complexes, deepwater Tarfaya-Agadir Basin, offshore Morocco: *Offshore Technology Conference*, p. 18, OTC 16741.
- Lee, H. J., W. R. Normark, M. A. Fisher, G. Greene, B. D. Edwards, and J. Locat, 2004b, Timing and extent of submarine landslides in southern California: *Offshore Technology Conference*, p. 11, OTC 16744.
- Macdonald, D. I. M., A. Moncrieff, and P. J. Butterworth, 1993, Giant slide deposits from a Mesozoic fore-arc basin, Alexander Island, Antarctica, *Geology Boulder*, United States, Geological Society of America (GSA) : Boulder, CO, United States, p. 1047.
- Manley, P. L., and R. D. Flood, 1988, Cyclic sediment deposition within Amazon deep-sea fan: *AAPG Bulletin*, v. 72, p. 912-925.

- Marr, J. G., P. A. Harff, G. Shanmugam, and G. Parker, 2001, Experiments on subaqueous sandy gravity flows: The role of clay and water content in flow dynamics and depositional structures: *GSA Bulletin*, v. 113, p. 1377-1386.
- Martinez, J. F., J. A. Cartwright, P. M. Burgess, and J. V. Bravo, 2004, 3D seismic interpretation of the Messinian unconformity in the Valencia Basin, Spain: *Memoirs of the Geological Society of London*, v. 29, p. 91-100.
- Martinez, J. F., J. A. Cartwright, P. M. Burgess, and J. V. Bravo, 2004, 3D seismic interpretation of the Messinian unconformity in the Valencia Basin, Spain: *Memoirs of the Geological Society of London*, v. 29, p. 91-100.
- Maslin, M., C. Vilela, N. Mikkelsen, and P. Grootes, 2005, Causes of catastrophic sediment failures of the Amazon Fan: *Quaternary Science Reviews*, v. 24, p. 2180-2193.
- Maslin, M., M. Owen, S. Day, and D. Long, 2004, Linking continental-slope failures and climate change: Testing the clathrate gun hypothesis: *Geology*, v. 32, p. 53-56.
- Maslin, M., N. Mikkelsen, C. Vilela, and B. Haq, 1998, Sea-level- and gas-hydrate-controlled catastrophic sediment failures of the Amazon Fan: *Geology*, v. 26, p. 1107-1110.
- Masson, D. G., B. van Niel, and P. P. E. Weaver, 1997, Flow processes and sediment deformation in the Canary debris flow on the NW African continental rise: *Sedimentary Geology*, v. 110, p. 163-179.
- Masson, D. G., M. Canals, B. Alonso, R. Urgeles, and V. Huhnerbach, 1998, The Canary debris flow; source area morphology and failure mechanisms: *Sedimentology*, v. 45, p. 411-432.
- Masson, D. G., M. Canals, B. Alonso, R. Urgeles, and V. Huhnerbach, 1998, The Canary debris flow; source area morphology and failure mechanisms, *Sedimentology, International*, Blackwell : Oxford-Boston, International, p. 411.
- McAdoo, B. G., L. F. Pratson, and D. L. Orange, 2000, Submarine landslide geomorphology, US continental slope, *Marine Geology*, Netherlands, Elsevier : Amsterdam, Netherlands, p. 103.
- McGilvery, T. A., D. L. R. Cook, H. H., N. C. Rosen, R. H. Fillon, and J. B. Anderson, 2003, The Influence of local gradients on accommodation space and linked depositional elements across a stepped slope profile, offshore Brunei: *Shelf Margin Deltas and Linked Down Slope Petroleum Systems: Global Significance and Future Exploration Potential*, p. 387-419.

- McGilvery, T. A., G. Haddad, and D. L. Cook, 2004, Seafloor and shallow subsurface examples of mass transport complexes, offshore Brunei: Offshore Technology Conference, p. 13, OTC 16780.
- McMurtry, G. M., P. Watts, G. J. Fryer, J. R. Smith, and F. Imamura, 2004, Giant landslides, mega-tsunamis, and paleo-sea level in the Hawaiian Islands: *Marine Geology*, v. 203, p. 219-233.
- Meade, R. H., F. H. Weibezahn, W. M. Lewis, D. Perez Hernandez, F. H. Weibezahn, H. Alvarez, and W. M. Lewis, 1990, Suspended-sediment budget for the Orinoco River: El Rio Orinoco como ecosistema--The Orinoco River as an ecosystem, *Impresos Rubel*, 55-79 p.
- Mize, K. L., L. J. Wood, and P. Mann, 2004, Controls on the morphology and development of deep-marine channels, eastern offshore Trinidad and Venezuela AAPG Annual Meeting Program, v. 13.
- Moiola, R. J., and G. Chanmugam, 1984, Submarine fan sedimentation, Ouachita Mountains, Arkansas and Oklahoma: *Transactions - Gulf Coast Association of Geological Societies*, v. 34, p. 175-182.
- Montoya, P., 2006, Salt tectonics and Sequence-Stratigraphic History of Minibasins near the Sigsbee Escarpment, Gulf of Mexico PhD Thesis thesis, University of Texas at Austin, Austin, 276 p.
- Morris, R. C., 1971, Classification and interpretation of disturbed bedding types in Jackfork flysch rocks (upper Mississippian), Ouachita mountains, Arkansas: *Journal of Sedimentary Research*, v. 41, p. 410-424.
- Moscardelli, L., L. J. Wood, and P. Mann, 2004, Debris flow distribution and controls on slope to basin deposition, offshore Trinidad AAPG Annual Meeting Program, v. 13.
- Moscardelli, L., L. Wood, and P. Mann, 2006, Mass-transport complexes and associated processes in the offshore area of Trinidad and Venezuela: *AAPG Bulletin*, v. 90, p. 1059-1088.
- Newton, C. S., R. C. Shipp, D. C. Mosher, and G. D. Wach, 2004, Importance of mass transport complexes in the Quaternary development of the Nile Fan, Egypt: Offshore Technology Conference, p. 10, OTC 16742.
- Newton, C., G. Wach, U. Dalhousie, C. Shipp, and D. Mosher, 2004, Importance of mass transport complexes in the Quaternary development of the Nyle Fan, Egypt: Offshore Technology Conference, p. 10.

- Nisbet, E., and D. J. W. Piper, 1998, Giant submarine landslides: *Nature* (London), v. 392, p. 329-330.
- Nissen, S. E., H. Norman, C. T. Steiner, and K. L. Cotterill, 1999, Debris flow outrunner blocks, glide tracks, and pressure ridges identified on the Nigerian continental slope using 3-D seismic coherency, *Leading Edge* Tulsa, OK, United States, Society of Exploration Geophysicists : Tulsa, OK, United States, p. 595.
- Norem, H., J. Locat, and B. Schieldrop, 1990, An approach to the physics and the modeling of submarine flowslides: *Marine Geotechnology*, v. 9, p. 93-111.
- Nota, D. J. G., 1958, *Sediments of the western Guiana shelf*, diss., Utrecht, Univ.
- O'Loughlin, K. F., and J. F. Lander, 2003, *Caribbean tsunamis – a 500 year history from 1498 – 1998: advances in natural and technological hazards research*: Boston, Kluwer Academic Publishers, 263 p.
- Pickering, K. T., and J. Corregidor, 2005, Mass-transport complexes (MTCs) and tectonic control on basin-floor submarine fans, middle Eocene, south Spanish Pyrenees, *Journal of Sedimentary Research*, United States, Society of Economic Paleontologists and Mineralogists : Tulsa, OK, United States, p. 761.
- Piper, D. J. W., C. Pirmez, P. L. Manley, D. Long, R. D. Flood, W. R. Normark, W. J. Showers, R. D. Flood, D. J. W. Piper, A. Klaus, S. J. Burns, W. H. Busch, S. M. Cisowski, A. Cramp, J. E. Damuth, M. A. Goni, S. G. Haberle, F. R. Hall, K.-U. Hinrichs, R. N. Hiscott, R. O. Kowsmann, J. D. Kronen, D. Long, M. Lopez, D. K. McDaniel, P. L. Manley, M. A. Maslin, N. Mikkelsen, F. Nanayama, W. R. Normark, C. Pirmez, J. R. dos Santos, R. R. Schneider, W. J. Showers, W. Soh, and J. Thibal, 1997b, Mass-transport deposits of the Amazon Fan: *Proceedings of the Ocean Drilling Program, Scientific Results*, v. 155, p. 109-146.
- Piper, D. J. W., E. W. R. Behrens, H. H., N. C. Rosen, R. Fillon, and J. Anderson, 2003, Downslope sediment transport processes and sediment distributions at the East Breaks, Northwest Gulf of Mexico: Shelf Margin Deltas and Linked Down Slope Petroleum Systems: *Global Significance and Future Exploration Potential*, p. 359-385.
- Piper, D. J. W., M. Deptuck, R. D. Flood, D. J. W. Piper, A. Klaus, S. J. Burns, W. H. Busch, S. M. Cisowski, A. Cramp, J. E. Damuth, M. A. Goni, S. G. Haberle, F. R. Hall, K.-U. Hinrichs, R. N. Hiscott, R. O. Kowsmann, J. D. Kronen, D. Long, M. Lopez, D. K. McDaniel, P. L. Manley, M. A. Maslin, N. Mikkelsen, F. Nanayama, W. R. Normark, C. Pirmez, J. R. dos Santos, R. R. Schneider, W. J. Showers, W. Soh, and J. Thibal, 1997a, Fine-grained turbidites of the Amazon Fan; facies characterization and interpretation: *Proceedings of the Ocean Drilling Program, Scientific Results*, v. 155, p. 79-108.

- Pirmez, C. H., Richard N., and J. D. Kronen, Jr., 1997, Sandy turbidite successions at the base of channel-levee systems of the Amazon Fan revealed by FMS logs and cores; unraveling the facies architecture of large submarine fans, Proceedings of the Ocean Drilling Program, Scientific Results, United States, Texas A & M University, Ocean Drilling Program : College Station, TX, United States, p. 7.
- Pirmez, C., J. Marr, C. Shipp, and F. Kopp, 2004, Observations and numerical modeling of debris flows in the Na Kika Basin, Gulf of Mexico: Offshore Technology Conference, p. 13, OTC 16749.
- Popenoe, P., E. A. Schmuck, and W. P. Dillon, 1993, The Cape Fear landslide; slope failure associated with salt diapirism and gas hydrate decomposition: U. S. Geological Survey Bulletin, p. 40-53.
- Posamentier, H. W., and V. Kolla, 2003, Seismic Geomorphology and Stratigraphy of Depositional Elements in Deep-Water Settings: Journal of Sedimentary Research, v. 73, p. 367-388.
- Posamentier, H., 2004, Stratigraphy and geomorphology of deep-water mass transport complexes based on 3D seismic data: Offshore Technology Conference, p. 7, OTC 16740.
- Rothwell, R. G., J. Thomas, and G. Kaehler, 1998, Low-sea-level emplacement of very large late Pleistocene "megaturbidite" in the Western Mediterranean Sea: Nature (London), v. 392, p. 377-380.
- Shackleton, N. J., 1987, Oxygen isotopes, ice volume and sea level: Quaternary Science Reviews, v. 6, p. 183-190.
- Shanmugam, G., 2000, 50 years of the turbidite paradigm (1950s-1990s); deep-water processes and facies models; a critical perspective: Marine and Petroleum Geology, v. 17, p. 285-342.
- Shanmugam, G., R. B. Bloch, S. M. Mitchell, G. W. J. Beamish, R. J. Hodgkinson, J. E. Damuth, T. Staume, S. E. Syvertsen, and K. E. Shields, 1995, Basin-floor fans in the North Sea; sequence stratigraphic models vs. sedimentary facies: AAPG Bulletin, v. 79, p. 477-512.
- Shanmugam, G., R. J. Moiola, and J. K. Sales, 1988, Duplex-like structures in submarine fan channels, Ouachita Mountains, Arkansas: Geology, v. 16, p. 229-232.
- Shipp, C., J. A. Nott, and J. A. Newlin, 2004, Physical characteristics and impact of mass transport complexes on deepwater jetted conductors and suction anchor piles: Offshore Technology Conference, p. 11, OTC 16751.

- Sohn, Y. K., 2000, Depositional Processes of Submarine Debris Flows in the Miocene Fan Deltas, Pohang Basin, SE Korea with Special Reference to Flow Transformation: *Journal of Sedimentary Research*, v. 70, p. 491-503.
- Strachan, L. J., 2002, *Geometry to Genesis: A Comparative Field Study of Slump Deposits and Their Modes of Formation*: PhD Dissertation thesis, Cardiff University, Cardiff, 412 p.
- Sullivan, S., L. J. Wood, and P. Mann, 2004, Distribution, nature and origin of Mobile mud features offshore Trinidad: *Salt-Sediment Interactions and Hydrocarbon Prospectivity: Concepts, Applications, and Case Studies for the 21st Century*, p. 840-867.
- Sutter, J. R., 2006, Shelf margin systems: Interface between shallow water sediment sources and deep water sinks: *External Controls on Deep Water Depositional Systems: Climate, Sea-Level and Sediment Flux*, p. 78.
- Sydow, J. C., J. Finneran, A. P. R. Bowman, H. H., N. C. Rosen, R. H. Fillon, and J. B. Anderson, 2003, Stacked shelf-edge reservoirs of the Columbus Basin, Trinidad, West Indies: *Shelf Margin Deltas and Linked Down Slope Petroleum Systems: Global Significance and Future Exploration Potential*, p. 411-465.
- Sydow, J. C., J. Finneran, A. P. R. Bowman, H. H., N. C. Rosen, R. H. Fillon, and J. B. Anderson, 2003, Stacked shelf-edge reservoirs of the Columbus Basin, Trinidad, West Indies: *Shelf Margin Deltas and Linked Down Slope Petroleum Systems: Global Significance and Future Exploration Potential*, p. 411-465.
- Syvitski, J., and C. Schafer, 1996, Evidence for an earthquake-triggered basin collapse in Saguenay Fjord, Canada, *Sedimentary Geology*, Netherlands, Elsevier: Amsterdam, Netherlands, p. 127.
- Thompson, L. G., E. Mosley-Thompson, M. E. Davis, P. N. Lin, K. A. Henderson, J. Cole-Dai, J. F. Bolzan, and K. B. Liu, 1995, Late Glacial Stage and Holocene tropical ice core records from Huscaran, Peru: *Science*, v. 269, p. 46-50.
- Twichell, D. C., W. C. Schwab, C. H. Nelson, and N. H. Kenyon, 2006, The effects of submarine canyon and proximal fan processes on the depositional systems of the distal Mississippi Fan: *External Controls on Deep Water Depositional Systems: Climate, Sea-Level and Sediment Flux*, p. 81.
- Urgeles, R., G. Lastras, M. Canals, V. Willmott, A. Moreno, D. Casas, J. Baraza, and S. Berne, 2003, The BIG'95 debris flow and adjacent unfailed sediments in the NW Mediterranean Sea: geotechnical-sedimentological properties, and dating: *Advances in natural and technological hazards research*: Dordrecht, The Netherlands, Kluwer, 479 - 490 p.

- Van Andel, T. H., 1967, The Orinoco Delta: *Journal of Sedimentary Research*, v. 37, p. 297-310.
- Wach, G., A. H. Bouma, T. Lukas, H. D. Wickens, R. K. R. Goldhammer, H. H., N. C. Rosen, R. H. Fillon, and J. B. Anderson, 2003, Transition from shelf margin delta to slope fan—outcrop examples from the Tanqua Karoo, South Africa: *Shelf Margin Deltas and Linked Down Slope Petroleum Systems: Global Significance and Future Exploration Potential*, p. 849-861.
- Warne, A. G., R. H. Meade, W. A. White, E. H. Guevara, J. Gibeaut, R. C. Smyth, A. Aslan, and T. Tremblay, 2002, Regional controls on geomorphology, hydrology, and ecosystem integrity in the Orinoco Delta, Venezuela: *Geomorphology*, v. 44, p. 273-307.
- Weimer, P., 1989, Sequence stratigraphy of the Mississippi Fan (Plio-Pleistocene), Gulf of Mexico: *Geo-Marine Letters*, v. 9, p. 185 - 272.
- Weimer, P., 1990, Sequence stratigraphy, seismic geometries, and depositional history of the Mississippi Fan, deep Gulf of Mexico: *AAPG Bulletin*, v. 74, p. 425-453.
- Weimer, P., and C. Shipp, 2004, Mass transport complex: Musing on the past uses and suggestions for future directions: *Offshore Technology Conference*, p. 10, OTC 16752.
- Winker, C. D., 1996, High-resolution seismic stratigraphy of a late Pleistocene submarine fan ponded by salt-withdrawal minibasins on the Gulf of Mexico continental slope, p. 619-628.
- Winker, C. D., J. R. W. Booth, P., R. M. Slatt, J. Coleman, N. C. Rosen, H. Nelson, A. H. Bouma, M. J. Styzen, and D. T. Lawrence, 2000, Sedimentary dynamics of the salt-dominated continental slope, Gulf of Mexico: Integration of observations from the seafloor, near-surface, and deep subsurface: *Deep-Water Reservoirs of the World*, p. 1059-1086.
- Wood, L. J., 2000, Chronostratigraphy and Tectonostratigraphy of the Columbus Basin, Eastern Offshore Trinidad: *AAPG Bulletin*, v. 84, p. 1905-1928.
- Wood, L. J., S. Sullivan, and P. Mann, 2004, Influence of mobile shales in the creation of successful hydrocarbon basins: *Salt-Sediment Interactions and Hydrocarbon Prospectivity: Concepts, Applications, and Case Studies for the 21st Century*, p. 892-930.
- Wynn, R. B., 2006, Timing and relation to climate/sea-level of giant landslides and turbidity currents on the Northwest African continental margin, from Morocco to Senegal: *External Controls on Deep Water Depositional Systems: Climate, Sea-Level and Sediment Flux*, p. 87.

Wynn, R. B., D. G. Masson, D. A. Stow, and P. P. Weaver, 2000, The Northwest African slope apron: a modern analogue for deep-water systems with complex seafloor topography: *Marine and Petroleum Geology*, v. 17, p. 253-265.



## **Vita**

Lorena Moscardelli was born in Caracas, Venezuela on August 2, 1977, to Domenico Moscardelli and Rosa Solange Jimenez de Moscardelli. After graduating from the Colegio Francia, she attended the Universidad Central de Venezuela, where she graduated in 2000 with a B.Sc. in geological engineer with an honorary mention for being the top student of her graduating class.

In 2000, she began to work with the National Oil Company of her home country as an exploration geologist for oil fields in offshore eastern Venezuela (Plataforma Deltana project). In the fall semester of 2003, she entered the Jackson School of Geosciences of the University of Texas at Austin to pursue a Ph.D. degree in Geological Sciences. During her Ph.D. studies, she was a graduate research assistant for the Quantitative Clastic Laboratory at the Bureau of Economic Geology, where she conducted research in the southeastern part of the Caribbean under the supervision of Dr. Lesli Wood. Lorena also worked as a summer intern in a production project in the Hugoton Basin for OXY in 2005, and as a seismic interpreter for an exploration project in the deep water blocks of the Gulf of Mexico for BHP in 2006.

Permanent address: Av. Francisco de Miranda, Edf. Monte Ararat, Piso 10, Apt I, Petare, Caracas, Venezuela.

This dissertation was typed by Lorena Gina Moscardelli. All figures were created by the author in Landmark Graphics Corporation®, Microsoft Office ® and Illustrator ®.